

Thermo-Catalytic Reforming of Woody Biomass

by

Manjot Kaur Gill

A thesis submitted in partial fulfillment of the requirements for the degree of

Master of Science

in

Chemical Engineering

Department of Chemical and Materials Engineering
University of Alberta

© Manjot Kaur Gill, 2020

ABSTRACT

Depletion of fossil fuels and greenhouse gas emissions from the usage of fossil fuels are the major environmental concerns in today's world. Biomass is one such renewable resource which can be converted to solid and liquid biofuels. A novel technology, known as Thermo-Catalytic Reforming, could be a promising solution to these issues. The TCR technology integrates intermediate pyrolysis with a post-reforming stage to convert biomass into a high-quality bio-oil, biochar, and syngas. Although there are several conventional pyrolysis-based bio-oil technologies in various stages of development, the challenge with most of these bio-oils is their properties (low pH, high viscosity, immiscibility with hydrocarbons and unstable over time). This process can convert any type of biomass and organic feedstock into a variety of energy products (biochar, bio-oil and permanent gases) and will help address the challenges with the bio-oil produced from conventional pyrolysis.

As a first part of the study, the thermal and kinetic behavior of corn stover, wheat straw and softwood were studied using thermogravimetric analysis (TGA) to understand its kinetic behavior. The TGA experiments were carried out using SDT Q600, TA instrument at three different heating rates (2, 5 and 10 °C/min) in an inert atmosphere. The TGA experiments showed that the decomposition of agricultural residues was significantly lower than the woody biomass due to high volatiles and low ash content in the latter. The TGA data was further used to calculate the activation energy of softwood using three different models. It was observed that the

activation energy increased at the beginning with increase in conversion from 0.1 to 0.35, and then decreased after further increase in conversion from 0.4 to 0.8.

Following the kinetic study, the experiments were carried out using various wood biomass feedstocks such as hardwood pellets, softwood pellets and softwood chips in a 2 kg/h laboratory scale TCR plant. The pelletized feedstock was fed through the hopper and pyrolyzed in a screw/auger reactor. The pyrolysis products are then passed through a catalytic reformer, where the produced bio-char acts as a catalyst to aid in the production of gases and bio-oil. The results revealed that the composition of the biomass had minimal effect on the product yield (~ 18 wt % biochar, 2.5 – 5 wt % bio-oil, ~60 wt % gases) and quality at a reforming temperature of 600 °C. In order to understand the properties of products, characterization tests such as ultimate analysis and GC-MS was performed on bio-oil and elemental analysis, BET and SEM were carried out on biochar. The TCR gases had a higher heating value between 12.5 – 12.8 MJ/kg and hydrogen content of 13 – 15 vol %. The produced TCR bio-oil had low water content and high heating value. The high quality of the bio-oil is reflected in the low O/C ratio of 0.15. The TCR biochar from all three woody feedstocks had a high heating value and high carbon content, low O/C and H/C ratio.

The parametric study was conducted for the softwood pellets to observe the effect of reformer temperature (500 – 700 °C), reactor temperature (400 – 550 °C) and biochar pre-filling on the product yield and properties. It was observed that as the

reformer temperature increases to 700 °C, the gas yield increases at the expense of reduction in bio-oil and biochar. The produced bio-oil had lower oxygen and water content, low TAN, and viscosity. The biochar produced had excellent structural and morphological properties. The optimum reactor temperature for the TCR of softwood pellets was found to be 500 °C in terms of both bio-oil quality and yield. The biochar pre-filling had negligible effect on the bio-oil quality and yield.

Keywords

Thermo-Catalytic Reforming; TCR; Bio-oil; Biochar; Biomass; Softwood; Hardwood

PREFACE

This thesis is an original research conducted by the author, Manjot Gill at the University of Alberta, Edmonton, Canada. Most of the experiments and characterizations were conducted at the Department of Chemical Engineering, with elemental analysis conducted at the Department of Chemistry, and the morphology test conducted at the Department of Earth and Atmospheric Sciences.

Dr. Rajender Gupta and Dr. Amit Kumar were the principal advisors on this work and were involved at every step during the research in development of process, implementation, and documentation edits.

Dedicated to my Parents, Husband & Teachers

ACKNOWLEDGEMENTS

I would like to thank my supervisor, Dr. Rajender Gupta for providing me with the opportunity to conduct this research. Without his immense knowledge, and invaluable advice, this research would not have been possible. I would also like to thank Dr. Amit Kumar for his guidance, insightful comments and suggestions that helped broaden and develop the research.

This work would not have been possible without the funding provided by Future Energy Systems, Alberta Economic Development and Trade, Alberta Innovates and WestJet. In addition, I would also like to thank Fraunhofer UMSICHT for the training they provided to operate and maintain the TCR experimental unit.

I am highly thankful to Dr. Vinoj Kurian for providing immense assistance in the lab whenever required in addition to his teachings and valuable suggestions throughout the research. I thank Dr. Kurian for always reviewing my work and providing insightful suggestions for the betterment for my work. I would also like to thank Dr. Deepak Pudasainee for training me to operate TGA, LECO TGA and BET, and for his helpful suggestions regarding experimental process and lab conduct. I thank Dr. Md Khan for his training to operate and build the micro GC experimental setup. I would also like to acknowledge the assistance provided by Nathan Gerein and Gubin Ma to operate SEM. A warm thanks to Bijay Dhakal for helping me with the experimental work, without whom this work would not have been complete on time. I would also

like to acknowledge Wasel-Ur Rahman and Dr. Madhumita Patel for providing suggestions and various discussions related to the experimental work.

I thank Ankit Mathanker and Ananthan Santhanakrishnan for being the best office and lab partners and their involvement in much needed brainstorming to figure out various solutions.

Lastly, I would like to express my deep gratitude to my parents, siblings (Harminder & Gurasis) and husband, Jaspreet Gill, for believing in me and supporting me in this journey.

Table of Contents

Chapter 1 Introduction	1
1.1 Background	1
1.2 Research objectives.....	5
1.3 Thesis outline	6
Chapter 2 Literature Review.....	8
2.1 Biomass.....	8
2.1.1 Cellulose.....	10
2.1.2 Hemi-cellulose.....	11
2.1.3 Lignin	12
2.2 Pyrolysis of biomass	15
2.2.1 Slow Pyrolysis.....	17
2.2.2 Intermediate Pyrolysis.....	18
2.2.3 Fast Pyrolysis.....	19
2.3 Reactor Configuration.....	20
2.3.1 Auger/Screw reactor	21
2.3.2 Pyroformer	22
2.4 Thermo-catalytic reforming (TCR) Technology.....	24
2.4.1 Advantages of TCR over other technologies	27
2.4.2 Summary of TCR experiments	28
Chapter 3 Kinetic study of Biomass Pyrolysis	37
3.1 Biomass Characterization Methods	37
3.1.1 Proximate Analysis	37
3.1.2 Thermogravimetric Analysis	38
3.1.3 Ultimate Analysis.....	40
3.1.4 Heating Value.....	41
3.2 Kinetic Models.....	41
3.2.1 Kissinger-Akahira-Sunose method (KAS).....	43
3.2.2 Flynn-Wall-Ozawa method (FWO)	43
3.2.3 Distributed Activation Energy Model (DAEM)	44

3.3	Results and Discussion	46
3.3.1	Ultimate and Proximate Analysis.....	46
3.3.2	Thermogravimetric Analysis	47
3.3.3	Estimation of kinetic parameters.....	50
Chapter 4	Thermo-Catalytic Reforming of Woody Biomass	55
4.1	Feedstock Preparation & Characterization.....	55
4.2	Lab Scale TCR	57
4.2.1	Experimental Procedure	62
4.2.2	Experimental Plan.....	64
4.3	Product Characterization Methods	65
4.3.1	Bio-oil Characterization.....	66
4.3.2	Produced Gas Characterization	69
4.3.3	Bio-char Characterization.....	71
4.4	Product Yield and Characterization Results.....	73
4.4.1	Biochar Characterization	76
4.4.2	Bio-oil Characterization.....	79
4.4.3	Permanent gas composition and properties	82
4.5	Parametric Study.....	84
4.5.1	Effect of Reforming Temperature.....	84
4.5.2	Effect of Reactor Temperature.....	97
4.5.3	Effect of Biochar Pre-filling	102
Chapter 5	Conclusion and Future Work	106
5.1	Conclusion	106
5.2	Future Work.....	107
References		109
Appendix A		114

List of Figures

Figure 2.1. Biomass Classification based on its existence in nature.....	9
Figure 2.2. Molecular structure of cellulose [20]	10
Figure 2.3. Major types of hemicelluloses in softwoods and hardwoods [20]	12
Figure 2.4. Model structure of spruce lignin [25]	14
Figure 2.5. Structure of coumaryl alcohol (H), coniferyl alcohol (G), and sinapyl alcohol (S)[25]	14
Figure 2.6. Primary mechanisms involved in the conversion of biomass [26]	15
Figure 2.7. Auger/Screw pyrolysis reactor [24].....	22
Figure 2.8. Internal mechanics of a Pyroformer reactor: 106 External Screw Shaft, 108 Internal Screw Shaft, 64 Feed Inlet Pipe, 62,60,52,50 Electrical Heating Bands, 58,56,54 Supports, 88,90 External Screw Slot, 80 External Screw, 70 Internal Screw, 68 Solid drop out pipe, 66 Gas Outlet Pipe [13]	23
Figure 2.9. Experimental set up with a Pyroformer reactor [14].....	24
Figure 2.10. Schematic diagram of the TCR plant [31].	25
Figure 3.1 Proximate Analysis, LECO TGA 701	38
Figure 3.2 Thermogravimetric analyzer SDT Q600, TA Instruments	39
Figure 3.3 CHNS Analyzer	40

Figure 3.4 TGA curves of corn stover, wheat straw and softwood as a function of temperatures at a heating rate of 10 °C/min in nitrogen atmosphere.....	47
Figure 3.5 DTG curves of corn stover, wheat straw and softwood as a function of temperature at a heating rate of 10°C/min in nitrogen atmosphere.....	48
Figure 3.6 TGA curve of softwood at four different heating rates.....	49
Figure 3.7 DTG curve of softwood at four different heating rates	49
Figure 3.8 Linear fit plots to calculate activation energy for pyrolysis of softwood at different conversion degree using KAS model.....	50
Figure 3.9 Linear fit plots to calculate activation energy for pyrolysis of softwood at different conversion degree using FWO model.....	51
Figure 3.10 Activation energy as a function of conversion for FWO, KAS and DAEM models.....	53
Figure 3.11 Experimental and modified DAEM curves for pyrolysis decomposition of softwood at 2, 5 and 10 °C/min	54
Figure 4.1 Feedstock: (a) Hardwood Pellets, (b) Softwood Pellets, (c) Softwood Chips	56
Figure 4.2 Schematic diagram of TCR-2 laboratory plant: (1) Hopper, (2) Screw Conveyer Feeder, (3) Auger Reactor, (4) Reformer, (5) Condensers, (6) Bio-oil Container, (7) Gas Wash Bottle, (8) Filters	58
Figure 4.3 Conical separating funnel: (a) At the end of experiment, (b) After 24 hours into separation	66

Figure 4.4 Mettler Toledo T50 for TAN measurement	67
Figure 4.5 Gas Chromatography Mass Spectroscopy (GC-MS)	69
Figure 4.6 CP-4900 Micro Gas Chromatograph used for gas analysis	70
Figure 4.7 Scanning Electron Microscope Zeiss Sigma 300 VP-FESEM.....	72
Figure 4.8 BET set-up, Quantachrome IQ.....	73
Figure 4.9 Energy flow from the feed to products for different biomass feedstock	76
Figure 4.10 TCR-2 Biochar (a): Hardwood Pellets (b): Softwood Pellets (c): Softwood Chips.....	77
Figure 4.11 Composition of the TCR gases as a function of time throughout the experiment.....	83
Figure 4.12 Product distribution and yield at three different reforming temperatures for a reactor temperature of 450°C	85
Figure 4.13 SEM images of the (a) softwood pellets (b) Biochar (450, 500) (c) Biochar (450, 600) (d) Biochar (450, 700)	89
Figure 4.14 Graphical representation of effect of reforming temperature on the TCR- 2 gases produced from softwood pellets at a fixed pyrolysis temperature of 450 °C	97
Figure 4.15 Influence of reactor temperature on the product yield and distribution at a fixed reforming temperature of 600 °C	98
Figure 4.16 Influence of reactor temperature on the composition of the TCR bio-oil at a fixed reformer temperature of 600 °C	101

Figure 4.17 Influence of reactor temperature on the TCR gas composition at a fixed reforming temperature of 600 °C.....	102
Figure 4.18 Influence of biochar pre-filling on the product yield at a reactor temperature of 450 °C and a reformer temperature of 500 °C	103
Figure 4.19 Influence of biochar pre-filling on the product yield at a reactor temperature of 450 °C and a reformer temperature of 600 °C	103
Figure 4.20 Influence of biochar pre-filling on the gas composition at a reactor temperature of 450 °C and a reformer temperature of 500 °C	104
Figure 4.21 Influence of biochar pre-filling on the gas composition at a reactor temperature of 450 °C and a reformer temperature of 600 °C	105
Figure 4.22 Composition of the TCR gases as a function of time throughout the experiment in the presence and absence of pre-existing biochar bed (solid line: presence of biochar pre-filling, dotted line: absence of biochar pre-filling).....	105

List of Tables

Table 2.1: Ultimate analysis and proximate analysis for different biomass feed stocks used in the TCR technology.....	32
Table 2.2: Operating conditions and product streams (wt %) for different TCR experiments.....	33
Table 2.3: Bio-oil composition and physical properties from different TCR experiments.....	34
Table 2.4: Gaseous products compositions and physical properties from different TCR experiments.....	35
Table 2.5: Biochar compositions and physical properties from different TCR experiments.....	36
Table 3.1 Ultimate and proximate analysis of different biomass feedstocks.....	46
Table 3.2 Calculated activation energy for pyrolysis of softwood using FWO and KAS models.....	52
Table 4.1 Ultimate and proximate analysis of different TCR biomass feedstocks ...	57
Table 4.2 Experiments performed on TCR-2.....	65
Table 4.3 Product yield of TCR-2 products (Mass Balance)	74
Table 4.4 Characterization of the TCR-2 biochar produced from woody feedstock	78
Table 4.5 Characterization of the TCR-2 bio-oil produced from woody feedstock .	79
Table 4.6 Summarized GC-MS analysis results for TCR bio-oil produced from different woody biomass feedstocks	81

Table 4.7 Composition of the TCR gases produced from different woody feedstocks at a pyrolysis temperature of 450 °C and a reforming temperature of 600 °C	82
Table 4.8 Post-Reforming Reactions identified in the Reformer by Neumann, Meyer [37].....	84
Table 4.9 Characterization of the TCR-2 biochar produced from woody feedstock at different reforming temperatures	87
Table 4.10 BET surface area, pore volume and average pore radius for softwood pellets biochar at different reformer temperatures	90
Table 4.11 Characterization of the TCR-2 bio-oil produced from woody feedstock at different reforming temperatures	91
Table 4.12 Summarized GC-MS results for bio-oil produced at different reforming temperatures.....	93
Table 4.13 Detailed GC-MS results for the bio-oil produced at different reforming temperatures.....	93
Table 4.14 Composition of the TCR-2 gases produced from softwood pellets at different reforming temperatures at a fixed pyrolysis temperature of 450 °C.....	96
Table 4.15 Characterization of TCR biochar at different reactor temperatures and a fixed reforming temperature of 600 °C.....	100
Table 4.16 Characterization of TCR bio-oil at different reactor temperatures and a fixed reforming temperature of 600 °C.....	100

List of Acronyms

TCR – Thermo-Catalytic Reforming
CHP – Combined Heat and Power
DP – Degree of polymerization
TGA – Thermogravimetric Analysis
DTG – Derivative thermogravimetric
KAS – Kissinger-Akahira-Sunose method
FWO – Flynn-Wall-Ozawa method
DAEM – Distributed Activation Energy Model
GC-MS – Gas chromatography mass spectroscopy
SEM – Surface electron microscopy
BET – Brunauer-Emmett-Teller
HHV – Higher Heating Value
LHV – Lower Heating Value
TAN – Total Acid Number
PAH – Poly aromatic hydrocarbon
MAH – Mono aromatic hydrocarbon
MSW – Municipal solid waste
O/C – Oxygen to carbon ratio
H/C – Hydrogen to carbon ratio
GHG – Greenhouse gas emissions
AD – Anaerobic digestion

Chapter 1

Introduction

1.1 Background

The modern economic sector still uses large amount of energy produced from conventional energy sources, i.e. fossil fuels, which includes coal, petroleum, and natural gas. Fossil fuels still accounts for 19 % of total energy production [1], because they are cheap, convenient, reliable, available, stable, abundant, and have an economic benefit and high calorific value. However, the use of fossil fuels has an adverse effect on the environment. In 2017, the oil and gas sector accounted for 27 % of total emissions, as reported by Government of Canada [2]. There has been an 84 % increase in total GHG emissions from oil and gas sector from 1990 till 2017 [2]. One of the strategies for GHG emissions reduction is replacement of fossil fuels with renewable energy sources. Therefore, it is crucial to explore alternative energy sources, such as renewable sources.

The primary sources of renewable energy are wind, hydro, solar, geothermal, and biomass. Canada is one of the world leaders in the production and use of energy from renewable sources. According to the data published by Natural Resources Canada [1], 67 % of Canada's energy is produced from renewable sources. Hydro has the highest share of generation at 60 % and the remaining 7 % is produced from

other non-hydro renewables [1]. Biomass only makes up 1.8 % of Canada's energy generation [1].

Lignocellulosic biomass is the most abundant renewable resource in existence and is the only source of renewable fixed carbon. In Canada, there are 347 million hectares of forest, an estimated 9% of the world's forests [3]. With proper harvesting practices and land use planning, these forests can be used as a resource for biofuels. In Western Canada, more than 27 million tonnes of agricultural residue are available, after the removal of the straw used for soil conservation and livestock feeding and bedding. These lignocellulosic feedstocks are good candidates for the production of renewable energy. The main sources of lignocellulosic biomass are forest residues, agricultural residues, animal manure, sewage sludge and by-products. Energy produced from this source is promising because it does not contribute to extra CO₂ emissions and it reduce our dependence on fossil fuels. Currently, lignocellulosic biomass use is limited because of its low heating value and low product yield per unit area of biomass compared to fossil fuels.

Historically, consumption of biomass was very important for home energy use, as Canadians burned wood for heating and cooking. While some households still use wood as a primary or secondary source of heat, the percentage has declined to less than 5 per cent, as other sources of energy have taken precedence (namely oil, hydroelectricity and natural gas) [4]. Recently, due to increasing concern over the

environment, there has been growing interest in production of green and sustainable energy from renewable sources, such as biomass.

There are many existing conversion technologies for biomass conversion to biofuels, such as, combustion, pyrolysis, gasification, torrefaction, hydrothermal liquefaction, and anaerobic digestion. Pyrolysis of biomass for biofuels production has been studied extensively over the past 25 years and it is still a current topic for research. Pyrolysis of biomass converts the solid feedstock to liquids (bio-oil), gases, and a solid (biochar) product. Pyrolysis is generally classified into three type: slow, intermediate, and fast pyrolysis based on the heating rates and the feedstock residence time. These process parameters cause significant differences in terms of the product distribution of biochar, non-condensable gas, and liquids (aqueous and organic phase). There have been extensive studies done on slow and fast pyrolysis of different types of biomass [5-9], but the studies done on intermediate pyrolysis are scant [10-14]. The intermediate pyrolysis operates at relatively moderate temperatures ($\sim 400-500$ °C), moderate heating rates ($1-2$ °C/s) and the feedstock residence time is in the range of approximately 5-15 minutes and the vapor residence time in the range of seconds.

Even though, biomass fast pyrolysis is one of the cheapest route towards renewable liquid fuels, its commercialization poses multi-scale challenges, such as, characterization of feed, products and reaction intermediates at molecular scales, and understanding the complex reaction network taking place in different reaction

configurations [15]. In addition, the crude pyrolysis oil is not immediately usable due to undesirable properties, such as, low energy content, and highly corrosive nature due to high oxygenates content. Therefore, it needs to be upgraded and fractionated to desired specifications [15]. Currently, many researchers are focusing on further development of fast pyrolysis process, but not enough attention is being given to intermediate pyrolysis.

In this study, the intermediate pyrolysis is of interest, as it produces fuels with higher energy density than that of the original biomass, which makes them easier to transport and store, and to produce on-demand energy and heat in combined heat and power (CHP) units. Fraunhofer UMSICHT has implemented a thermo-catalytic reforming (TCR) process in a patented TCR[®] reactor [16]. This technology is based on intermediate pyrolysis and subsequent post-reforming of pyrolysis products into a hydrogen rich syngas, biochar with similar properties to that of anthracite coal, and bio-oil with significantly improved physical and chemical properties. The presence of catalytic reforming of pyrolysis products is the key difference from other existing technologies. Due to the catalytic reforming of pyrolysis products at high temperatures (600-750 °C), the produced bio-oil is of superior quality compared to fast pyrolysis bio-oil. The TCR bio-oil has much higher energy content, low oxygen content, viscosity, and total acid number (TAN), thus resulting in improved flow characteristics as well as making the fuel less corrosive.

The TCR reactor has not been implemented in Canada as of till date. So, this study focuses on implementing the TCR reactor in Canadian weather conditions using the available Canadian biomass feedstocks.

1.2 Research objectives

The novel contribution of this research is in the area of renewable fuel production from lignocellulosic biomass feedstocks. The aim of this research is to assess the use of Canadian lignocellulosic biomass to produce and store energy in the form of bio-oil, biochar and hydrogen-rich syngas, which will help mitigate GHG emissions.

The TCR experiments will be carried out in a laboratory-scale 2 kg/h plant using several Canadian biomass feedstocks such as, hardwood pellets, softwood pellets and softwood chips. The specific objectives of this research are to:

1. Perform thermogravimetric study to understand the pyrolysis kinetics and thermochemical properties of four Canadian lignocellulosic biomass (Corn Stover, Wheat Straw, and Softwood chips).
2. Optimize the operating conditions for the thermo-catalytic reforming of lignocellulosic biomass using laboratory-scale TCR-2 unit.

Special attention is given to the effect of the following operating parameters on product yield and quality:

- Reforming temperature (500 – 700 °C)
- Reactor temperature (400 – 550 °C)

- The effect of biochar pre-filling (Part of the biochar produced from previous experiments is added to the reformer to create a biochar bed for catalytic action from the beginning of the experiment) will also be investigated.
3. Characterization of various TCR products (syngas, bio-oil and biochar) will be performed in terms of chemical composition, morphology and physical properties to optimize the operating conditions.

1.3 Thesis outline

This thesis consists of five chapters. The following description outlines each chapter in this thesis:

The **first chapter** briefly introduces the renewable fuels, technologies, and overall objectives of this research.

The **second chapter** reviews in detail the available literature on the biomass characteristics and pyrolysis of biomass. This chapter discusses the different types of pyrolysis, reaction mechanism, and available reactor configurations for pyrolysis of biomass. This chapter also introduces the thermo-catalytic reforming (TCR) technology and reviews in detail the available literature on thermo-catalytic reforming (TCR) technology.

The **third chapter** investigates the pyrolysis kinetics and thermochemical properties of the feedstock using a thermogravimetric analyzer. The **fourth chapter**

contains the experimental details and the results obtained from all the TCR experiments. The experimental details include the description of TCR reactor, feed preparation and the analytical methods used to characterize the feedstock and produced products. The results include mass and energy balance, and product analysis. This chapter also investigates the effect of different operating conditions on the product yield and quality.

Finally, the **fifth chapter** provides the outcomes obtained in this study and future work that needs to be done.

Chapter 2

Literature Review

2.1 Biomass

Biomass is the total mass of living matter. Biomass is a generic term for the plant (phytomass) and animal (zoomass) biomass. The term biomass is used for all organic materials, which are combustible in nature, mainly plant and animal origin present in land and aquatic environments. Plants produce biomass continuously by the process of photosynthesis [17]. Biomass stores solar energy in the chemical form, and it is the most versatile resources on earth. Unlike fossil fuels, biomass is a renewable energy resource that is available in abundant wherever there is plant growth and production. Biomass can be classified according to Panwar [18] and it is presented in Figure 2.1. It can be grouped as [18]:

- i. Agricultural and forestry residues: silviculture crops.
- ii. Herbaceous crops: weeds, Napier grass.
- iii. Aquatic and marine biomass: algae, water hyacinth, aquatic weeds, plants, sea grass beds, kelp, and coral reef, etc.
- iv. Waste: municipal solid waste, municipal sewage sludge, animal waste and industrial waste, etc.

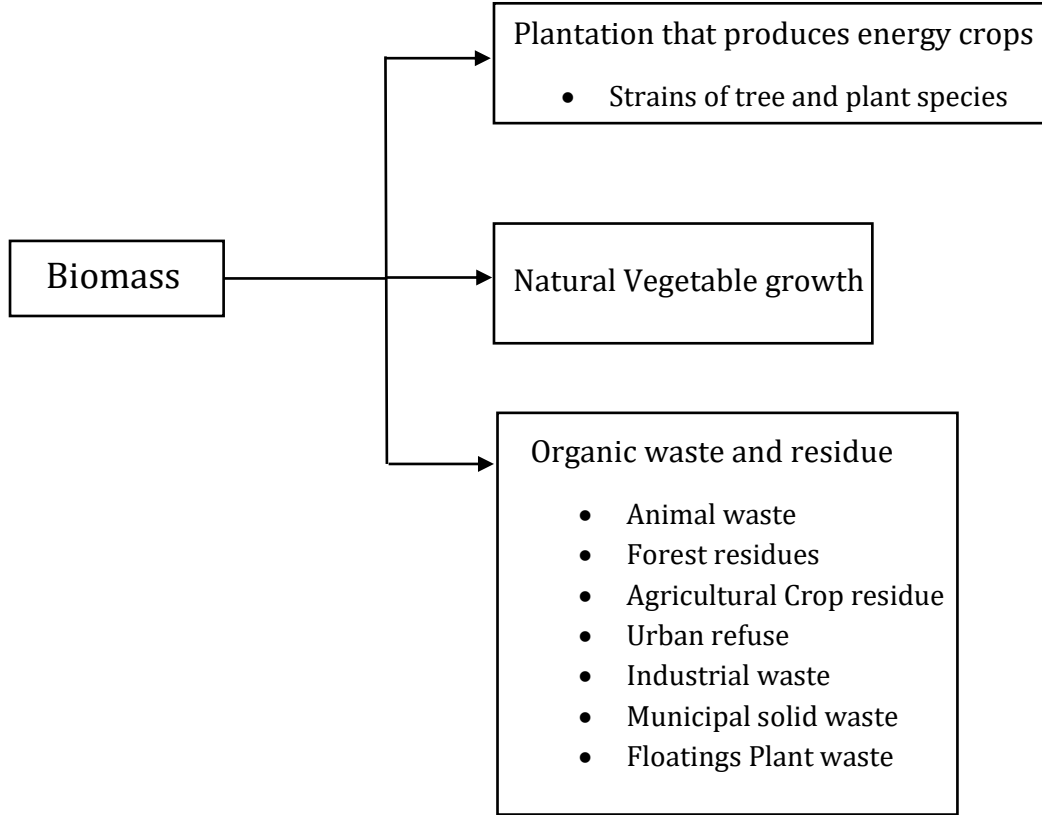


Figure 2.1. Biomass Classification based on its existence in nature

The conversion of biomass to solid and liquid fuels depends upon the chemical composition and physical properties of the biomass. The three main components of biomass are cellulose, hemi-cellulose and lignin. Other than these three components, biomass also contains trace amounts of extractives and inorganic components. The chemical and physical properties of the biomass depend on the amounts of cellulose, hemi-cellulose, and lignin in the biomass. The proportion of these components varies depending on the biomass type. Normally, biomass

contains 40-60 wt % of cellulose, 20-40 wt % of hemicellulose and 10-25 wt % of lignin on dry basis [19].

2.1.1 Cellulose

Cellulose is the most abundant organic polymer present in the cell walls of the plant cells. Cellulose is a linear homopolysaccharide built up of β -D glucopyranose units covalently linked with 1 \rightarrow 4 glycosidic bonds, with an average molecular weight of 100,000 [20]. Each glucose unit is inverted with respect to its neighbors, and the resulting disaccharide repeat occurs hundreds of times in a single cellulose molecule. Generally, biomass contains around 40 – 60 % of the cellulose. Figure 2.2 shows the molecular structure of cellulose.

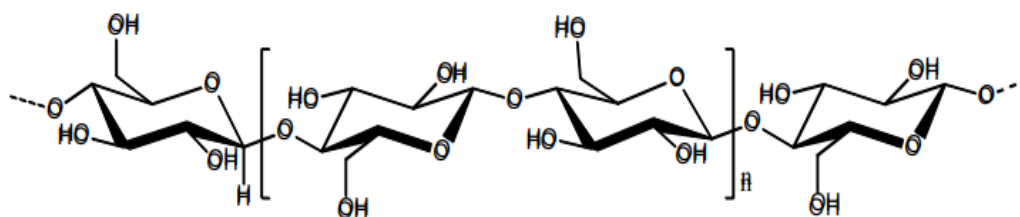


Figure 2.2. Molecular structure of cellulose [20]

The cellulose chain has hydrophilic sides and is hydrophobic on its end. The cellulose chains adhere to one another to form crystalline material, known as microfibril through intermolecular hydrogen bonding [21]. Microfibrils are connected and held together by cross-linking glycan molecules to form fibers. Due to the highly organized structure and the intermolecular hydrogen bonds, cellulose has a relatively high degree of crystallinity averaging 50-70% [20]. The fibrous structures and the strong hydrogen bonding also gives cellulose a high tensile

strength and makes the fibers insoluble in most solvents [22]. Cellulose polymers have a high degree of polymerization (DP) of 500 – 15000 [23].

2.1.2 Hemi-cellulose

Hemicelluloses are complex polysaccharides present in the cell wall, which consist of branched structures that varies with the type of biomass. Hemicellulose surrounds the cellulose fibers and serves as a connecting link between cellulose and lignin [24]. Unlike cellulose, which is a homopolysaccharide, hemicellulose is a heteropolysaccharide. Hemicellulose is composed of two or more monomer units, mainly hexoses (D-glucose, D-mannose, D-galactose) and pentoses (D-xylose, L-arabinose) [21]. In contrast to cellulose, hemicellulose polymers are short with a DP of 50-200 [23]. Most of the hemicelluloses in the cell walls is non crystalline [23]. Figure 2.3 shows some of the major hemicelluloses found in softwood and hardwood.

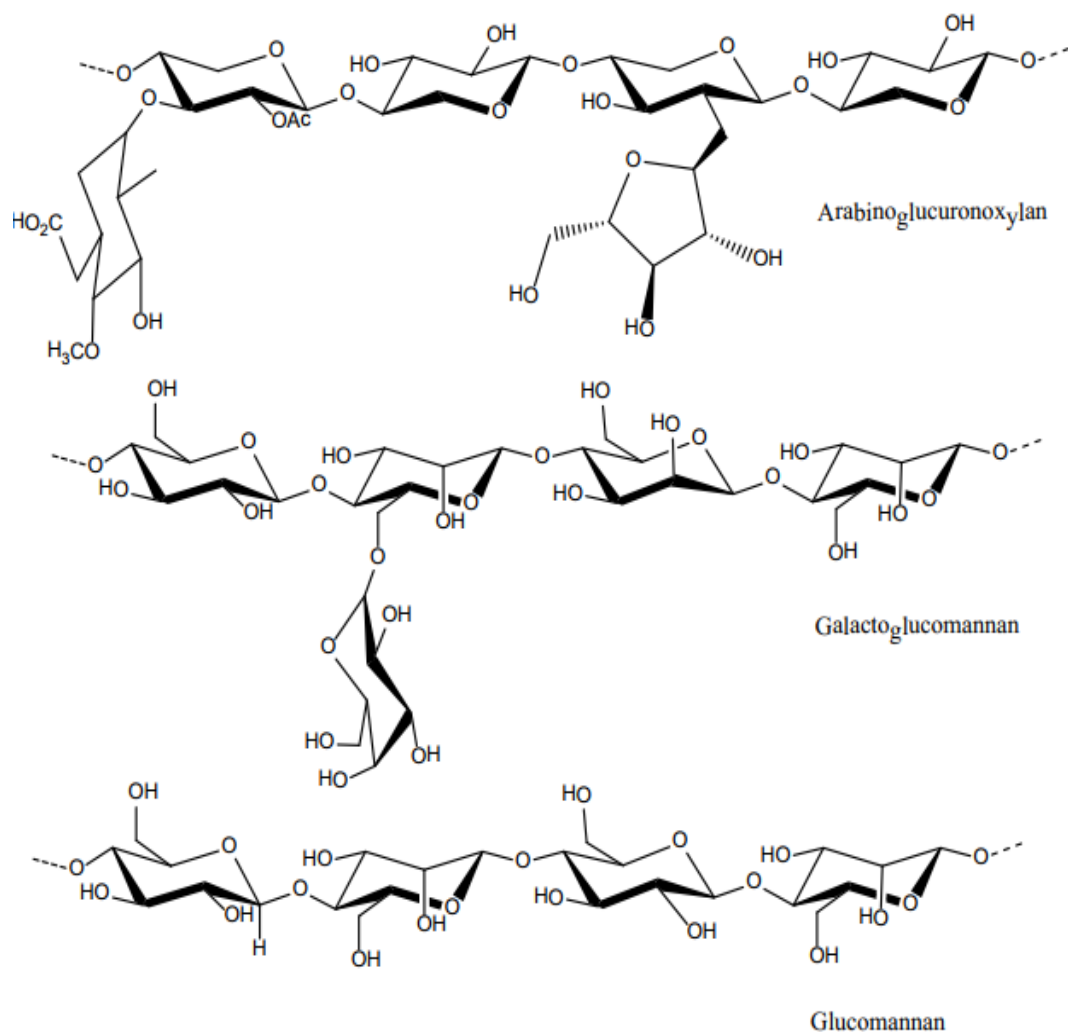


Figure 2.3. Major types of hemicelluloses in softwoods and hardwoods [20]

2.1.3 Lignin

Lignin is the second most abundant biomass component and is distinctly different from cellulose and hemicellulose. Lignin is an aromatic, three dimensional and cross-linked phenol polymer (Figure 2.4) that consists of a non-regular arrangement of three monolignols [21, 24]. These three monolignols are coumaryl alcohol (H), coniferyl alcohol (G), and sinapyl alcohol (S) [25]. The proportions of

these three monolignols distinctly differ in every plant depending on the plant species and its geographic location. Lignin is mainly located in the outer layer of the fibers and provides the structural rigidity by holding the polysaccharide fibers together. Physically, lignin fills up the empty spaces between the cellulose microfibrils coated with hemicellulose, thus playing a binding role between hemicellulose and cellulose within the cell wall [24]. The percentage of lignin may vary from 23-33 % in softwoods to 16-25% in hardwoods [24]. Figure 2.5 indicates the structure of the three monolignols of lignin. Hardwoods mainly compose of coniferyl alcohol and sinapyl alcohol, whereas the main monolignol in softwood is coniferyl alcohol along with minor amounts of coumaryl alcohol [21]. Since, coniferyl alcohol and sinapyl alcohol are methoxylated, it results in higher methoxyl content in hardwoods compared to softwoods.

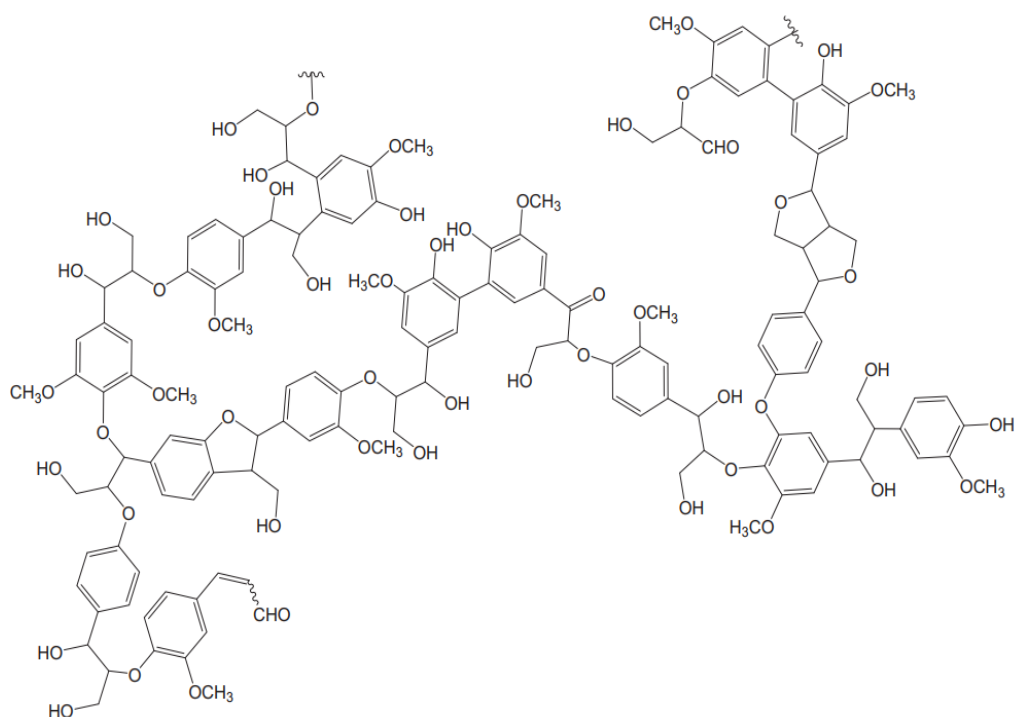


Figure 2.4. Model structure of spruce lignin [25]

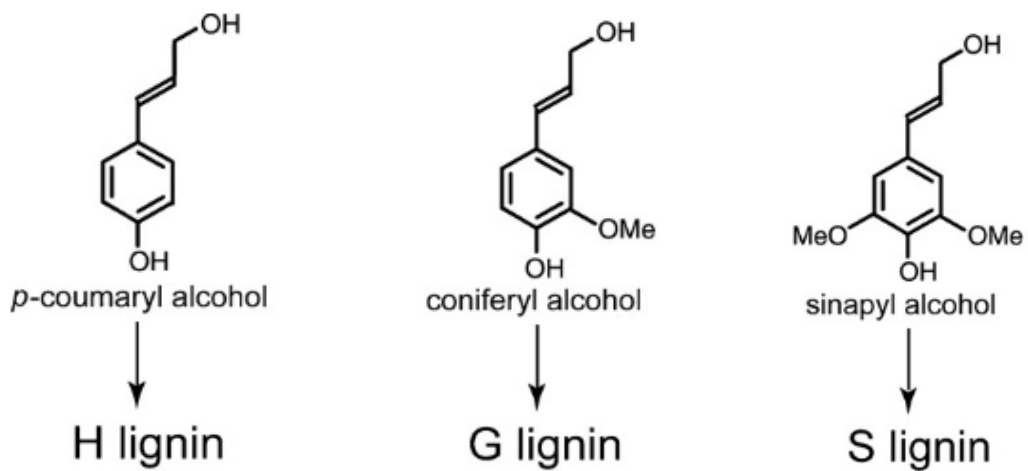


Figure 2.5. Structure of coumaryl alcohol (H), coniferyl alcohol (G), and sinapyl alcohol (S)[25]

2.2 Pyrolysis of biomass

Pyrolysis is a thermochemical process that is able to convert biomass to liquids (bio-oil), gases, and solid (biochar) products. It is the chemical decomposition of carbon-based materials through the application of heat in the absence or near absence of oxygen. The solid, liquid, and gaseous product yields are influenced by the conditions of pyrolysis. The mechanism behind pyrolysis can be defined by the superposition of three primary mechanisms (i.e. char formation, depolymerization and fragmentation) (Figure 2.6), and of secondary mechanisms [26].

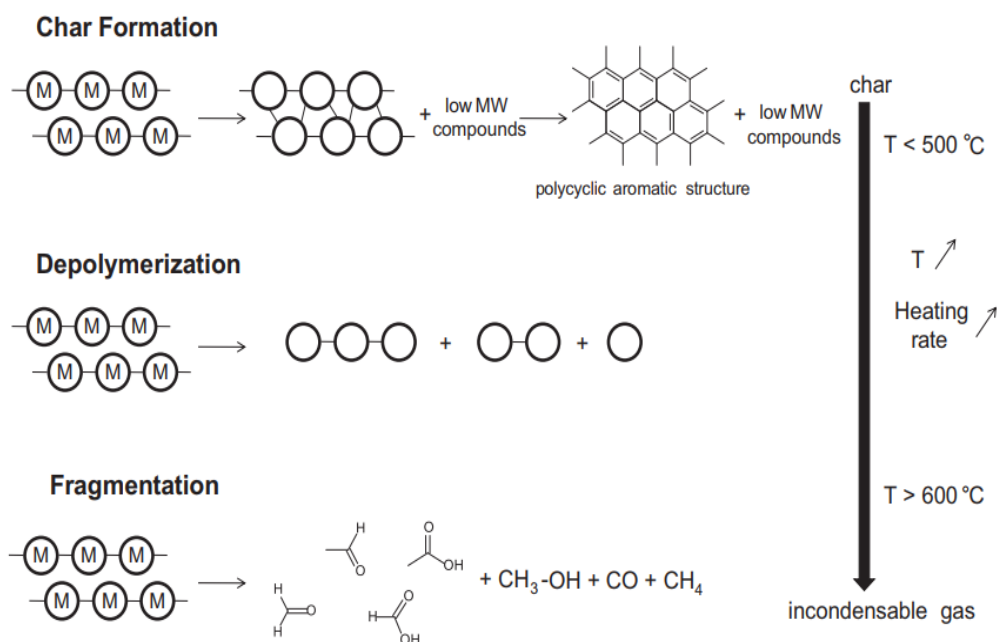


Figure 2.6. Primary mechanisms involved in the conversion of biomass [26]

Char formation: Char is a solid residue and has an aromatic polycyclic structure [26]. It is primarily carbon ($\sim 85\%$), but it also contains some oxygen and hydrogen [27]. It is formed by the intra- and intermolecular rearrangement reactions which

gives the char higher degree of reticulation and thermal stability [26]. The main step in the char formation is the formation of benzene rings and the re-arrangement of these rings to form polycyclic structures. Char formation is usually favored at lower temperatures and lower heating rates. Biochar can be used for soil applications, such as soil amendment or as an agent for soil remediation, carbon sink, and improving water quality [8].

Depolymerization: The breaking of the bonds between the monomer units in the biomass polymer is called as depolymerization. Depolymerization is favored by higher heating rates. As the bonds rupture, two new chains are formed and these chain ends undergo stabilization reactions [26]. This results in a decrease in the degree of polymerization of the chain until the produced molecules become volatile. The condensable molecules formed are often found in the liquid fraction of the products in the form of derived monomer, dimer or trimer [26].

Fragmentation: Fragmentation results in the formation of non-condensable gas by the linkage of many covalent bonds of the biomass polymer, even within the monomer units [26]. This also leads to the formation of small chain organic compounds, which can be condensed at ambient temperatures. Higher the pyrolysis temperature, more the non-condensable gas fraction of the products.

Pyrolysis can be classified based on the heating rate, residence time of biomass and the temperature. Therefore, pyrolysis can be classified into following three categories:

- i. Slow Pyrolysis
- ii. Intermediate Pyrolysis, and
- iii. Fast Pyrolysis

Each type of pyrolysis process can deal with different types of biomass, but often the shape and the moisture content of the biomass are very critical in deciding between different pyrolysis processes. Finely ground and dry biomass is used in fast pyrolysis, whereas the intermediate pyrolysis is able to process larger particles (pellets and chips) and biomass with moisture content of up to 40 %. Slow pyrolysis is more tolerant to the moisture content in the feedstock and can also handle sizes as large as logs of wood. The liquid, gas and biochar produced from different pyrolysis processes have very different qualities and will be discussed in depth in the next section.

2.2.1 Slow Pyrolysis

Slow pyrolysis is a batch process, which is carried out at low temperatures, slow heating rates, and for longer residence times. Slow pyrolysis of lignocellulosic biomass mostly produces biochar and gaseous products. Slow pyrolysis occurs at lower temperatures (300 – 550 °C) and heating rates (0.01 – 80 °C/min), and has a longer vapor residence time (that can last minutes, hours or even days) [21]. The primary aim of the slow pyrolysis process is the production of char. For example, carbonization is the oldest form of slow pyrolysis, and has been in use for thousands of years. Carbonization involved heating of the wood in the absence of oxygen to a

temperature of 400 °C over an extended period, which used to be several days in ancient times to maximize the char formation. The vapors are usually not condensed in this process but can be used for providing heat directly or indirectly to the process. Torrefaction is another slow pyrolysis process in the temperature range of 225-300 °C in the absence of oxygen. It is a mild pyrolysis process, which improves the energy density of biomass, reduces its oxygen-to-carbon ratio, and reduces its hygroscopic nature [27]. The torrefaction process removes CO_2 and H_2O from the biomass, resulting in lower oxygen-to-carbon and hydrogen-to-carbon ratio of the biomass. During this process the biomass dries and partially devolatilizes, which decreases its mass while preserving its energy content [21]. The most common example of torrefaction is the process of roasting coffee beans. As the green beans are heating from 200-300 °C, the surface of the beans darkens. It also modifies the structure of the biomass, making it more brittle, which is caused by the depolymerization of hemicellulose. As mentioned before, the energy density of the biomass increases, which is due to the relatively higher reduction in mass compared to the lower reduction in the energy content of the biomass.

2.2.2 Intermediate Pyrolysis

Intermediate pyrolysis takes place at moderate heating rates (100-500 °C/min), temperature range of 350-550 °C and a solid residence time of several minutes, up to 10 minutes [10]. The vapor residence times are very much dependent on the reactor type and are in the range of 2-4 seconds. Due to the lower heating rates

compared to fast pyrolysis (1000 °C/min), there is lower tar formation due to more controlled reactions taking place rather than the thermal cracking of the biomass [10]. In recent years, there have been many developments in the intermediate pyrolysis process and significant amount of work is being done to enhance the production of high-grade bio-oil. Yang, Brammer et al. (2014) studied the intermediate pyrolysis of wood and barley straw pellets for producing sustainable liquid, gaseous and solid fuels [14]. The bio-oil yields obtained were 34.1 wt % and 12.0 wt % for wood and barley straw respectively [14]. Both feedstocks produced similar char yield of about 30 wt %, and gas yield of approximately 20 wt % [14]. Some of the common technologies used in the intermediate pyrolysis are haloclean rotary kiln, pyroformer and a hot gas filtration unit [10].

2.2.3 Fast Pyrolysis

In the fast pyrolysis process, biomass is treated at high temperatures of 500 - 1000 °C, with high heating rates of ~1000 °C/min, and short hot vapor residence time of 0.5-5 s. The short hot vapor residence times are typically less than 2 s to minimize secondary reactions [5]. According to literature review, fast pyrolysis of wood typically produces a maximum yield of 60-75 wt % of liquid bio-oil, 15-25 wt % of solid char, and 10-20 wt % of non-condensable gases [5, 18]. Onay, Beis [28] studied the fast pyrolysis of rapeseed in a well-swept fixed bed reactor and reported an oil yield of 68 % at a final pyrolysis temperature of 550 °C, and a heating rate of 300 °C/min. In other experiment, Onay and Kockar [7] studied the effects of pyrolysis

temperature, heating rate, particle size and sweep gas flow rate on the pyrolysis product yields and their chemical compositions. Onay and Kockar [7] reported an oil yield of 36.8 % at pyrolysis temperature of 400 °C, which increased to a maximum value of 63.1 % at a final pyrolysis temperature of 550 °C, and increasing the temperature further to 700 °C, the oil yield decreases to 57.5 %. Fast pyrolysis of biomass has been studied in many different reactor configurations. Some of the reactor configurations used in the fast pyrolysis are bubbling fluid beds, circulating fluid beds, ablative pyrolysis, and rotating cone technology [6].

2.3 Reactor Configuration

The design of the pyrolysis reactor is one of the key factors in determining the product distribution, both qualitatively and quantitatively. The essential features of the pyrolysis reactors are the high heat transfer, moderate and carefully controlled temperature, and rapid cooling and quenching of the pyrolysis vapors, while providing simple process operation and the potential for scale-up. Some of the traditional reactor configurations that have been used for slow and fast pyrolysis are as follows: Fixed bed reactor, Fluidized bed reactor, Ablative reactor, and Rotating cone configuration.

In fixed bed reactors, the biomass material travels downwards by gravity while being thermally decomposed into biochar, bio-oil, and gaseous products by gasifying agents such as air, steam, or oxygen. Fluidized bed reactors are partly filled with bed material (mostly sand) and additives. The heat is supplied by heating the

walls of the reactor and by injecting the hot fluidizing gas at the bottom of the reactor. Ablative reactors involve “melting” or “thermal erosion” of biomass, where the feedstock particles are pressed against the reactor wall and the heat is transferred from the hot surface to the feedstock particles to “melt” the biomass particle. The rotating cone reactors are used to produce bio-oil from biomass with negligible char formation [29]. Biomass particles and the heat carrier particles (sand) are fed near the bottom of the rotating cone, where the particles are mixed together and transported upwards by the rotating action of the cone. The particles remain close to the wall and experience a high heating rate.

The reactor configurations commonly used in the intermediate pyrolysis are explained in detail in the following section.

2.3.1 Auger/Screw reactor

Auger (or screw) reactor (Figure 2.7) consists of a helical screw rotating in an enclosed tubular shell. The solid biomass is conveyed through the reactor by the rotating screw, while the heat required for pyrolysis is transported along the tubular wall of the reactor. The speed of the screw can be changed accordingly to control the residence time of the biomass in the reactor. Thus, the screw serves two purposes: firstly, it mixed the feed particles and secondly, it controls the residence time of the solids in the reactor.

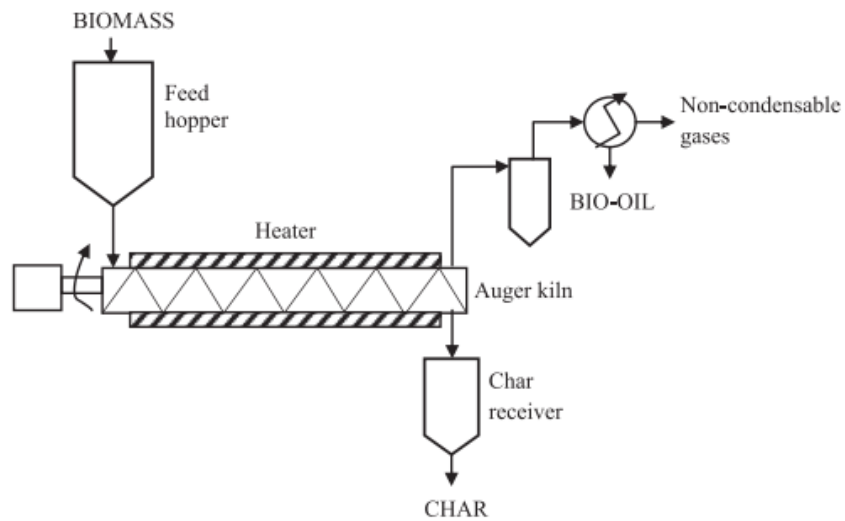


Figure 2.7. Auger/Screw pyrolysis reactor [24].

2.3.2 Pyroformer

The Pyroformer consists of a horizontal carbon steel vessel with two co-axial rotating screws [14]. The inner screw conveys the mixture of fresh feedstock and char forward through the reactor and the outer screw returns a portion of the char backwards for recycle (Figure 2.8). This ensures a good mixing of the feedstock with the hot char, which acts both as a heat carrier and as a catalyst aiding in the secondary cracking reactions of pyrolysis vapors. This results in the production of more permanent gases (H_2 and CO), lower molecular weight condensable organics, and less heavy tars. Both screws are driven by electric motor and the electrical heaters heat the reactor to reach the desired reaction temperature.

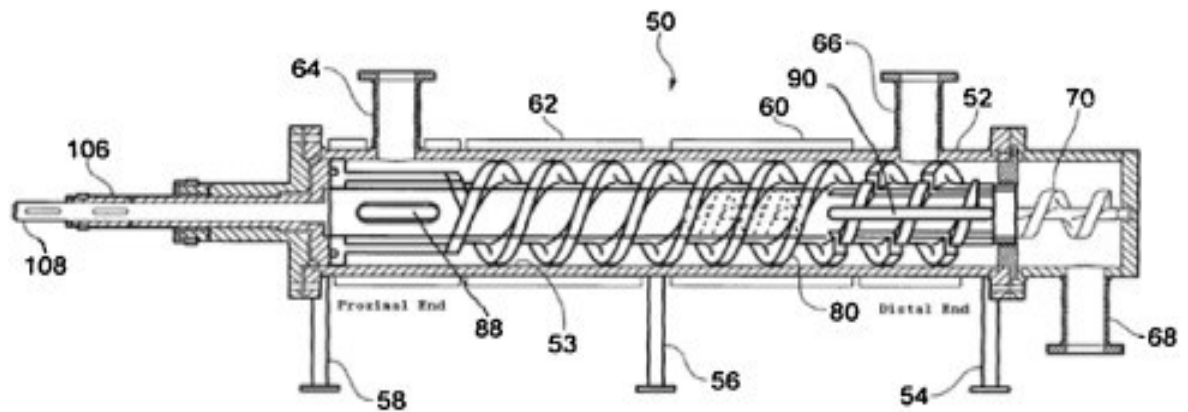


Figure 2.8. Internal mechanics of a Pyroformer reactor: 106 External Screw Shaft, 108 Internal Screw Shaft, 64 Feed Inlet Pipe, 62,60,52,50 Electrical Heating Bands, 58,56,54 Supports, 88,90 External Screw Slot, 80 External Screw, 70 Internal Screw, 68 Solid drop out pipe, 66 Gas Outlet Pipe [13]

The pyroformer unit set up is shown in Figure 2.9. The set up usually comprises of a screw feeder, pyroformer reactor, hot gas filter candles, shell and tube water-cooled condensers and an electrostatic precipitator. The screw feeder continuously feeds fresh biomass to the pyroformer. The pyrolysis vapors leaving the pyroformer pass through hot gas filter candle to ensure the removal of entrained char and ash particulates. The filtered vapors are then condensed in the condensers to form bio-oil and the remaining permanent gases pass through the electrostatic precipitator for aerosol removal.

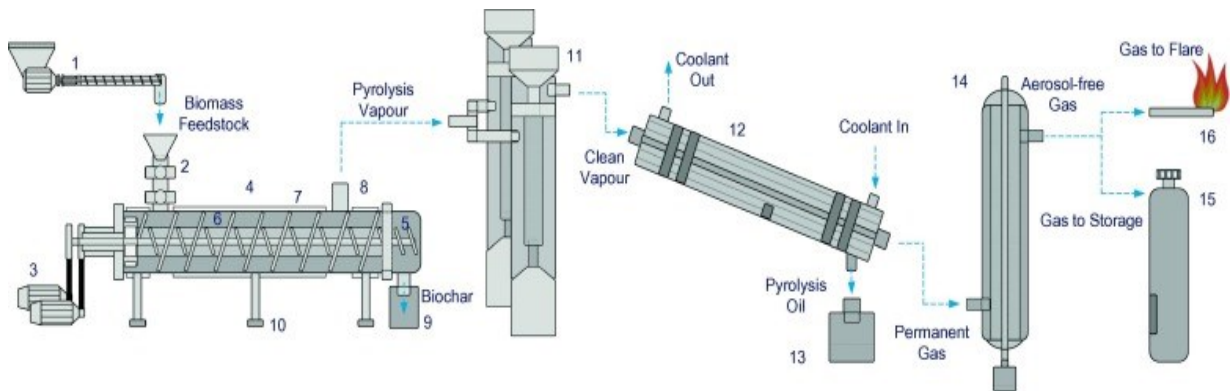


Figure 2.9. Experimental set up with a Pyroformer reactor [14].

2.4 Thermo-catalytic reforming (TCR) Technology

Several technologies have been developed for the conversion of biomass/organic waste to fuels and chemicals or liquid fuels or intermediates that can be used for fuel production. One of the key pathways is to convert biomass/organic waste directly to a dense liquid, generally known as bio-oil, through thermo-chemical conversion or conventional pyrolysis. Although there are several conventional pyrolysis-based bio-oil technologies in various stages of development, a challenge with most of these bio-oils is their properties. Bio-oil produced from existing technologies has low pH and high viscosity and is typically unstable over time. These properties have a key impact on the overall feasibility and economics of the use of biomass-based feedstock for the conversion to fuels and chemicals. These properties need to be improved in order for bio-oil to be used in the production of fuels and chemicals.

The TCR technology was developed at Fraunhofer UMSICHT in Sulzbach-Rosenberg, Germany in 2013. The TCR technology converts solid biomass to high quality energy in a multi-stage thermal process. The TCR technology is based on the intermediate pyrolysis and subsequent downstream post-reforming of pyrolysis products into a hydrogen rich syngas, bio-char with similar properties to anthracite coal, and a bio-oil with significantly improved physical and chemical properties [30]. The catalytic reforming of the pyrolysis products at elevated temperatures (500–750 °C) is the key difference from the other existing technologies. A schematic diagram of the process involved in the TCR technology is illustrated in Figure 2.10.

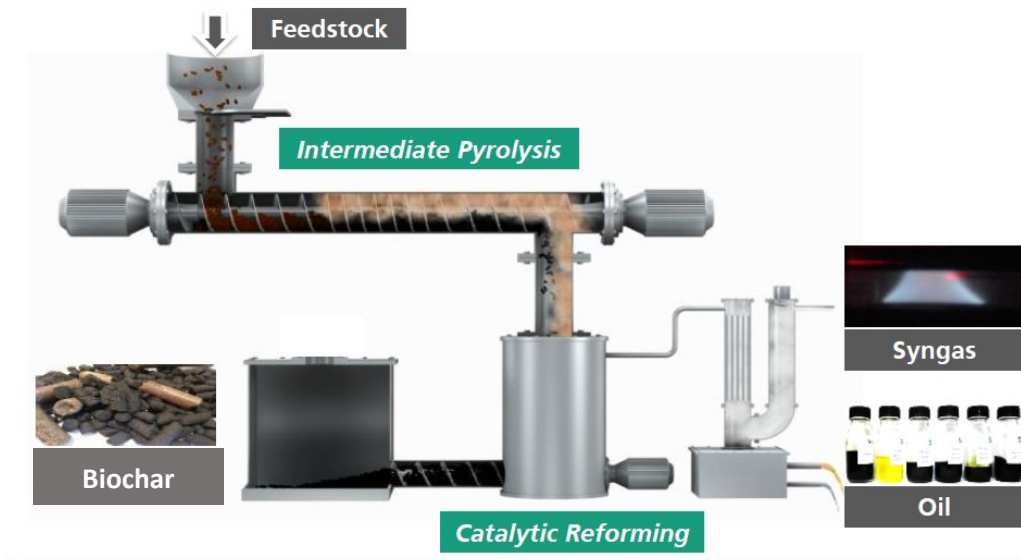


Figure 2.10. Schematic diagram of the TCR plant [31].

The TCR technology consists of two consecutive reactors that are externally heated using electric heaters. The first reactor is a horizontal tubular auger type reactor followed by a vertical fixed bed reactor for additional reforming of the pyrolysis

products at elevated temperatures. The two reactors are connected in series and all the reactions are carried out in the complete absence of oxygen. The unique feature of the TCR technology is the partial internal recycling of the solid bio-char. The horizontal screw reactor has two coaxial rotating screws. The purpose of the first screw is to move the feedstock through the reactor, whereas the second screw serves two purposes: mixing and recycling. The recycling and the mixing of the biochar with dried feedstock is achieved by the unique design of the middle screw. A small portion of biochar is moved back along the reactor to mix with the fresh dried feedstock.

The whole system using TCR technology mainly consists of feed hopper, TCR reactors (auger screw reactor and fixed bed reformer), condensing unit, filtration system and a gas analyzer. The intermediate pyrolysis occurs at varying temperatures between 400 – 600 °C depending on the feedstock followed by post reforming happening at elevated temperatures between 500 – 750 °C. The average residence time of the feedstock varies between 5 min and 10 min [32-41].

Fraunhofer UMSICHT has successfully tested the TCR technology at a 2 kg/h unit level (further referred to as TCR-2) in the city of Sulzbach-Rosenberg, Germany, and is currently operating a unit with a capacity of 30 kg/h (TCR-30), and a unit with a capacity of 300 kg/h (TCR-300). The major difference between the TCR-2 and TCR-300 is the heating of the TCR reactors. The TCR-2 and TCR-30 reactors are electrically heated, whereas the TCR-300 reactors are heating by the burning of

propane gas. Experiments have been carried out using several feedstock such as municipal solid waste (MSW) [40], sugarcane bagasse [32], co-form rejects [38], pulper rejects [39], wheat husk [42], digestate [35-37] and woodchips [33].

2.4.1 Advantages of TCR over other technologies

The advantages of TCR compared to other technologies are that it produces low oxygenated high-energy dense liquids that are easily transportable and storable, energy dense chars and hydrogen rich synthesis gas. The TCR technology can be applied for all kind of residues with HHV higher than 8 MJ/kg and a water content up to 70 wt% [37]. The TCR can process biomass with high ash and moisture content and low ash melting points.

The quality of the TCR bio-oils is very different from other pyrolysis bio-oils. Neumann, Jäger [36] investigated the conversion of TCR liquids from digestate as a feedstock for subsequent hydrocarbon production. The generated bio-oil had a molar O/C ratio of 0.09 [36], whereas the bio-oils produced from other intermediate pyrolysis technologies had a molar O/C ratio in the range of 0.29-0.31 [13, 41, 43]. The TCR bio-oil has higher carbon content at 77.6 wt% [36] compared to pyroformer bio-oil at 62.6 wt% [14]. The TCR bio-oil had other outstanding properties as well, such as low water content of 2.2 wt% and low total acid number (TAN) of 2.1mgKOH g⁻¹ [36]. Furthermore, the TCR bio-oil produced had low viscosity of 4.43mm²s⁻¹, which is comparable to common biofuel like biodiesel (3.5-5mm²s⁻¹) [36]. The TCR bio-oils have high stability compared to bio-oils produced

from other pyrolysis technologies. Approximately 80% of the TCR bio-oil was distillable at atmospheric pressure and 350 °C, forming a highly viscous vacuum oil fraction and low viscosity distillate fraction. The bio-oil produced from TCR is completely miscible with biodiesel at all compositions and has been successfully utilized in diesel engine already [44]. The TCR fuel produced from sewage sludge was successfully used for test drive in vehicles without any further engine modifications [45].

Furthermore, the biochar from TCR is of interest as a potential fertilizer and soil conditioner in agricultural as well as garden and landscape applications. It can also be used as a filter for water, air and gas purification [46]. TCR char can be used to substitute the char used in barbeque, which is obtained from tropical forests [46]. Additionally, it can also be used as a catalyst for several chemical and biochemical conversion processes. For example, in TCR trials, biochar obtained was used as a catalyst in the reformer to obtain products with even better quality.

2.4.2 Summary of TCR experiments

Ouadi, Jaeger [40] explored the thermo-catalytic reforming of municipal solid waste in a 2 kg/h continuous pilot scale TCR reactor (TCR-2). The intermediate pyrolysis occurred at 450 °C and the catalytic reforming at 700 °C. The results indicated a yield of 19 wt% of aqueous phase, 6 wt % of organic phase bio-oil, 44 wt% of syngas, and a 31 wt% of bio-char. The bio-oil had a higher heating value (HHV) of 38 MJ/kg, oxygen content <7 wt% and water content <4 wt%.

Ouadi, Greenhalf [38] investigated the thermo-catalytic reforming of co-form rejects (waste cleansing wipes). The intermediate pyrolysis and reforming took place at 450 °C and 700 °C, respectively. The co-form reject pellets were successfully converted into 12 wt% bio-oil, 9 wt% aqueous phase liquid, 8 wt% char, and 71 wt% syngas. The bio-oil had an HHV of 39.36 MJ/kg, which is comparable to biodiesel. In addition, the oxygen and water content in the bio-oil was very low at 3.90 and 0.1 wt% respectively, which also contributed towards higher HHV.

Conti, Jäger [30] explored the thermo-catalytic reforming of biomass waste streams (digestate, sewage sludge, paper sludge, and wood chips) in a TCR-2 reactor. The intermediate pyrolysis was conducted at 400 °C and the post catalytic reforming at 700 °C. The bio-oil produced from all different biomass waste streams had a high HHV (35 -38 MJ/kg), despite the type of biomass used.

Jäger, Conti [33] evaluated the thermo-catalytic reforming of three different woody biomass (pruning olive trees, evergreen oak trees, and vine) in a 2 kg/h laboratory-scale plant. The results revealed that, at the reforming temperature of 700°C, the composition of biomass had only a minor effect on the composition and characterization of the products. The gases produced from all three biomass types had high hydrogen content at 33-36 vol % and had high HHV between 14.6 – 14.9 MJ/kg. The bio-oil produced was of very high quality; depicted by its low O/C ratio of 0.15 ± 0.04 , low water content, low TAN, and high HHV. The author concluded that

quality of bio-oil produced from fast pyrolysis is only comparable to TCR oil after additional intense hydro-deoxygenation treatment.

Ouadi, Greenhalf [39] investigated the thermal conversion of pre-treated pulper reject waste using a TCR-2 reactor. The results showed a conversion of approximately 40 % of the original feedstock energy into solid and liquid energy vectors, and over 30% of the energy converted into the gas products. The study showed that the TCR technology was able to tolerate high plastic content in the feedstock and produced liquid fuel analogue to the fossil fuels. The bio-oil produced was comparable to that of bio-oil produced using MSW waste by Ouadi, Jaeger [40]. The most abundant components in the bio-oil were oleic acid methyl ester (18.90 %) and naphthalene (16.23 %). Overall, the TCR technology proved a promising route for pulper rejects to produce energy vectors.

Neumann, Meyer [37] demonstrated the TCR technology using digestate as feedstock. In this study, the post reformer temperature was varied between 500-750°C to achieve optimized fuel products. The results revealed that, with the increase in the reformer temperature at 750°C, there was increase in hydrogen rich permanent gases, and the bio-oil produced was highly deoxygenated with significantly improved fuel physical properties, low viscosity, and TAN.

Santos, Ouadi [42] studied the conversion of wheat husk into fuels using the TCR technology in a 2 kg/h continuous pilot scale reactor. The bio-oil obtained had high heating value (HHV) of 26 MJ/kg, compared to the original feedstock with HHV of

17.8 MJ/kg. The TAN and viscosity of the bio-oil was reported as 29.9 mg KOH/g and 145.2 cSt, which was considerably higher compared to the other TCR oils. However, this could be contributed to the type of feedstock and the lower reforming temperature of 600°C compared to other experiments carried out at 700-750°C. The author concluded that the wheat husk oil could be used as a direct engine oil, if upgraded via hydro-processing; or blended with crude oil for further refining.

Table 2.1 – Table 2.5 shows details of the experiments that have been carried out using TCR technology by Fraunhofer UMSICHT.

Table 2.1 and Table 2.2 lists the biomass type, operating conditions, and the product yields for the specific experiment. The results of these experiments in terms of product characterization are listed in Table 2.3, Table 2.4 and Table 2.5

Biomass Type	Ultimate Analysis of Feedstock (wt %)						Proximate Analysis of Feedstock (wt %)					References
	C	H	N	S	O (a)	H ₂ O	Ash	Volatiles	Fixed Carbon	Moisture	HHV (MJ/kg)	
MSW	45	6.4	0.3	0.1	47.7	8	0.6				17.8	[30]
Digestate stream	34.8	4.3	1.9	0.4	43.8	11	14.8				16.9	[30]
Digestate (from AD plant)	41.6	5.1	1.6	0.3	31.6	d.b.	8.7	53.6	26.6	11.1	17.1	[35]
MSW	43.1	6.1	1	0.3	31.4	d.b.	18.1	68.5	13.4	10	18.3	[40]
Digestate (from AD plant)	51.8	6.3	2.8	0.6	38.5	d.b.	17.9	46.3	20.8	15	14	[37]
Olive (OL)	44.9	6.5	0.4	0.06	46	d.b.	2.16			8.7	19.3	[33]
Evergreen Oak (EO)	44.2	6.3	0.5	0.04	45.4	d.b.	3.6			10	19.6	[33]
Vine shoots (VS)	47.8	6.2	0.6	0.05	41.2	d.b.	4.08			7.6	19.2	[33]
Co-form Rejects	58.9	6.1	0.4	0.2	30.2	d.b.	4.1	82.7	7.7	5.5	20.4	[38]
Pulper Rejects	53.3	7.5	0.5	<0.1	29.6	d.b.	8.8	73.5	10.1	7.6	22.9	[39]
Wheat Husk	42	6.3	1.9	<0.1	47.4	d.b.	2.3	71.4	19.3	7	17.8	[42]

Table 2.1: Ultimate analysis and proximate analysis for different biomass feed stocks used in the TCR technology.

n/d: not disclosed; d.b.: dry basis

Biomass Type	Operating Parameters					Product Streams (wt %)					References
	Mass Flow of feedstock (kg/h)	Pyrolysis Temperature (°C)	Reformer Temperature (°C)	Heating Rate (°C/s)	Residence Time (minutes)	Bio-Oil	Gaseous Products	Biochar	Aqueous Phase	Ash	
MSW	2	400	700	2	5	4.23	62.7	14.67	18.66	---	[30]
Digestate stream	2	400	700	2	5	5.78	31.81	39.9	23.11	---	[30]
Digestate (from AD plant)	1.6	400	500	---	5	11	27	36	26	---	[35]
	1.6	400	550	---	5	10	32	33	25	---	
	1.6	400	600	---	5	9	34	33	24	---	
	1.6	400	700	---	5	8	41	31	20	---	
	1.6	400	750	---	5	6	44	29	21	---	
MSW	2	450	700	1	10	6	44	31	19	--	[40]
Digestate (from AD plant)	1.6	450	NR	1	5	11.69	18.18	22.08	29.87	17.92	[37]
	1.6	450	500	1	5	12.99	20.26	20	29.09	17.66	
	1.6	450	750	1	5	3.64	35.84	15.84	25.71	17.66	
Olive (OL)	2	400	700	0.83 - 5	12	3.9	60	20.48	16.09	---	[33]
Evergreen Oak (EO)	2	400	700	0.83 - 5	12	2.93	58.05	22.44	17.07	---	[33]
Vine shoots (VS)	2	400	700	0.83 - 5	12	4.88	58.05	23.41	14.63	---	[33]
Sugarcane bagasse	2	400-500	NR	1.5	---	---	24.6	32	39.3 (b)	---	[32]
	2	400-500	500	1.5	---	---	34.8	27.24	33.85 (b)	---	
	2	400-500	600	1.5	---	---	42.8	25.29	31.12 (b)	---	
	2	400-500	700	1.5	---	---	57.39	23.56	19.56 (b)	---	
Co-form Rejects	2	350 - 450	700	1	several minutes	12	71	8	9	---	[38]
Pulper Rejects	2	450	700	1	<10	8	53	24	15	---	[39]
Wheat Husk	1.4	430	600	1	5-10	5.8	29.6	21.7	32.8	---	[42]

Table 2.2: Operating conditions and product streams (wt %) for different TCR experiments

(a): calculated by difference, d.b: dry basis, NR: Not reforming (b): include oil + water (Ahmad, E., et al. (2018) only specified an oil composition varying between 17-21wt %)

Biomass Type	Pyrolysis Temperature (°C)	Reformer Temperature (°C)	Bio-oil Composition (wt %) and physical properties (dry basis)										References
			C	H	N	S	O (a)	H2O	Ash	HHV (MJ/kg)	TAN (mg KOH/g)	viscosity (cSt)	
MSW	400	700	73.2	8	1.5	0.3	17	9.5	< 0.05	35.3	5.4	---	[30]
Digestate stream	400	700	75.8	7.4	6	1.9	8.9	3.9	< 0.05	35.6	4.9	---	[30]
Digestate (from AD plant)	400	500	---	---	---	---	---	---	---	---	---	---	[35]
	400	550	---	---	---	---	---	---	---	---	---	---	
	400	600	---	---	---	---	---	---	---	---	---	---	
	400	700	---	---	---	---	---	---	---	---	---	---	
	400	750	76.6	7.7	2.2	0.6	11.2	1.7	< .05	33.9	4.9	40	
MSW	450	700	83.7	7.5	1.8	0.2	6.7	3.2	< 0.05	38.2	2.9	6.5	[40]
Digestate (from AD plant)	450	NR	75.1	7.6	4.9	1.2	10.6	< 2	0.6	34.4	23.7	n.d.	[37]
	450	500	78	8.3	5.2	1.2	7	< 2	0.2	36.7	8.8	n.d.	
	450	750	79.6	7	5.2	1.1	7	< 2	0.1	35.2	5.1	40	
Olive (OL)	400	700	75.2	7.4	2.2	0.3	14.9	8.2	<0.05	33.6	9.3		[33]
Evergreen Oak (EO)	400	700	72.2	7	2.6	0.3	17.9	6	<0.05	32.8	14.6		[33]
Vine shoots (VS)	400	700	78.6	7.2	2.5	0.3	11.4	8.4	<0.05	35.5	30.1		[33]
Sugarcane bagasse	400-500	NR	59.9	7.4	0.9	0.2	31.6	28.8	<0.1	21.1	12.4		[32]
	400-500	500	53.7	9.7	1.1	0.3	35.2	25.6	<0.1	24.3	11.1		
	400-500	600	71.4	5.4	1.3	0.1	21.8	7.2	<0.1	28.8	12.3		
	400-500	700	80	7.9	1.7	0.2	10.2	2.6	<0.1	33.9	16.1		
Co-form Rejects	350 - 450	700	87.6	8.11	0.27	0.05	3.8	0.1	0.1	39.26	0.78	1.66	[38]
Pulper Rejects	450	700	84.2	7.86	0.52	0.13	7	0.2	0.1	40.17	38.49	2.44	[39]
Wheat Husk	430	600	56.3	7.8	4.8	1.4	29.7	<1.0	<.001	26	29.9	145.2	[42]

Table 2.3: Bio-oil composition and physical properties from different TCR experiments.

Biomass Type	Pyrolysis Temperature (°C)	Reformer Temperature (°C)	Gas Composition (vol %)						Non traceable (a)	HHV (MJ/Nm ³)	References
			H ₂	CH ₄	CO	CO ₂	C _x H _y				
MSW	400	700	24.6	12.27	20.46	21.17	1.6	21.5	---	[30]	
Digestate stream	400	700	33.45	8.19	14.94	23.13	2.31	20.29	---	[30]	
Digestate (from AD plant)	400	500	8.9	12.24	20.51	48.67	---	---	---	[35]	
	400	550	23.44	10.91	16.2	36.89	---	---	---		
	400	600	28.33	6.95	13.39	29.71	---	---	---		
	400	700	32.93	4.88	19.36	24.19	---	---	---		
	400	750	34.13	6.89	15.51	23.1	---	---	---		
MSW	450	700	36	14	12	21	6	11* (N ₂)	17.23	[40]	
Digestate (from AD plant)	450	NR	7	6	43	40	---	4	9.7	[37]	
	450	500	21	5	14	40	---	20	13.1		
	450	750	37	3	12	28	---	20	14.4		
Olive (OL)	400	700	33.16	11.58	15.79	27.37	1.58	10.52		[33]	
Evergreen Oak (EO)	400	700	35.26	11.58	16.84	27.89	0.53	7.9		[33]	
Vine shoots (VS)	400	700	35.4	11.58	15.26	26.32	1.05	10.39		[33]	
Sugarcane bagasse	400-500	NR	6.6	17.9	46.3	35.2	2.8		12.55	[32]	
	400-500	500	11.29	19.5	33.65	32.21	2.4	0.72	13.76		
	400-500	600	20.91	14.42	29.08	27.04	2.16	6	15.29		
	400-500	700	28.7	12.5	22.59	24.27	1.923	10	16.17		
Co-form Rejects	350 - 450	700	13.04	13	12.25	3.1	5	53.61	11.02	[38]	
Pulper Rejects	450	700	29.33	0.0	7.4	11.68	5	46.59	---	[39]	
Wheat Husk	430	600	19.4	12.3	26.4	26.9	3.6	11.4	20.6	[42]	

Table 2.4: Gaseous products compositions and physical properties from different TCR experiments.

Biomass Type	Pyrolysis Temperature (°C)	Reformer Temperature (°C)	Char composition (wt %) and physical properties								References
			C	H	N	S	O (a)	H ₂ O	Ash	HHV (MJ/kg)	
MSW	400	700	84.9	1.7	0.4	0.1	9.8	0.3	3.2	30.6	[30]
Digestate stream	400	700	48.3	2	1.5	0.3	0.1	0.6	47.8	17.5	[30]
Digestate (from AD plant)	400	500	---	---	---	---	---	---	---	---	[35]
	400	550	---	---	---	---	---	---	---	---	
	400	600	---	---	---	---	---	---	---	---	
	400	700	---	---	---	---	---	---	---	---	
	400	750	65	1.2	1.5	0.3	2.2	0.7	29.1	23.9	
MSW	450	700	47.3	0.8	1	0.3	5.7	1.6	44.9	17	[40]
Digestate (from AD plant)	450	NR	72.5	6.1	3	0.5	17.9	3.3	35.8	16.7	[37]
	450	500	83.7	4.7	2.7	0.5	8.4	2.1	38.4	18.9	
	450	750	92.2	5	2.1	0.7	0	2.2	41.6	17.3	
Olive (OL)	400	700	84.2	1.2	0.8	0.1	1.5	0.4	12.2	30.3	[33]
Evergreen Oak (EO)	400	700	78.1	1.2	0.9	0.1	1.6	0.4	18.1	27.3	[33]
Vine shoots (VS)	400	700	70.8	1	0.9	0.1	0.7	0.6	23.1	25.5	[33]
Sugarcane bagasse	400-500	NR	63.63	1.31	0.55	0.21	1.84	d.b	32.46	222.1	[32]
	400-500	500	67.9	1.6	0.52	0.51	-1.03	d.b	30.5	24	
	400-500	600	65.84	0.87	0.48	0.04	0.2	d.b	32.57	23.1	
	400-500	700	64.47	0.7	0.54	0.03	2.11	d.b	32.15	21.2	
Co-form Rejects	350 - 450	700	83.9	1.66	0.49	0.06	1.9	d.b	11.9	30.79	[38]
Pulper Rejects	450	700	66.7	1.68	0.45	0.12	4.94	d.b.	26.1	25.16	[39]
Wheat Husk	430	600	76.5	2.2	3.3	0.1	6.1	d.b.	11.8	28.4	[42]

Table 2.5: Biochar compositions and physical properties from different TCR experiments

Chapter 3

Kinetic study of Biomass Pyrolysis

The following chapter investigates the pyrolysis kinetics and thermochemical properties of three different types of lignocellulosic biomass using a thermogravimetric analyzer. In addition, the kinetic study was also conducted to assess different kinetic models for biomass being a mixture of components with different activation energies. The three selected biomass feedstocks are corn stover, wheat straw, and softwood chips. These feedstocks were collected from nearby farm areas located in Northern Alberta.

3.1 Biomass Characterization Methods

3.1.1 Proximate Analysis

The proximate analysis of the biomass feedstock was conducted in LECO TGA 701 (Figure 3.1) to determine the percentages of moisture, volatile, fixed carbon, and ash using ASTM D7582. Approximately 1 g of prepared samples were placed in the ceramic crucibles and for accuracy all the experiments were repeated three times. The moisture content was measured in the nitrogen atmosphere at 107 °C until constant mass was achieved and the percentage moisture was calculated from the loss of mass in the sample (ASTM E1756-08) [47]. The volatiles and the fixed carbon were measured by heating up the same sample till 900 °C in nitrogen atmosphere,

with a heating rate of 40 °C/min and a holding time for 15 minutes. The ash content was measured in the same experiment by lowering the temperature to 500 °C and then heating up to 575±25 °C, in an oxygen atmosphere. The ash content was then determined by the calculation from the mass of residue remaining at the end of heating period.



Figure 3.1 Proximate Analysis, LECO TGA 701

3.1.2 Thermogravimetric Analysis

The thermogravimetric analysis experiments were carried out using SDT Q600, TA instrument (New Castle, DE, USA) (Figure 3.2). To maintain pyrolysis conditions, high-purity nitrogen was used as carrier gas at a constant flow rate of 45 mL/min throughout the run. About 10 mg of prepared biomass samples were placed in the

alumina crucible and for accuracy all the experiments were repeated three times. The biomass samples were prepared by grinding the supplied feedstock to less than 1 mm using a grinder and sieved through mechanical screens ranging from a mesh size of 2 mm to less than 0.125 mm. The particle size chosen for these TGA experiments was 0.425 – 1 mm. For all feedstocks, thermogravimetric analyses were performed at three different heating rates: 2, 5, and 10 °C/min. The temperature used for the decomposition study ranges from room temperature to 900 °C. At the end of all the experiments, the isothermal condition was maintained for 15 minutes. During the experiments, weight loss was monitored with temperature and time in a nitrogen-controlled atmosphere. A Type R thermocouple was used to monitor the temperature in the thermogravimetric analyzer. The mass loss data and derivative thermogravimetric (DTG) curves obtained from the TGA instrument was analyzed using TA instruments Universal Analysis 2000 software.



Figure 3.2 Thermogravimetric analyzer SDT Q600, TA Instruments

3.1.3 Ultimate Analysis

The prepared sample for feedstock, biochar and bio-oil were analyzed in the Chemistry laboratory, University of Alberta for CHNS analysis (Figure 3.3). The oxygen content was determined by the difference (Equation 1).

$$O (wt\%) = 100 - \sum CHNS (wt \%) + Ash(wt \%) \quad \text{Equation 1}$$

The C, H, N analysis was carried out according to ASTM E777 and ASTM E778. The sulfur content was measured according to ASTM E775. The experiments were carried out in a Carlo Erba EA1108 Elemental Analyzer.



Figure 3.3 CHNS Analyzer

3.1.4 Heating Value

The higher heating value HHV (MJ/kg) was determined using the unified correlation for fuels developed by Channiwala and Parikh [48] where C, H, S, O, N and A are carbon, hydrogen, sulfur, oxygen, nitrogen and ash weight fraction respectively, see (Equation 2):

$$\text{HHV} \left(\frac{\text{MJ}}{\text{kg}} \right) = 0.3491 (C) + 1.1783(H) + 0.1005(S) - 0.1034(O) - 0.0151(N) - 0.0211(A) \quad \text{Equation 2}$$

The lower heating value (LHV) is calculated by Equation 3[49] with hydrogen content determined by CHNS and the moisture content.

$$\text{LHV} \left(\frac{\text{MJ}}{\text{kg}} \right) = \text{HHV} \left(\frac{\text{MJ}}{\text{kg}} \right) - 2.441(m_{H_2O} + 9 * m_H) \quad \text{Equation 3}$$

Where, m_{H_2O} = mass of water, and m_H = mass of hydrogen

3.2 Kinetic Models

The decomposition of biomass into volatiles and char in the absence of oxygen can be illustrated by Equation 4.



The global kinetics of the biomass pyrolysis reaction can be described by Equation 5:

$$\frac{d\alpha}{dt} = k(T) * f(\alpha) = A * \exp\left(-\frac{E}{RT}\right) * f(\alpha) \quad \text{Equation 5}$$

where, α is the extent of reaction (conversion), t is the time (min), $k(T)$ is the rate constant of the reaction (s^{-1}), and $f(\alpha)$ is the function of the reaction mechanism, A is the pre-exponential factor (s^{-1}), E is the apparent activation energy (kJ mol^{-1}), R is the gas constant ($8.314 \text{ J K}^{-1}\text{mol}^{-1}$), and T is the absolute temperature (K)

The extent of reaction, α , is defined by Equation 6:

$$\alpha = \frac{m_i - m_t}{m_i - m_f} \quad \text{Equation 6}$$

where m_i and m_f are initial and final mass of the sample (kg), and m_t is the actual mass at time t (kg).

The mathematical expression for the reaction model, $f(\alpha)$ is represented by Equation 7:

$$f(\alpha) = (1 - \alpha)^n \quad \text{Equation 7}$$

where n is the order of the reaction. For this study n was considered to be 1.

The substitution of Equation 7 in Equation 5 results in Equation 8 which is the fundamental expression used to calculate the kinetic parameters for solid state decomposition reactions.

$$\frac{d\alpha}{dt} = A * \exp\left(-\frac{E_a}{RT}\right) (1 - \alpha) \quad \text{Equation 8}$$

For non-isothermal thermogravimetric experiments at the linear heating rate $\beta = dT/dt$, Equation 8 can be revised as follows:

$$\frac{d\alpha}{dT} = \frac{A}{\beta} * \exp\left(-\frac{E_a}{RT}\right) * (1 - \alpha) \quad \text{Equation 9}$$

The non-isothermal methods for kinetic analysis can be broadly classified into two groups: model-fitting and model-free (iso-conversional). For this study, we will look into three different kinetic models: Kissinger-Akahira-Sunose method, Flynn-Wall-Ozawa method, and distributed activation energy model.

3.2.1 Kissinger-Akahira-Sunose method (KAS)

Kissinger-Akahira-Sunose [50-52] developed an iso-conversional linear integral method to determine the activation energy (E_a), based on the following equation [53, 54].

$$\ln\left(\frac{\beta}{T^2}\right) = \ln\left(\frac{AR}{g(\alpha)E_a}\right) - \frac{E_a}{RT} \quad \text{Equation 10}$$

where $g(\alpha)$ is the integral function of the conversion and is constant at a fixed conversion.

For a constant value of conversion (α), the values of $\ln\left(\frac{\beta}{T^2}\right)$ at different heating rates are plotted against corresponding $1/T$ values. The activation energy (E_a) can then be calculated from the slope of straight-line plots.

3.2.2 Flynn-Wall-Ozawa method (FWO)

The FWO method was derived by Joseph Flynn, Leo Wall, and Takeo Ozawa and the final equation [55] is described by Equation 11. This method is also an integral iso-

conversional model-free method, where activation energy is assumed to vary with the increase in conversion.

$$\ln\beta = \ln\left(\frac{AE_a}{Rg(\alpha)}\right) - 5.331 - 1.0516 \frac{E_a}{RT} \quad \text{Equation 11}$$

where $g(\alpha)$ is the integral function of the conversion and is constant at a fixed conversion.

The plot of $\ln\beta$ versus $1/T$, at a fixed conversion for different heating rates helps in evaluating the activation energy from the slope of the straight-line plots. This calculated activation energy is named apparent activation energy since it is the sum of chemical reactions and physical processes that occur during conversion.

3.2.3 Distributed Activation Energy Model (DAEM)

The distributed activation energy model assumes that the pyrolysis of a complex fuel is carried out as the first-order decomposition of many different chemical groups, where the decomposition of each group is characterized uniquely by its activation energy [56]. The complexity of the fuel is such that a continuous distribution of activation energies is assumed where the mass of volatile material with activation energies between the initial activation energy and the activation energy at some point in time can be related as a function of activation energy and time [57]. The mathematical expression was shown by Scott, Dennis [57] as follow:

$$M_v(t) = \int_0^\infty m(E, t) dE \quad \text{Equation 12}$$

Where $M_v(t)$ the total mass of the volatile matter at time t , and E is the activation energy.

The final equation for the DAEM was given by Scott, Dennis [57] as follow:

$$\frac{M_v(t)}{M_{v0}} = \int_0^\infty g(E) * e^{(-A(E) * \int_0^t \exp(-\frac{E}{RT}) dt)} dE = \int_0^\infty g(E) * \psi(E, t) dE \quad \text{Equation 13}$$

Where M_{v0} is the initial mass of the volatile matter, $\psi(E, t)$ is the double exponential term, and $g(E)$ is the activation energy distribution.

There have been numerous approximations to solve the closed form of the double integral term in the DAEM (Equation 13), to reduce the complexity of the model. One of the modifications was presented by Scott, Dennis [57], which led to the development of modified DAEM.

The modified DAEM proposes that the reactions in a complex solid fuel occur in parallel and assumes that at each fractional conversion, a single reaction is dominant. For two different heating rates, at a fixed conversion, it is assumed that the i^{th} reaction is the only reaction taking place at this conversion. This led to the development of Equation 14 by Scott, Dennis [57], which provides an easier and faster way for calculating Activation Energy as compared to traditional DAEM.

$$\frac{1}{\beta_1} \left[T_0 e^{\left(-\frac{E_i}{RT_0}\right)} - \frac{E_i}{R} \int_{\frac{E}{RT_0}}^\infty \frac{e^{-u}}{u} du - T_1 e^{-\frac{E_i}{RT_1}} + \frac{E_i}{R} \int_{\frac{E}{RT_1}}^\infty \frac{e^{-u}}{u} du \right] = \frac{1}{\beta_2} \left[T_0 e^{\left(-\frac{E_i}{RT_0}\right)} - \frac{E_i}{R} \int_{\frac{E}{RT_0}}^\infty \frac{e^{-u}}{u} du - T_2 e^{-\frac{E_i}{RT_2}} + \frac{E_i}{R} \int_{\frac{E}{RT_2}}^\infty \frac{e^{-u}}{u} du \right] \quad \text{Equation 14}$$

The TGA data for two different heating rates was used to calculate the activation energy from Equation 14 using the MATLAB software.

3.3 Results and Discussion

3.3.1 Ultimate and Proximate Analysis

The ultimate and proximate analysis was performed for all three biomass types: corn stover, wheat straw and softwood according to the methods listed in Section 3.1. The analysis results are listed below in Table 3.1.

Table 3.1 Ultimate and proximate analysis of different biomass feedstocks

	Corn Stover	Wheat Straw	Softwood
Ultimate Analysis (dry basis) (wt %)			
Carbon	41.5	42.24	48.52
Hydrogen	5.6	5.69	6.04
Nitrogen	1.2	0.76	<0.1
Sulfur	0.05	0.03	0
Oxygen (a)	50.25	51.08	45.45
Proximate analysis (wt %)			
Volatiles	76.32	75.4	77.45
Fixed carbon	17.62	18.3	15.42
Ash	6.06	6.3	0.34
Moisture	6.15	4.1	6.79
HHV (MJ/kg)	15.88	16.16	19.35

3.3.2 Thermogravimetric Analysis.

3.3.2.1 Thermal degradation of biomass in TGA

The thermogravimetric analysis of three different lignocellulosic biomass feedstocks: corn stover, wheat straw, and softwood are shown in Figure 3.4 and Figure 3.5. Figure 3.4 depicts the TGA curves of the three biomass feedstocks, whereas, Figure 3.5 shows the derivative thermogravimetric (DTG) curves for a heating rate of 10 °C/min in a nitrogen controlled atmosphere.

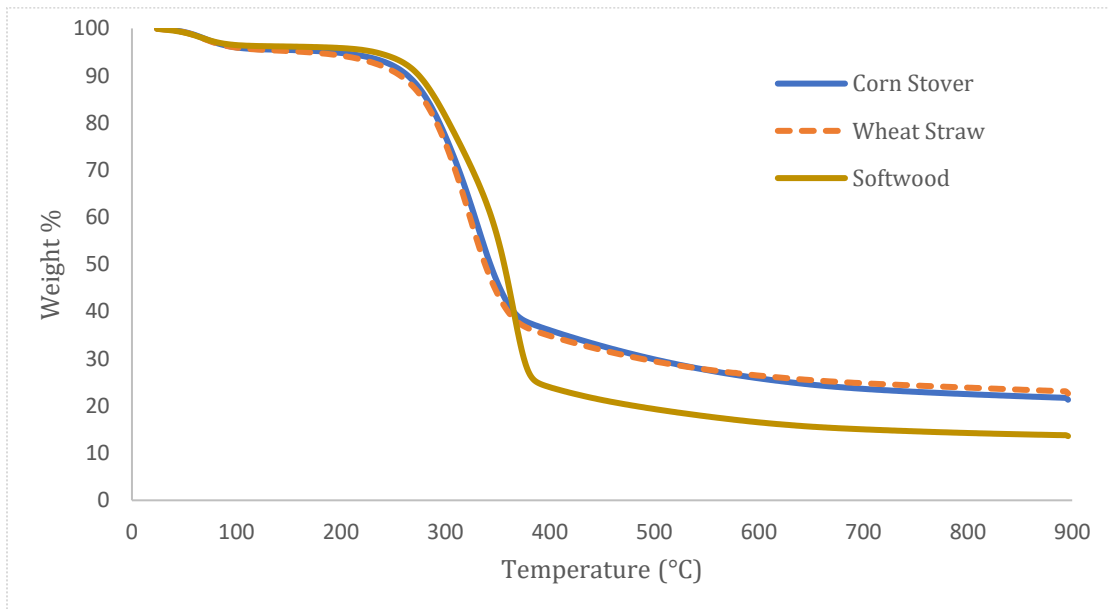


Figure 3.4 TGA curves of corn stover, wheat straw and softwood as a function of temperatures at a heating rate of 10 °C/min in nitrogen atmosphere

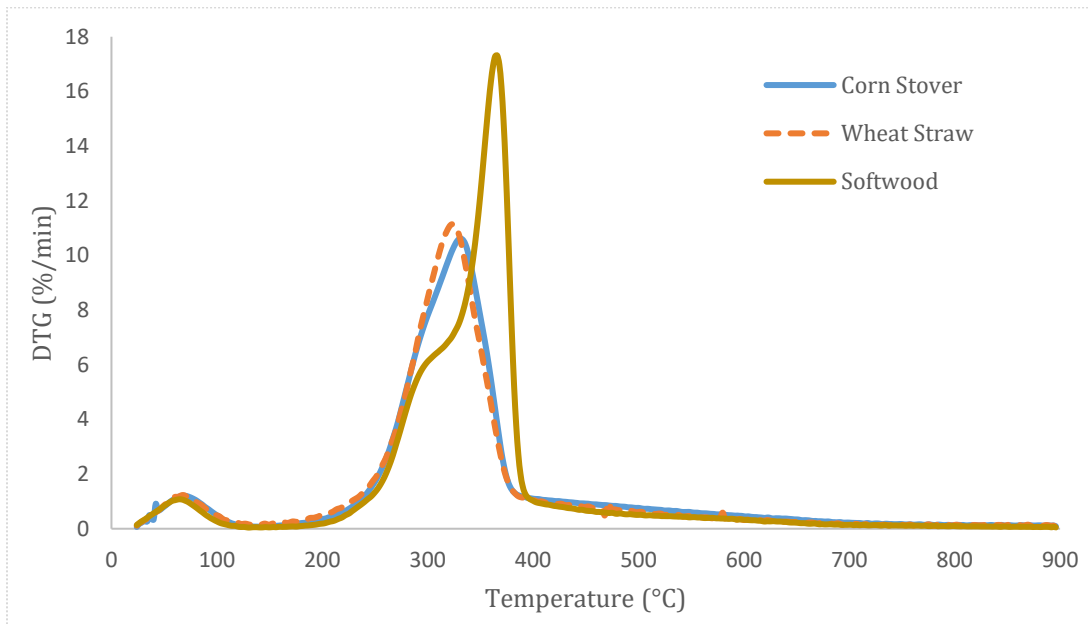


Figure 3.5 DTG curves of corn stover, wheat straw and softwood as a function of temperature at a heating rate of 10°C/min in nitrogen atmosphere

3.3.2.2 Effect of heating rate

The effect of heating rate on the TGA and the DTG curves for softwood is illustrated in Figure 3.6 and Figure 3.7. The response of all the feedstocks to the different heating rates was similar to that of softwood. It can be observed that the heating rate affected the TGA and DTG curves by changing the position of the peak temperature, biochar yield, and the decomposition rate at peak temperature. At a slower heating rate of 2 °C/min, the rate of weight loss is much lower than that at a higher heating rate of 15 °C/min, as can be seen in Figure 3.7. With the increase in heating rate, the rate of weight loss and the temperature at which maximum weight loss occurs increases from 329 °C at 2 °C/min to 366 °C at 15 °C/min. The maximum rate of weight loss of 17.31 %/min was observed at 15 °C/min at a temperature of

366 °C. The rate of weight loss at 2 °C/min was much lower at a value of 2.63 %/min at a temperature of 329 °C.

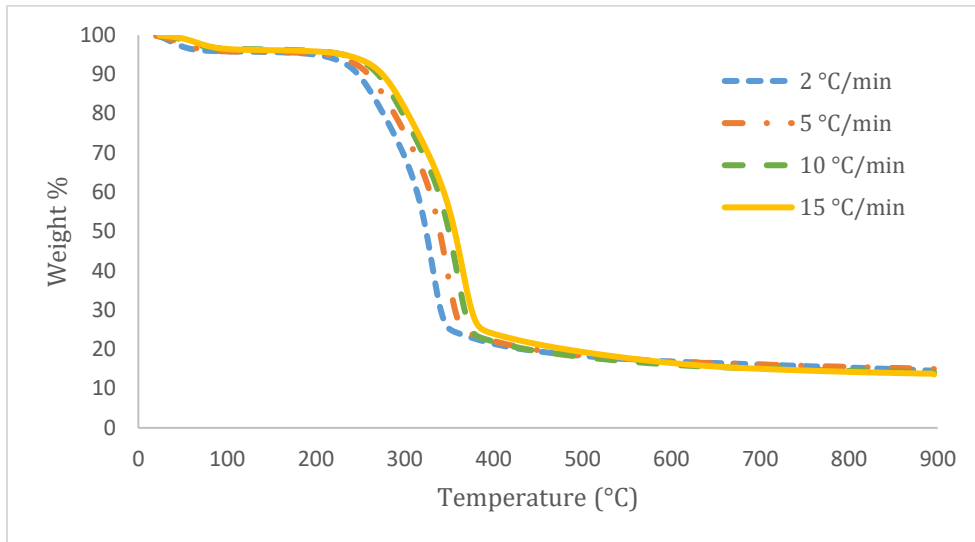


Figure 3.6 TGA curve of softwood at four different heating rates

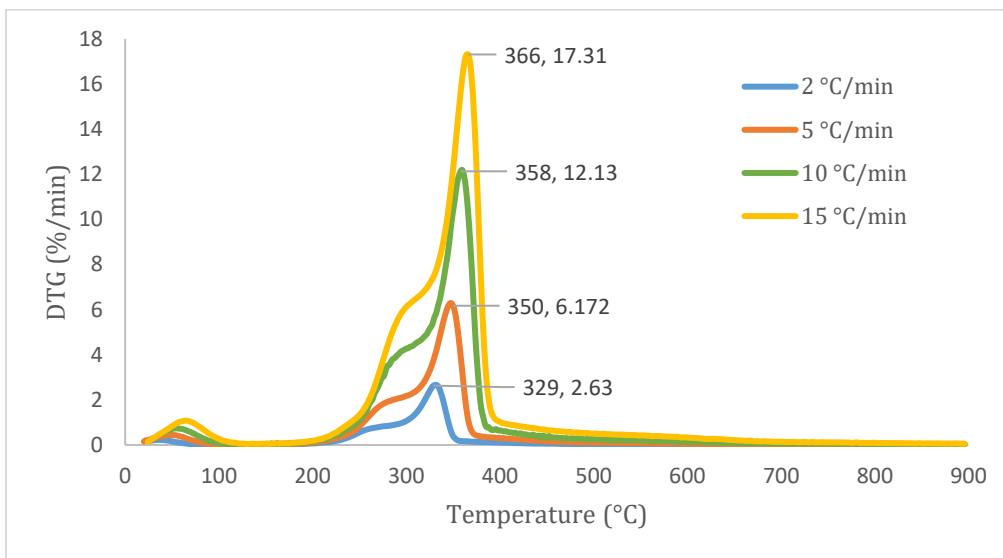


Figure 3.7 DTG curve of softwood at four different heating rates

3.3.3 Estimation of kinetic parameters

The activation energy (E_a) values of the softwood were calculated from individual slopes of linear model equations $\ln\left(\frac{\beta}{T^2}\right)$ and $\ln(\beta)$ versus $1/T$ for KAS and FWO, respectively (Figure 3.8 and Figure 3.9). These plots give the apparent activation energy values for different stages of solid phase reactions at different values of conversion.

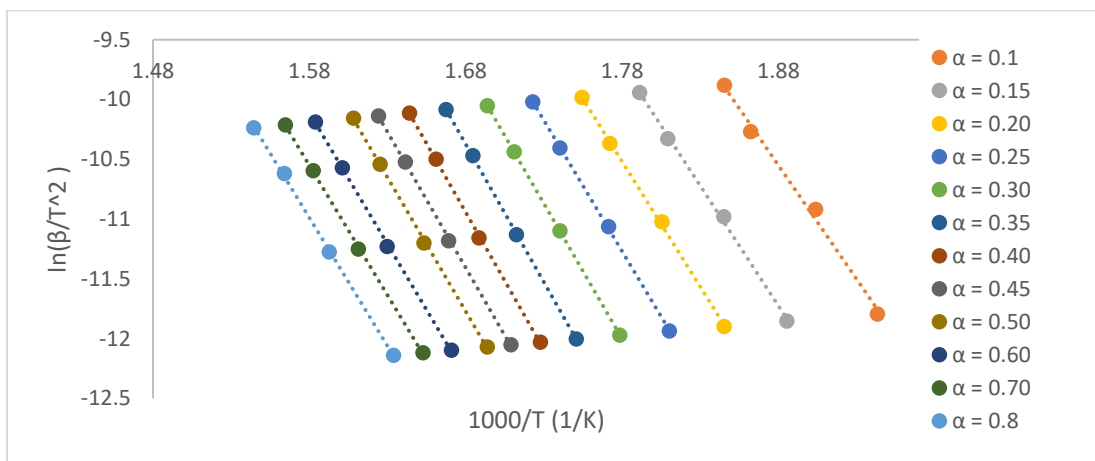


Figure 3.8 Linear fit plots to calculate activation energy for pyrolysis of softwood at different conversion degree using KAS model

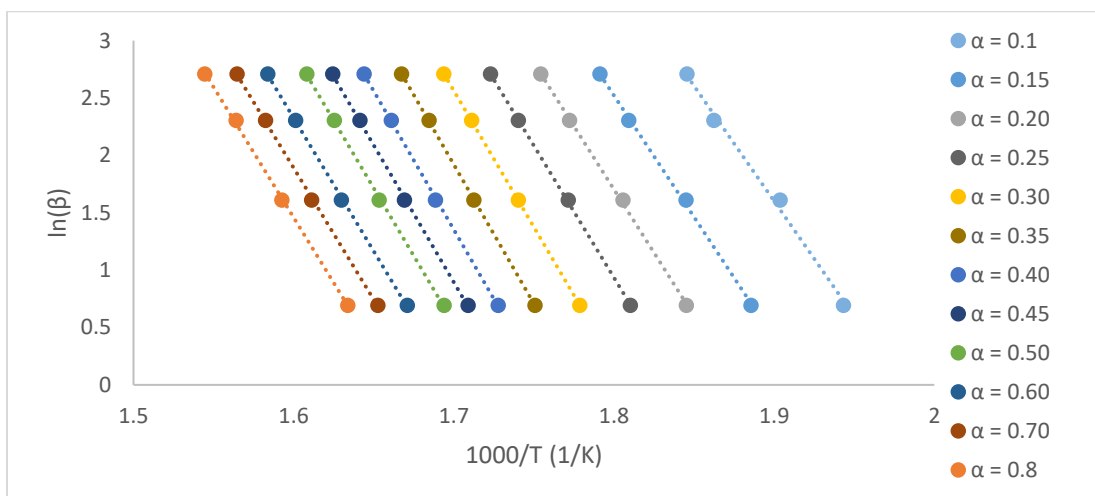


Figure 3.9 Linear fit plots to calculate activation energy for pyrolysis of softwood at different conversion degree using FWO model

In order to calculate the activation energy using modified DAEM, experiments were performed at three different heating rates of 2, 5 and 10 °C/min. The data obtained from these three heating rates was inputted into the algorithm created to solve Equation 14, which was solved for apparent activation energy at different conversions.

The calculated E_a using the FWO KAS and modified DAEM for the softwood at different conversions are reported in Table 3.2. It was observed that for all three models, similar trend was observed. The activation energy increased at the beginning with increase in α from 0.1 to 0.35, and then decreased after further increase in α from 0.4 to 0.8. Values above 0.8 conversion are not included since their behavior is not linear. The observed trend is in accordance with results reported by Gašparovič, Labovský [58], who reported the DAEM kinetic parameters for wood. Initially, the molecule bonds present are not broken or damaged, so they require more energy to ensure the decomposition of these molecules. Decomposition of these molecules lead to formation of less stable molecules which are easier to decompose, so require less amount of energy. Also, the initial conversion of 30 % ($\alpha = 0.3$) results in formation of more pores leading to more pore volume and surface area, which enhances diffusion related conversion. As a result, the activation energy decreases after a certain conversion ($\alpha = 0.35$) is achieved. Another contributing factor for the increase in activation energy could be due to

pyrolysis of cellulose being endothermic, whereas, the pyrolysis of hemicellulose and lignin is exothermic. At a conversion of 0.35, with the temperature in the range of 300 – 400 °C, the cellulose is almost entirely decomposed, with mostly lignin remaining, which decomposes in a wide range of temperature of 160 – 900 °C. Thus, the amount of activation energy decreases at higher conversions.

Table 3.2 Calculated activation energy for pyrolysis of softwood using FWO and KAS models

α	FWO		KAS		DAEM
	E_a (kJ/kg)	R^2	E_a (kJ/kg)	R^2	E_a (kJ/kg)
0.1	158.61	0.99	158.08	0.99	171.79
0.15	167.32	0.99	166.97	0.99	173.72
0.2	174.25	0.99	174.06	0.99	177.73
0.25	181.75	0.99	181.80	0.99	180.61
0.3	187.90	1	188.10	1	182.51
0.35	191.65	0.99	191.88	0.99	182.75
0.4	190.86	0.99	190.92	0.99	181.03
0.45	188.74	0.99	188.58	0.99	178.30
0.5	186.46	0.99	186.09	0.99	175.66
0.6	183.42	0.99	182.74	0.99	173.34
0.7	181.38	0.99	180.48	0.99	171.07
0.8	179.66	0.99	178.53	0.99	170.63

The average activation energy calculated using FWO and KAS are 181 kJ/kg and 180.68 kJ/kg, respectively. The average R^2 values for both FWO and KAS were found to be 0.99. But the average activation energy calculated by modified DAEM was

slightly lower at 176.6 kJ/kg. The comparison of the calculated activation energies using the three models is shown in Figure 3.10.

Ding, Ezekoye [59] compared the pyrolysis behaviors of hardwood and softwood. The author reported an average activation energy for softwood at 183.43 kJ/kg at conversion values above 0.2 and 188.12 kJ/kg for conversion values below 0.2 using the FWO method. The trend in the activation energy reported was opposite of what was observed in this study. The results indicated that the softwood activation energy decreased until conversion value of 0.2 and at value above 0.2, the activation energy kept constant.

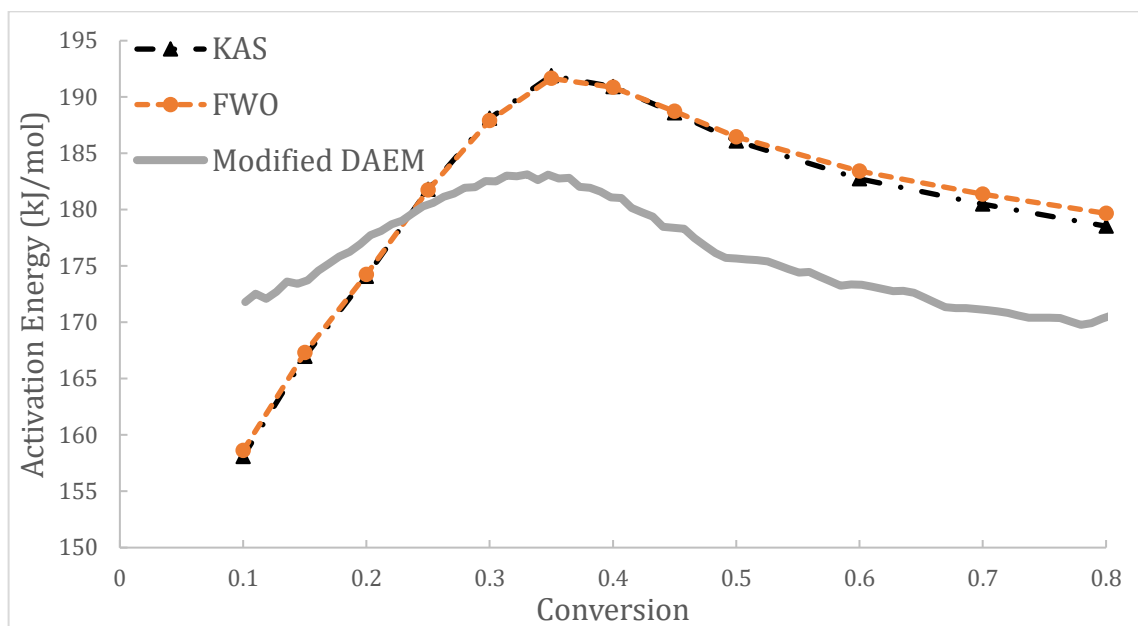


Figure 3.10 Activation energy as a function of conversion for FWO, KAS and DAEM models

Modified DAEM has been proven to be an effective tool for predicting the thermal decomposition of various biomass feedstocks [53, 55, 57, 58]. A comparison of

experimental and calculated modified DAEM mass loss curves of the thermal decomposition of the softwood at the heating rates of 2, 5 and 10 °C/min are shown in Figure 3.11. The quality of fit obtained in all the cases was above 90 %. Thus, the modified DAEM can describe the decomposition curve without much deviation. It was observed that the predicted TGA curves using modified DAEM were much more accurate fit (~90 %) to the experimental data compared to FWO and KAS, Similar results were obtained for corn stover and wheat straw as well and the images are displayed in Appendix A.

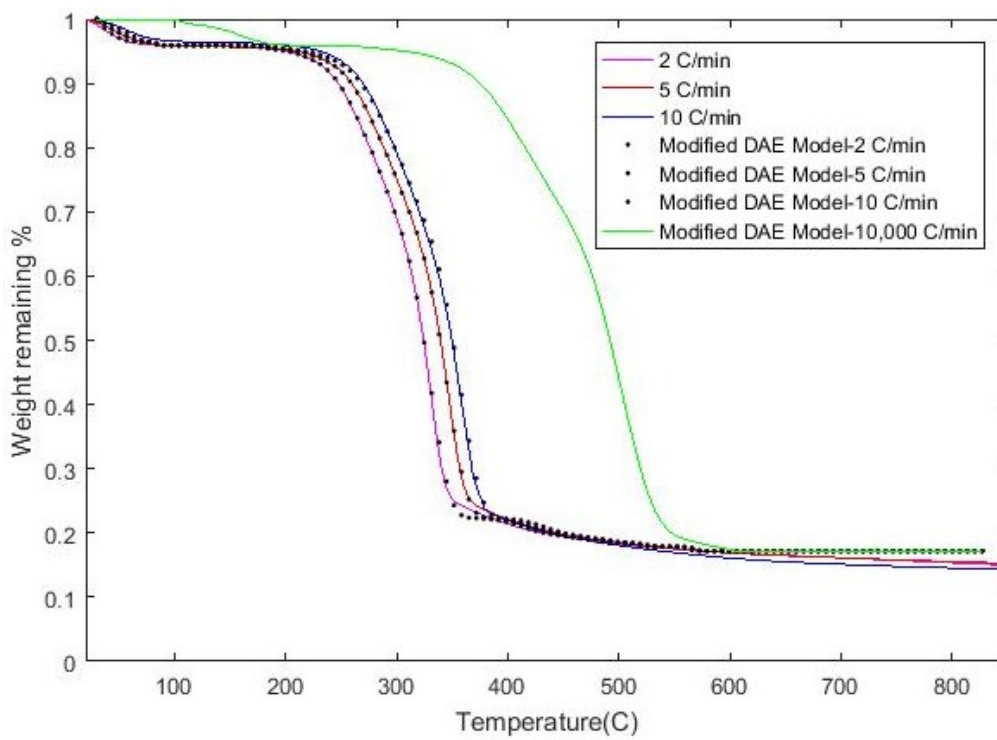


Figure 3.11 Experimental and modified DAEM curves for pyrolysis decomposition of softwood at 2, 5 and 10 °C/min

Chapter 4

Thermo-Catalytic Reforming of Woody

Biomass

The following chapter contains a comprehensive description of the experimental set-up and the results of the TCR experiments. The experimental details include feedstock preparation, experimental set up of the TCR-2 plant, and the analytical methods used to characterize the feedstock and the TCR products. The results of the TCR experiments are presented in the form of mass and energy balance, chemical composition, physical properties, and morphology study.

4.1 Feedstock Preparation & Characterization

The TCR plant is designed for pelletized or granulated feedstocks. The size of the granules must be between 3 – 20 mm. The pellets should preferably have a diameter of 6 mm and a length between 10 – 25 mm. The robustness of the process enables the utilization of various biogenic feedstock, however very fine material e.g. sand- or dust-like particle must not be used, due to their conveying properties. Larger particle must not be used either, as they are more likely to cause a blockage in the system and their limitation of heat transfer. The water content should be between 5 – 25 %.

For this study, three different lignocellulosic biomass feedstocks were selected: hardwood pellets, softwood pellets and softwood chips. The hardwood pellets were bought from Canadian Tire for the preliminary runs to test the machine. The softwood pellets and chips were supplied by Vanderwell Contractors in Slave Lake, Alberta. The hardwood and softwood pellets had a diameter of 6 – 8 mm and a length of 20 – 30 mm. The softwood chips were received as a part of the saw dust which was classified in a standard chip classifier (BM&M Inc., Surrey, BC, Canada). The saw dust was classified into five nominal sizes of ~67.2 mm, ~19.2 mm, ~6.4 mm, ~3.2 mm, and <~3.2 mm, which were labelled after the size of the classifier sieves opening.

The ultimate and proximate analysis of the three different feedstocks (Figure 4.1) used in the TCR-2 were performed according to the methods listed in Section 3.1, and are summarized in Table 4.1.



Figure 4.1 Feedstock: (a) Hardwood Pellets, (b) Softwood Pellets, (c) Softwood Chips

Table 4.1 Ultimate and proximate analysis of different TCR biomass feedstocks

	Hardwood Pellets	Softwood Pellets	Softwood Chips
Ultimate Analysis (dry basis) (wt %)			
Carbon	47.74	48.27	48.52
Hydrogen	5.94	6.09	6.04
Nitrogen	0.13	<0.1	<0.1
Sulfur	0	0	0
Oxygen (a)	46.19	45.64	45.45
Proximate analysis (wt %)			
Volatiles	77.23	77.20	77.45
Fixed carbon	17.95	16.19	15.42
Ash	1.42	1.15	0.34
Moisture	3.4	5.46	6.79
HHV (MJ/kg)	18.89	19.31	19.35

(a): calculated by difference

The elemental composition and proximate analysis of the three woody feedstocks were similar to that published in literature [33]. The three feedstocks have almost similar elemental compositions, with carbon content varying from 47 – 48 wt %, and oxygen content from 45 – 46 wt %. The only major difference can be seen in the fixed carbon and ash content through the proximate analysis. The pellets, both hardwood and softwood have higher ash content at 1.42 wt % and 1.15 wt % respectively, whereas the softwood chips have significantly lower ash content at 0.34 wt %.

4.2 Lab Scale TCR

The experimental setup is shown schematically in Figure 4.2. The setup consists of feed hopper, TCR reactors (intermediate pyrolysis auger reactor combined with a

fixed bed-reforming reactor), condensers, bio-oil container, gas wash bottle, filters and a gas analyzer. The TCR plant was designed and assembled in 2018 at Fraunhofer UMSICHT in Sulzbach-Rosenberg, Germany. The experiments carried out in the TCR-2 are designed to be a batch process, so it does not require continuous feeding or bio-char extraction system.

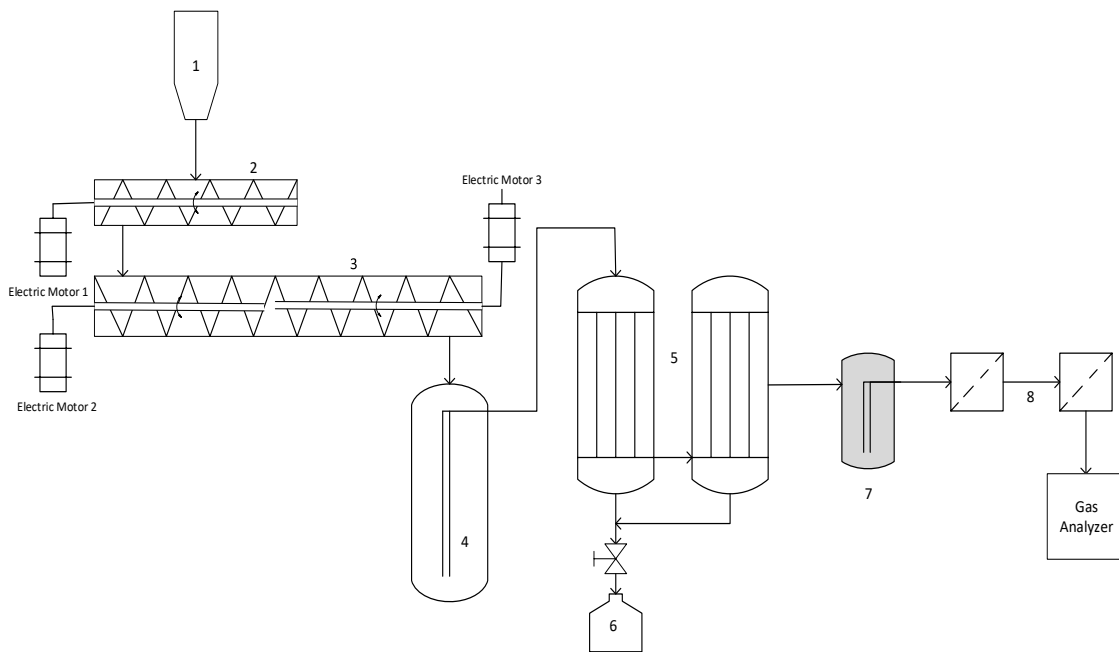


Figure 4.2 Schematic diagram of TCR-2 laboratory plant: (1) Hopper, (2) Screw Conveyor Feeder, (3) Auger Reactor, (4) Reformer, (5) Condensers, (6) Bio-oil Container, (7) Gas Wash Bottle, (8) Filters

The design of the TCR reactor allows for a maximum capacity of 6 kg of the solid pelletized feedstock in the hopper. The hopper is placed on the top of the feeding screw conveyor, the purpose of which is to transfer the feed from the hopper to the reactor. The feeding screw conveyor moves the feedstock to the reactor by pulsing the feedstock to ensure no blockage or overfeeding, which may reduce the efficiency of the experiment.

The first reactor is a horizontal tubular auger reactor, which can be divided into two different zones based on the temperature [32-35, 38-40]. The first zone (Zone 1) is the drying zone, where the moisture and the light volatiles vaporize from the solid biomass [32]. The temperature in the zone 1 can be varied between 200 °C – 300 °C. The feed is conveyed by the means of a screw within this zone. The temperature in the second zone (Zone 2) is usually between 400 °C – 500 °C and can be referred to as the pyrolysis zone. Majority of the volatiles and oxygenates are removed in zone 2 and the char is produced [32, 38]. This zone can be further divided into two sub-zones due to the design of the screw: mixing zone (zone 2a) and transportation zone (zone 2b).

The horizontal screw reactor has two coaxial rotating screws. The purpose of the first screw is to move the feedstock through the reactor, whereas the second screw serves two purposes: mixing and recycling. The unique design of the second screw is such that it mixes the feedstock with the char and recycles a portion of char within the screw reactor. Within the pyrolysis zone 2, a portion of the solid char is moved back to the beginning of the pyrolysis zone. The dried feedstock coming from the drying zone 1 is thus mixed with the entirely and partially pyrolyzed solids. Mixing of the dried feedstock with the solid recycled char has many advantages. The recycled solid particles in the zone 2 have a higher surface temperature and is therefore significantly higher than the feedstock from zone 1. Thorough mixing of the solid particles with the recycled particles by the screw results in enhanced heat

transfer between the particles. The horizontal screw reactor is heated by three electric ceramic heaters.

The two screws within the horizontal auger reactor are separately controlled by an electric motor. The motor for the first screw is placed on the side of the feed inlet. The second screw is controlled by a motor that is placed on the hot side of the reactor. Due to this, the flange sealing must be suitable for temperatures beyond 673 K. Graphite seals with a purity of 99.85 wt% are in use. To reduce the complexity of plant, these seals are also used on the cold side of the reactor.

The solid pyrolysis products are transported forward by the rotation of the second screw in the horizontal auger reactor to the transition zone between the two reactors. The transition zone between the two reactors is also heated by an electric heater and is maintained at 500 °C. The solid particles are partially carried by the gaseous products and gravity to the vertical reformer reactor.

The reformer is also heated by three electric ceramic heaters. The temperature in the reformer is usually between 600°C - 750°C depending on the feedstock and the desired products. Like the horizontal screw reactor, the temperature in the reformer is monitored and controlled by three temperature sensors to prevent damage caused by overheating. The presence of the riser in the middle of the reformer ensures that the gaseous components completely react with biochar before leaving the reformer. The solid products, i.e. pelletized biochar remains within the reformer

for the duration of the experiment and can only be removed after the completion of the experiment.

The riser exits the reformer with a vertical 90° bend into the countercurrent condenser. The connecting pipe between the reformer and the condenser is also heated by an electric heater and is maintained at 550 °C to ensure that the product gases do not condense in the connecting pipe.

The hot gases exiting the reformer are cooled in two condensers in series. These condensers are cooled by water flowing through the condensers using the counter-current principle. The condensable substances are collected in a collection container below the first condenser. Adapters with ball valves and a by-pass connection to the second condenser enable removal of condensate during plant operation.

The cooled gas stream passes a gas wash bottle – filled with aqueous phase collected from previous experiments followed by 5-inch polypropylene foam 5- μ m. After these gas treatments, the gases pass through a diaphragm gas meter to measure the gas volume. A part of the gas is then sent to gas measurement system for analysis and the remaining is vented out through the exhaust.

The control system is based on the Siemens Simatec S7-1200 and visualized with Siemens WinCC Runtime Advanced. All frequency inverters of the screw motors can be controlled and adjusted through the user interface. The feeder screw is equipped with an automatization and enables feeding rates beyond the capacity of the frequency inverters. This is achieved by a definable pause and run times or also

referred to as pulse mode further on. The lab scale plant of the Thermo-Catalytic Reforming technology has also been described in several publications [14, 30, 32-36, 38-40, 42, 43].

4.2.1 Experimental Procedure

A detailed inspection of the plant must be performed prior to every operation of the plant. Initial inspection includes ensuring the plant is fully assembled with all screw connections joined and intact. All of the chain guards, drive chains and the gears should be installed, functional and free of damage. The heater elements and the thermocouples should be connected properly and in good condition. The cooling water inlet to the condenser and the outlet water tube from the condenser must be connected and free from damage. Ensure that the CO monitor is always working and wear personal CO detectors during the experiment. Given that the preliminary inspection is successful, the start-up phase can be started.

Start-up phase includes preparing documentation sheets. Then turn on the power supply to the TCR plant and open the software 'Wincontrol' in the attached computer. Record the weight of the filter cartridges and the bio-oil glass bottles before connecting to the plant. A pressure test is performed at pressures between 50 - 100 mbar to ensure there are no leaks in the system. The plant is flushed with nitrogen and the gas outlet is closed by a ball valve. As soon as the pressure level is 100 mbar, the nitrogen flow is stopped, and the ball valve closed to prevent backflow. If the pressure drop is below 5 mbar per minute at pressures within 50-

100 mbar, the system can be considered as 'leak free' or 'gas tight'. It is mandatory to ensure that there is no oxygen in the system, so the system is flushed with nitrogen for approximately 10 minutes or until the oxygen concentration in the system is less than 0.5 %. The feeder nitrogen valve is turned off after the system is ensured to be free of oxygen, but the bearings nitrogen valve (x2) must be on throughout the experiment. Once the preliminary checks are complete, the plant is heated up to the operating temperatures. The plant is heated up by turning on the electric heaters (screw reactor and reformer) and setting it to desired temperature in the software. Also, turn on the reactor screws and the cooling water flow into the condensers. When the screw reactor and the reformer are almost heated up, open the hopper and fill the feeder with the weighed feedstock and close the hopper. In addition, weigh the aqueous phase and fill the gas wash bottle with the measured aqueous phase. Perform a quick leak test again and purge the system with nitrogen for 5 minutes or until the oxygen concentration in the system is less than 0.5 %. The experiment can be started by turning on the feeding screw conveyer. Record the gas flow readings every 15 minutes and collect the condensate every 15 minutes by opening the release valve.

The experiment is successfully finished when there is no more feedstock in the hopper and the gas is no longer being produced within the system. Following the completion of the experiment, all the electric heaters (screw reactor and reformer) are turned off. Once the temperature in the screw reactor and reformer is below 300 °C, the operating screws in the screw reactor can be turned off. In addition, shut

down the cooling water flow and the nitrogen flow in the system before turning off the power supply to the plant.

Post processing phase of the experiment is started after the plant has cooled down to room temperatures. The primary focus of this phase is to measure the relevant quantities for mass balance calculations and collect product samples for analysis. The aqueous phase is collected from the gas wash bottle and the condensate is collected by unscrewing the bio-oil collection bottle. The biochar is to be collected from the reformer. Therefore, the reformer is disassembled to extract the biochar. The screw reactor and the hopper are cleaned to remove any unreacted feedstock or residues to account for losses in the mass balance calculations. Because the TCR is set up as a batch process, evaluating the data requires an interval determination: only the data from the steady-state-operation of the plant is used to represent the experiment. Therefore, it is essential to utilize the gas composition and property data from this specific steady-state interval. It can be assumed that steady state operation has been reached when gas composition and the gas building rate is stable with only small variation over time.

4.2.2 Experimental Plan

The total number of experiments conducted in the lab scale TCR plant are shown in Table 4.2. Experiments were carried out for the three different feedstocks: hardwood pellets, softwood chips and softwood pellets. The temperatures were varied between 400 – 550 °C, and 500 – 700 °C for the horizontal reactor and the

vertical reformer, respectively. In addition, at a fixed reformer temperature, biochar collected at the same temperature was added prior to the experiment to create a pre-existing biochar bed. It is crucial to ensure the pre-existing biochar bed should be the biochar collected at the same conditions. Using the biochar from different experimental conditions, such as lower reformer temperatures, will result in reforming of the biochar bed, leading to additional gases and condensate. This could lead to incorrect mass and energy balance.

The initial experiments were carried out for all three feedstocks: hardwood pellets, softwood pellets and softwood chips. But the parametric study was only conducted for the softwood pellets feed.

Table 4.2 Experiments performed on TCR-2

Feedstock	Reactor Temperature (°C)	Reformer Temperature (°C)	Number of experiments
Hardwood Pellets	500	550, 600, 650*	4
Softwood Chips	400, 450	600*	2
Softwood Pellets	400*, 450*, 500*, 550*	500*, 600*, 700	13

*: At this temperature, an additional experiment was carried out with a pre-existing char bed.

4.3 Product Characterization Methods

The measurement devices used for TCR experiments can be categorized into on-line and off-line devices. At the end of the experiment, the produced condensate (aqueous phase + bio-oil) is transferred from the collection vessel to the conical separating funnel (Figure 4.3 (a)). The condensate is stored in the separating funnel for 20 hours so that the two phases with different densities are separated by gravity.

The organic oil phase with higher density than aqueous phase stays at the bottom and the aqueous phase at the top (Figure 4.3 (b)). After the reactors have cooled down, the biochar is collected by removing the bottom of the reformer.



Figure 4.3 Conical separating funnel: (a) At the end of experiment, (b) After 24 hours into separation

4.3.1 Bio-oil Characterization

The ultimate analysis of the bio-oil samples were performed, applying the same method as described in Section 3.1.3 for the determination of the elemental

compositions (C, H, N, S and O). The oxygen and water content of the bio-oil sample was determined by the Chemistry department at University of Alberta.

The heating value of the bio-oil was calculated using the same method described in Section 3.1.4.

The total acid number (TAN) was determined in accordance with ASTM D664-04 using Mettler Toledo T50 Figure 4.4. Approximately 0.25 g of bio-oil sample was dissolved in 60 ml of titration solvent and titrated with KOH solution to neutralize the acidic content in the sample.



Figure 4.4 Mettler Toledo T50 for TAN measurement

The viscosity of the bio-oil was determined by Anton Paar rotational rheometer – RheolabQC in accordance with ASTM D5018. The viscosity of all the bio-oil samples was measured at 40 °C.

The composition of the bio-oil was analyzed with gas chromatography mass spectroscopy (GC-MS) (Figure 4.5). The column used for the analysis was a 5% Phenyl Methyl Siloxane capillary column 30m × 0.25mm, 0.25µm film thickness. A small amount of bio-oil was dissolved in dichloromethane as solvent (10 wt %). The mixture was micro-centrifuged, and the supernatant was used for analysis after filtration using 2-micron PTFE filter. For analysis, 1µL of sample was injected in splitless mode with Helium as a carrier gas. The temperature profile for column heating in GC starts at 50°C with a hold time of 5 min followed by heating at ramp of 10°C min⁻¹ to reach 325°C and hold for 7.5 min. The temperature at auxiliary interface between GC and MS was maintained at 280°C. Likely compounds in sample were identified using NIST library for mass spectra. Compounds were quantified in terms of relative abundance of peak area (% peak area to the total area)



Figure 4.5 Gas Chromatography Mass Spectroscopy (GC-MS)

4.3.2 Produced Gas Characterization

The gas measurement devices are on-line, which means that the gas is monitored continuously for analysis through a tube connecting the TCR outlet with the devices. The volumetric determination of produced gas is determined by a residential natural gas diaphragm gas meter RS/2001 [60] for the hardwood pellets, but for softwood chips and pellets, the amount of gases were calculated by difference due to the malfunction of the gas meter.

The composition of the produced gas is determined by an on-line CP-4900 Micro Gas Chromatograph, (Figure 4.6). The micro GC is equipped with four independent column channels, but only three are in use for this equipment. Each column channel is a complete, miniaturized GC with electronic carrier gas control, micro-machined injector, narrow-bore analytical column and micro thermal conductivity detector (μ

TCD). The carrier gases used in this set-up are Helium and Argon. The principle behind separation is that as the components of a mixture move through a separation column, they undergo a number of processes, and hence the components exit the column at different times [61]. Even identical solute molecules, owing to the randomness of different processes, reach the detector at different times leading to a distribution [61]. The detectors can identify CO, CO₂, H₂, N₂, O₂, CH₄ and C_xH_y.



Figure 4.6 CP-4900 Micro Gas Chromatograph used for gas analysis

4.3.3 Bio-char Characterization

The ultimate analysis of the bio-char were performed, applying the same method as described in Section 3.1.3 for the determination of the elemental compositions (C, H, N, S and O).

The heating value of the biochar was calculated using the same method described in Section 3.1.4.

The proximate analysis was conducted for the solid biochar in accordance with methods described in 3.1.1.

The surface morphology of the bio-char was studied by performing scanning electron microscopy (SEM) using Zeiss Sigma 300 VP-FESEM (Figure 4.7) at Department of Earth and Atmospheric Sciences, University of Alberta. The bio-char pellets were attached to the top of the sample holder using a conductive carbon tape. Due to good conductivity of the bio-char samples, no additional coating was used. For the analysis, SEM scans were conducted at an accelerating voltage of 10 kV.



Figure 4.7 Scanning Electron Microscope Zeiss Sigma 300 VP-FESEM

Brunauer-Emmett-Teller (BET) experiments were performed to obtain the surface area of the bio-char on an Autosorb IQ instrument (Quantachrome Instruments, Boynton Beach, FL, U.S.A.) (Figure 4.8). For BET experiments, 9 mm cells were filled with sample till 3/4th of cell (bulb) volume. The sample were degassed by heating the sample in vacuum at 250°C at a heating rate of 5°C/min and the soak time was 4 hours. The adsorption and desorption isotherm of nitrogen was measured at a relative pressure range of 0-0.99 at 77 K. The multipoint BET surface areas were measured at a relative pressure range of 0.05–0.35 (unit).



Figure 4.8 BET set-up, Quantachrome IQ

4.4 Product Yield and Characterization Results

The biomass feedstock in pelletized and chips form were fed into a lab scale TCR-2 plant to produce gas, solid biochar, and liquid condensate. At a pyrolysis temperature of 450 – 500 °C, reformer temperature of 600 °C, and a solid residence time of ~5 minutes, the product yields for the three feedstocks are shown in Table 4.3. The biochar and bio-oil yield were determined gravimetrically, and the gas yield was calculated by difference.

Table 4.3 Product yield of TCR-2 products (Mass Balance)

Weight %	Hardwood Pellets	Softwood Pellets	Softwood Chips
Biochar	18.5	17.48	18.23
Bio-oil	2.7	4.16	4.92
Aqueous Phase	16.94	18.16	17.43
Gas (a)	61.86	60.2	59.42

(a): calculated by difference

The mass balance revealed an overall similar distribution. The only major difference can be seen in the bio-oil content. The bio-oil yield was lowest for the hardwood pellets (2.7 wt %), whereas the softwood pellets and chips had almost similar yield at 4.16 wt % and 4.92 wt %. The amount of aqueous phase produced was higher for softwood pellets (18.16 wt %) and chips (17.43 wt %) due to higher moisture content in the feedstock compared to hardwood pellets (16.94 wt %) which had the lowest moisture content, and thus lowest yield of aqueous phase. However, the presence of moisture also aids in the reforming of biochar to produce more gases and bio-oil [32]. Thus, lower moisture content in hardwood pellets also results in lower bio-oil yield. The amount of biochar produced is quite similar for all three feedstocks, hardwood pellets (18.5 wt %), softwood pellets (17.48 wt %), and softwood chips (18.23 wt %). It can be noted that, all three of the woody feedstocks produced very high amount of gas varying between 59 – 61 wt %. Overall, these mass balance results do not account for mass losses happening in the process, such as, sticking of liquid in the equipment.

The process energy flow depicted in Figure 4.9 was calculated from the mass balance (Table 4.3) and individual heating value of the TCR products. The TCR process is an endothermic process requiring an external source of heat input. The boundary conditions were set only around the TCR feed and product streams. It does not include the external source of heat input required for the operation of the TCR unit because the electrical energy required is very substantial and not relevant for a small lab scale unit. In case of larger capacity plants (300 kg/h), the syngas produced will be used to heat up the reactors, thus making energy balance to be conducted then more relevant. Approximately 74 – 80 % of the energy within the feedstock is transferred to the chemical energy within the products. Majority of the energy ~70 – 75 % is transferred to the syngas and the biochar. Only a small amount of energy ~4 – 8 % is transferred to the bio-oil due to the low yield of bio-oil from thermo-catalytic reforming of the woody biomass. The remaining energy which was unrecoverable was believed to be because of aqueous phase as well as heat losses within the system and surrounding environment.

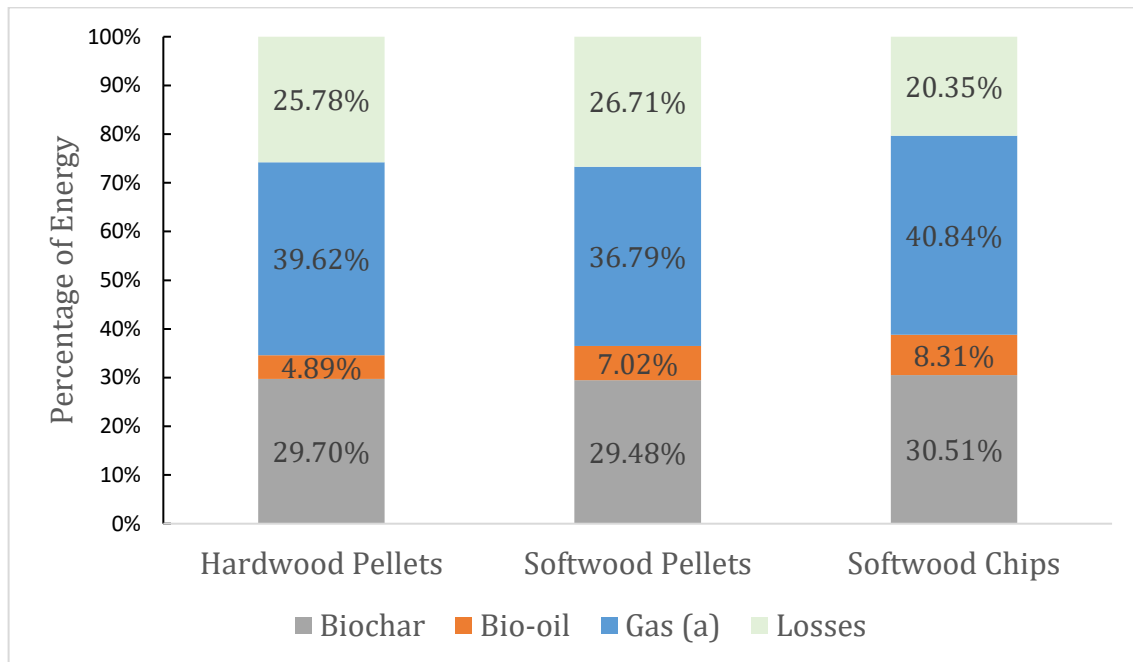


Figure 4.9 Energy flow from the feed to products for different biomass feedstock

4.4.1 Biochar Characterization

Figure 4.10 shows the TCR-2 biochar produced at a reformer temperature of 600 °C. The produced biochar had the same structure as the feedstock. The biochar from pelletized feedstock retained its pelletized form and that from the softwood chips was still in the form of chips. The size of the biochar pellets and chips reduced due to shrinkage resulting from release of gases from the biochar. The biochar pellets had an average diameter of 3 – 4 mm and length of 8 – 12 mm. The biochar chips had an average width of 1 – 2 mm and a length of 6 – 8 mm.

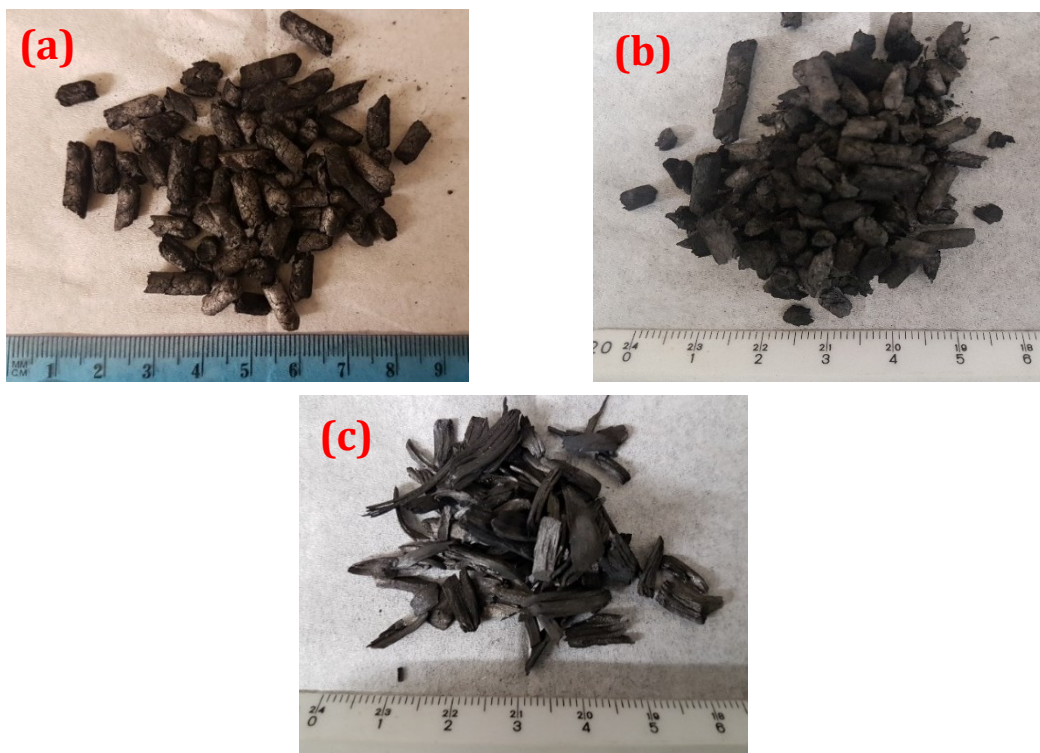


Figure 4.10 TCR-2 Biochar (a): Hardwood Pellets (b): Softwood Pellets (c): Softwood Chips

The elemental composition along with the calorific value for the biochar produced from all three feedstocks are listed in Table 4.4.

Table 4.4 Characterization of the TCR-2 biochar produced from woody feedstock

Ultimate Analysis (dry basis) (wt %)			
	Hardwood Pellets	Softwood Pellets	Softwood Chips
Carbon	88.37	93.26	93.01
Hydrogen	1.58	1.47	1.47
Nitrogen	0.25	0.13	0.13
Sulfur	0	0	0
Oxygen (a)	9.8	5.14	5.43
O/C	0.1108	0.0551	0.0583
H/C	0.0178	0.0157	0.0158
HHV (MJ/kg)	30.33	32.57	32.38

The carbon content of the biochar produced from hardwood (88.37 wt %) was lower than that produced from softwood (93.26 wt %). This is due to higher ash content in hardwood compared to softwood. As proven in literature, higher ash content has negative effect on the carbon content. The oxygen content was also significantly higher for hardwood pellets char (9.8 wt %) compared to softwood pellets char (5.14 wt %). The hydrogen and nitrogen content were similar for biochar produced from all three feedstocks. The effect of carbon and ash content was also observed in the HHV of the char. The hardwood pellet char had the lowest HHV at 30.33 MJ/kg, and the softwood pellets had the highest HHV at 32.57 wt %, which is close to that of anthracite coal (34 MJ/kg). The O/C and H/C ratio for the three biochar also lies in the range of 0.055 – 0.11 and 0.015 – 0.017, similar to anthracite coal, thus making

the TCR biochar much stable than fast pyrolysis biochar. The softwood pellets and chips, irrespective of structure produced biochar with similar properties.

4.4.2 Bio-oil Characterization

The liquid phase consisted of the organic bio-oil phase and the aqueous phase. The aqueous phase consisted of inherent moisture in the feedstock and out of product water. Due to difference in the density and polarity of the two phases, a distinct phase separation was achieved after 20 hours by gravity.

The obtained TCR-2 bio-oils were characterized by elemental analysis, moisture content, TAN, viscosity, and calorific value as can be seen in Table 4.5.

Table 4.5 Characterization of the TCR-2 bio-oil produced from woody feedstock

Ultimate Analysis (dry basis) (wt %)			
	Hardwood Pellets	Softwood Pellets	Softwood Chips
Carbon	81.1	78.04	78.49
Hydrogen	6.73	6.71	6.6
Nitrogen	0.69	0.42	0.51
Sulfur	0	0	0
Oxygen	11.48	14.09	13.02
H ₂ O (wt %)	----	5.25	----
TAN (mg KOH/g)	15 ± 1.15	7.11 ± 0.85	6.75 ± 0.72
Viscosity (mPas)	35.69	32.86	19.49
HHV (MJ/kg)	34.19	32.6	32.67

The TCR-2 bio-oils had a very high carbon content of >78 wt %. Bio-oil from the hardwood pellets had the highest carbon content (81.1 wt %). The hydrogen and nitrogen content were similar for all three bio-oils. The oxygen content in the bio-oil varied from 11- 14 wt %, with hardwood pellets bio-oil having the least oxygen content (11.48 wt %). The produced TCR-2 bio-oils had a TAN varying between 6- 15 mg KOH/g. The bio-oil produced from softwood chips had the lowest TAN (6.75 mg KOH/g) and viscosity (19.49 mPas). Like bio-char properties, the bio-oil produced from softwood pellets and chips irrespective of structure had similar properties. The TCR bio-oils produced have a heating value of 32 – 34 MJ/kg, which is close to that of biodiesel (37 MJ/kg), but less than that of propane (46 MJ/kg).

It is important to note that these properties are very different from that reported in studies done using fast pyrolysis of woody feedstocks. Haarlemmer, Guizani [62] performed a comparative study on the bio-oils obtained by hydrothermal liquefaction and fast pyrolysis of beech wood. The results reported that at a pyrolysis temperature of 500 °C, the produced bio-oil had a TAN of 89(±14) mg KOH/g, water content of 11(±1) % and oxygen content of 52.8 % [62]. Thus, even though the TCR bio-oil yield is very low compared to the fast pyrolysis bio-oils (17.2 %, organic fraction of the bio-oil [62]), the quality of the TCR bio-oil is far more superior compared to the fast pyrolysis bio-oil in terms of TAN, oxygen content and water content.

The TCR bio-oil was further analyzed in GC-MS to obtain its molecular composition using the method outlined in Section 4.3.1. The summary of the GC-MS results obtained for different biomass feedstocks are outlined in the Table 4.6. The different chemical compounds found in the bio-oil were grouped into 8 groups based on its structure and properties, such as: poly aromatic hydrocarbons (PAHs), mono aromatic hydrocarbons (MAHs), phenols, oxygen containing compounds (furans), acids, esters, and nitrogen containing compounds (pyridine). The majority of the compounds found in the TCR bio-oil were PAHs, which mainly included naphthalene, anthracene, and naphthalene derivatives. The MAHs mainly consisted of styrene, xylene, and its derivatives. Some oxygen containing compounds such as furan and its derivatives were also found in the TCR bio-oil produced from all three woody biomass feeds. Small amounts of nitrogen containing compounds such as pyridine were also detected.

Table 4.6 Summarized GC-MS analysis results for TCR bio-oil produced from different woody biomass feedstocks

Area %	Hardwood Pellets	Softwood Pellets	Softwood Chips
PAHs	54.31	54.47	61.79
MAHs	11.25	7.13	7.74
Phenols & Alcohols	23.05	26.85	14.98
O-compounds	5.47	7.68	5.57
Acids	1.28	0	0
Esters	3.63	1.26	7.94
N-compounds	0	1.75	1.62

4.4.3 Permanent gas composition and properties

The permanent gases mainly comprise of hydrogen, carbon monoxide, carbon dioxide, and methane, as shown in Table 4.7. The composition of the gases leaving the TCR unit for all three woody biomass feedstocks is quite similar. The hydrogen content of the gases varies between 13.39 – 15.70 vol %. The heating value of the TCR gases vary between 12.50 – 12.80 MJ/kg, which is very low compared to that of natural gas (47 – 52 MJ/kg). Thus, it can be said that the initial composition of the biomass feedstock had only a minor effect on the gas composition and characterization.

Table 4.7 Composition of the TCR gases produced from different woody feedstocks at a pyrolysis temperature of 450 °C and a reforming temperature of 600 °C

	Hardwood Pellets	Softwood Pellets	Softwood Chips
Gas Composition (Vol %)			
Hydrogen	15.70	13.39	13.62
Methane	27.93	28.46	29.14
Carbon monoxide	24.95	24.73	24.85
Carbon dioxide	30.38	31.58	30.98
C2	0.60	0.73	0.55
C3	0.44	0.68	0.45
C3+	0.00	0.44	0.40
HHV (MJ/kg)	12.80	12.50	12.70
LHV (MJ/kg)	11.70	11.40	11.60

Figure 4.11 shows the composition of the gases leaving the TCR unit as a function of time. It can be seen that initially; high amounts of carbon monoxide and methane is being produced with very small amounts of hydrogen and carbon dioxide. As the biochar is produced and it creates a biochar bed in the reformer, the gases undergo reforming reactions (Table 4.8) and the amount of hydrogen and carbon dioxide increases with time, whereas the methane and carbon monoxide content in the gases decreases with time. The composition of the gases leaving the TCR unit stabilizes after a certain time and remains almost constant until there is no feed in the hopper.

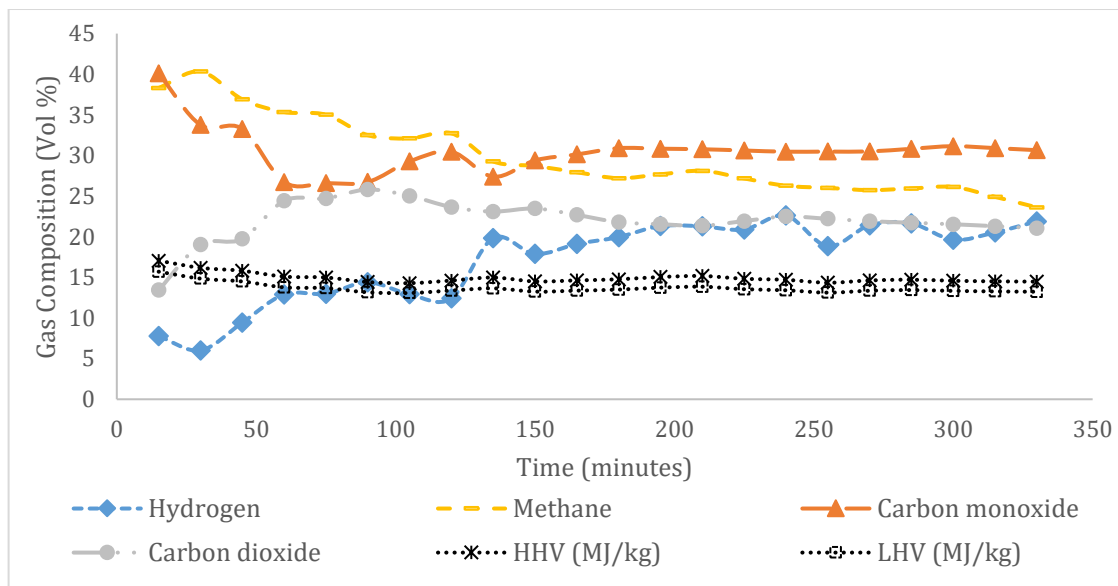


Figure 4.11 Composition of the TCR gases as a function of time throughout the experiment

Table 4.8 Post-Reforming Reactions identified in the Reformer by Neumann, Meyer [37]

Reaction	Enthalpy	Reaction No.
$CO_2 + C \leftrightarrow 2CO$	+172	1
$C + H_2O \leftrightarrow CO + H_2$	+131	2
$C + 0.5 O_2 \leftrightarrow CO$	-111	3
$CH_4 + H_2O \leftrightarrow CO + 3H_2$	+206	4
$CO + H_2O \leftrightarrow CO_2 + H_2$	-41.2	5
$C + 2H_2 \leftrightarrow CH_4$	-74.8	6

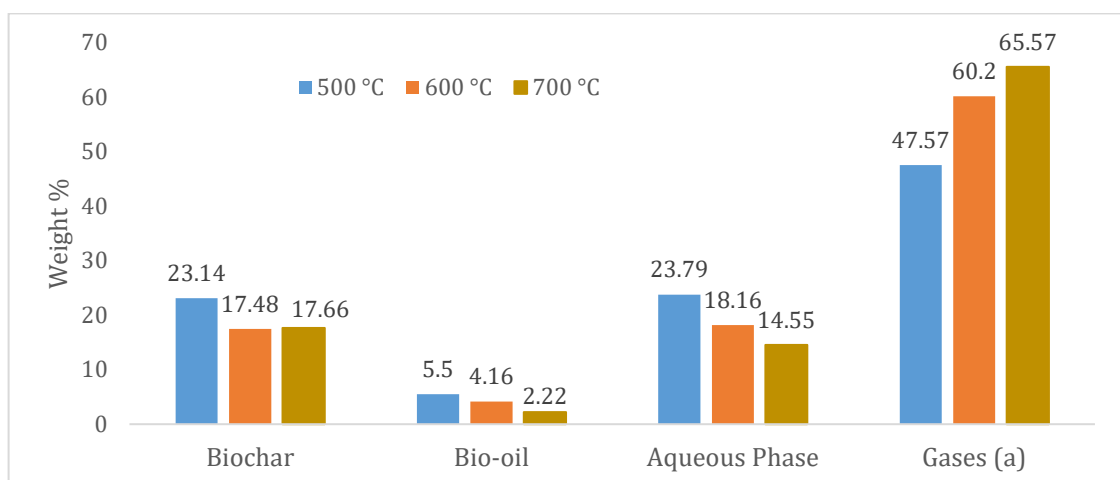
4.5 Parametric Study

4.5.1 Effect of Reforming Temperature

The reforming temperature is one of the most influential operating parameters in the TCR process. The extent of catalytic cracking of the biochar and the organic vapors depends on the reformer temperature. The parametric study was performed for the softwood pellets, where the pyrolysis temperature was fixed at 450 °C and the reformer temperature was varied at 500, 600 and 700 °C. The solid, liquid and gaseous product were collected and analyzed to understand the effect of reforming temperature on product yield and quality.

4.5.1.1 Product distribution and yields

Figure 4.12 shows the effect of reforming temperature on the product distribution and yields of liquid, gases, and solid products.



(a): calculated by difference

Figure 4.12 Product distribution and yield at three different reforming temperatures for a reactor temperature of 450°C

Increasing the reformer temperature from 500 °C to 700 °C shows a significant decrease in the bio-oil, biochar and aqueous phase yield, along with increase in the gases yield. Neumann, Meyer [37] investigated the effect of reforming temperature on product distribution and found a direct relationship with reforming temperature and attributed the product distribution to six primary post-reforming reactions, as shown in Table 4.8. The effect of reforming temperature on the biochar yield can be seen with 24 % reduction from 500 °C (23.14wt %) to 700 °C (17.66 wt %). This is due to conversion of char into permanent gases (as shown in Table 4.8 Reactions 1, 2, 3 & 6), where the fixed carbon in the char reacts with existing permanent gases to favor the formation of carbon monoxide, methane and hydrogen. The bio-oil yield also decreased by 60 % from 5.5 wt % (500 °C) to 2.22 wt % (700 °C). This reduction in the bio-oil yield at 700 °C is due to vapor cracking of organic vapors to form more permanent gases at higher reforming temperatures. The reduction in the aqueous

phase at 700 °C by 39 % from 23.79 wt % (500 °C) to 14.55 wt % (700 °C) is also due to forward water gas shift reaction (Table 4.8 Reaction 5), which promotes the formation of hydrogen at higher temperatures. Thus, at a reforming temperature of 700 °C, there was a 38 % increase in permanent gases produced from 47.57 wt % (500 °C) to 65.57 wt % (700 °C) at the expense of reduction in bio-oil, biochar and aqueous phase. These results are in agreement with Neumann, Meyer [37] and Ahmad, Jäger [32] which also showed an increase in gas production at the expense of reduction in bio-oil and biochar yield for the feedstocks: anaerobic digestate and sugarcane bagasse respectively.

4.5.1.2 Biochar characterization

The elemental analysis and the heating value of the biochar at increasing reforming temperatures can be seen in Table 4.9. There was an increase in the carbon content and decrease in the hydrogen and oxygen content of the biochar at higher reforming temperatures. The carbon content increased from 90.96 wt % (500 °C) to 93.54 wt % (700 °C). There was an overall decrease in the O/C and H/C ratio with increase in the reforming temperature, thus indicating higher stability of char. There was almost negligible effect in the heating value of the biochar, where it decreased from 33.96 MJ/kg (500 °C) to 32.37 MJ/kg (700 °C).

Table 4.9 Characterization of the TCR-2 biochar produced from woody feedstock at different reforming temperatures

Reforming Temperature	500 °C	600 °C	700 °C
Ultimate Analysis (dry basis) (wt %)			
Carbon	90.96	93.26	93.54
Hydrogen	2.44	1.47	1.23
Nitrogen	0.16	0.13	0.12
Sulfur	0	0	0
Oxygen (a)	6.45	5.14	5.11
O/C	0.07	0.06	0.05
H/C	0.03	0.01	0.01
HHV (MJ/kg)	33.96	32.57	32.37

The SEM images of the softwood pellets and the biochar obtained at different reforming temperatures are displayed in Figure 4.13. Biochar (450, 500) denotes biochar produced at a pyrolysis temperature of 450 °C and a reformer temperature of 500 °C. Similarly, biochar (450, 600) and biochar (450, 700) denote a reformer temperature of 600 °C and 700 °C, respectively. The biochar obtained at all reformer temperatures show thermal cracks and pores being formed, whereas, the raw softwood pellets has a lumpy dense structure. The increase in reforming temperature has further increased the intensity of the destruction of the fibers, thereby leading to dramatic increase of 2155 % in the BET surface area. The BET surface area at 500 °C was observed to be 13.11 m²/g, which increased to 129.17 m²/g (600 °C), and further increased to 295.74 m²/g at 700 °C. However, the average pore radius decreased, and the pore volume increased with increase in reformer temperature (Table 4.10). This confirms that the higher reformer

temperatures lead to more fiber destruction, thus formation of more pores, which leads to increase in the pore volume and thereby increases the BET surface area. The formation of pores at higher reforming temperatures can be clearly seen in Figure 4.13(d). The SEM images of biochar produced from hardwood pellets and softwood chips are displayed in Appendix A.

The pore volume measure by the BET only accounts for pore size smaller than 50 nm, but it can be seen in the SEM images that some of the pores are quite large at a size of 10 – 20 μm . So, the pore volume measured by BET underestimates the actual pore volume of the biochar sample. Therefore, the total pore volume was measured from the following correlation used by Brewer, Chuang [63].

$$Porosity = 1 - \frac{\rho_{apparent}}{\rho_{particle}} \quad \text{Equation 15}$$

Where, $\rho_{apparent}$ is the apparent density, and $\rho_{particle}$ is the particle density.

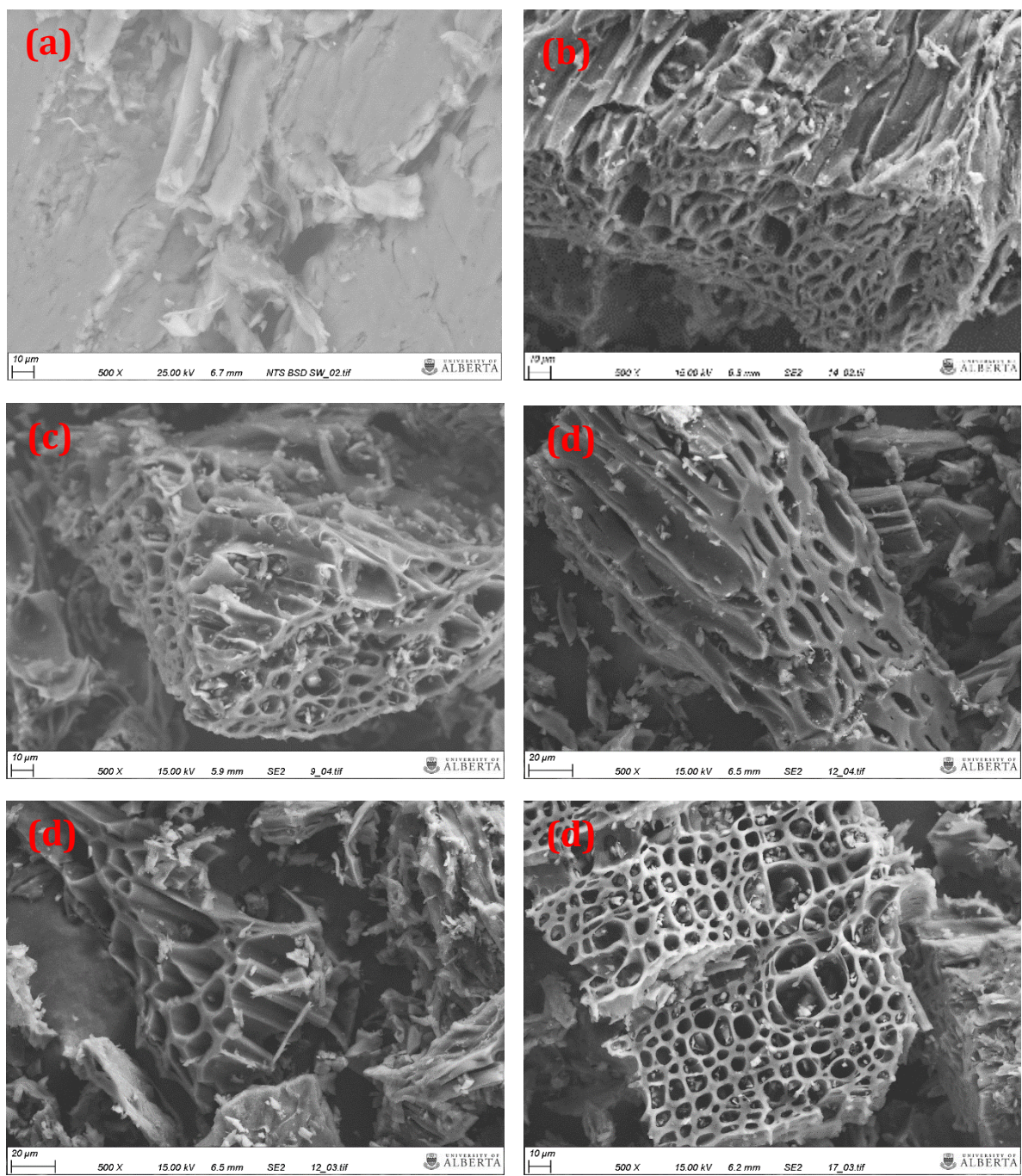


Figure 4.13 SEM images of the (a) softwood pellets (b) Biochar (450, 500) (c) Biochar (450, 600) (d) Biochar (450, 700)

Table 4.10 BET surface area, pore volume and average pore radius for softwood pellets biochar at different reformer temperatures

Reforming Temperature	500 °C	600 °C	700 °C
BET Surface area (m ² /g)	13.11± 3.5	129.17 ± 13	295.74 ± 30
Pore volume ¹ (cc/g)	0.0097	0.092	0.226
Average pore radius (nm)	1.48	1.53	1.49
Total Pore volume ² (cc/g)	1.606	1.755	1.976
Apparent density (g/cm ³)	0.44	0.42	0.39
Particle density ³ (g/cm ³)	1.5	1.6	1.7

¹measured by BET, pore volume for pore size less than 50 nm.

²calculates the total pore volume by the porosity correlation (Equation 15).

³particle density is assumed from the experiments performed by Brewer, Chuang [63] for fast pyrolysis of wood.

4.5.1.3 Bio-oil characterization

The elemental analysis, moisture content, TAN, viscosity and heating value of the bio-oils produced at three different reforming temperatures are listed in Table 4.11. The influence of reforming the bio-oil quality can be clearly seen through the result. Increase in reforming temperature led to increase in the carbon content and heating value of the bio-oil. At lower reforming temperatures of 500 °C, higher oxygen and water content was observed. Increase in reforming temperature also led to reduction of hydrogen, oxygen, nitrogen, and water content, resulting in much more stable oil at high reforming temperatures. It is important to note that the oxygen content decrease from 25.21 wt % (500 °C) to 11.78 wt % (700 °C) due to reforming of oxygenated compounds to form more permanent gases at higher reforming temperatures.

The TAN decreased from 15.14 mg KOH/g (600 °C) to 6.53 mg KOH/g (700 °C) due to catalytic cracking of organic acids in the reformer at higher reforming temperatures. The TCR-2 bio-oils have considerably lower TAN compared to bio-oil produced from the fast pyrolysis of wood (90-110 mg KOH/g) [62]. Liquid fuels with lower TAN's are favorable as they reduce wear and corrosion in downstream pipes and engine components. The viscosity of the bio-oil also decreased with increase in reforming temperature. Viscosity is an important feature in considering the fuel pumping and delivery aspects. Fuels with higher viscosities need additional measures for transportation.

Table 4.11 Characterization of the TCR-2 bio-oil produced from woody feedstock at different reforming temperatures

Reforming Temperature	500 °C	600 °C	700 °C
Ultimate Analysis (dry basis) (wt %)			
Carbon	67.48	78.04	80.44
Hydrogen	7.06	6.71	6.66
Nitrogen	0.26	0.42	0.35
Sulfur	0	0	0
Oxygen	25.21	14.09	11.78
H ₂ O (wt %)	7.34	5.25	3.41
TAN (mg KOH/g)	-	15.14 ± 3.45	6.53± 1.15
Viscosity (mPas)	-	32.86	13.77
HHV (MJ/kg)	29.26	32.6	34.25

The GC-MS analysis results for the bio-oil produced and at different reforming temperatures are displayed in Table 4.12 and Table 4.13. Since bio-oil is a very complex mixture of compounds, very small peaks unidentifiable peaks were ignored. It was observed that at a reformer temperature of 500 °C, majority of the bio-oil comprised of phenol and simple phenol derivatives such as phenol, 3-methyl, phenol, 2, 6-dimethyl and so on. The bio-oil at 500 °C also had some PAHs and MAHs along with furans and N-compounds and pyridine derivatives. Increasing the reforming temperature to 600 °C led to reduction of phenols, furans and MAHs, and increase in PAHs. This is due to breaking of phenolic compounds and furans into different compounds at higher reforming temperatures. Further increase in reforming temperature to 700 °C led to significant reduction in the phenolic compounds and furans along with increase in PAHs and MAHs. This indicates that at higher reforming temperatures phenol and its derivatives undergo secondary cracking reactions, such as deoxygenation reactions to yield more aromatics. The most abundant aromatic compound found in the TCR bio-oil produced at 700 °C was naphthalene and its derivatives at 20.54 % followed by phenanthrene at 8.59 %.

Thus, it can be said that higher reforming temperatures produce bio-oils with higher stability due to lower oxygen and water content, and improved physical properties.

Table 4.12 Summarized GC-MS results for bio-oil produced at different reforming temperatures

Area %	500 °C	600 °C	700 °C
PAHs	13.44	44.00	50.36
MAHs	20.05	6.80	13.68
Phenols & Alcohols	56.70	41.59	29.22
Furans	8.64	5.49	4.09
Acids	0.00	0.00	0.83
Esters	0.00	1.10	0.92
N-compounds	1.17	0.65	0.35

Table 4.13 Detailed GC-MS results for the bio-oil produced at different reforming temperatures

Reforming Temperature		500 °C	600 °C	700 °C
Library/ID	RT	% Area	% Area	% Area
1H-Imidazole, 1,5-dimethyl-	4.59	0.45	-	-
Bicyclo[4.2.0]octa-1,3,5-triene	6.01	-	-	0.52
Styrene	6.05	-	0.41	-
Phenol	8.91	1.79	2.82	2.40
Indene	9.71	-	3.81	8.76
Phenol, 2-methyl-	10.29	4.77	7.03	3.88
p-Cresol	10.82	12.36	-	-
Phenol, 3-methyl-	10.86	-	13.77	11.62
Phenol, 2,6-dimethyl-	11.06	0.64	-	-
1H-Indene, 1-methyl-	11.67	-	1.50	-
Benzene, 1-butynyl-	11.71	-	-	1.52
Phenol, 3,5-dimethyl-	11.91	9.50	-	-
Phenol, 2,4-dimethyl-	11.98	-	4.86	1.53
m-Cresyl acetate	12.08	-	-	0.95
Acetic acid, 4-methylphenyl ester	12.16	-	1.10	0.92
Azulene	12.23	6.84	-	-
Naphthalene	12.29	-	9.15	7.36
Phenol, 4-ethyl-	12.59	-	-	0.33
Phenol, 2-ethyl-	12.61	0.62	0.50	-
Benzofuran, 4,7-dimethyl-	12.72	-	0.50	0.29

Catechol	12.92	7.50	-	-
Benzaldehyde, 3-methyl-	12.92	-	-	0.86
Benzofuran, 2,3-dihydro-	13.08	-	2.30	1.07
Phenol, 4-ethyl-3-methyl-	13.23	1.69	-	-
Phenol, 3-ethyl-5-methyl-	13.56	0.67	0.77	-
1H-Imidazo(4,5-d)pyridazine	13.71	-	-	0.35
Phenol, 2,4,6-trimethyl-	13.73	-	0.47	-
1,2-Benzenediol, 3-methyl-	13.82	3.00	-	-
Naphthalene, 1-methyl-	13.91	1.43	-	-
Naphthalene, 2-methyl-	14.00	-	10.32	14.43
1,2-Benzenediol, 4-methyl-	14.42	-	0.33	-
Benzaldehyde, 3,5-dimethyl-	14.43	15.81	-	-
Benzofuran, 7-methyl-	14.52	-	0.39	-
Biphenyl	14.69	-	1.17	-
1,3-Benzenediol, 4,5-dimethyl-	14.78	1.83	-	-
Benzaldehyde, 4-(1-methylethyl)-	15.07	4.25	-	-
4-Ethylcatechol	15.19	2.43	-	-
Phenol, 3-butoxy-	15.60	12.30	-	-
Naphthalene, 1,3-dimethyl-	15.10	-	2.06	2.08
Naphthalene, 1,6-dimethyl-	15.28	-	1.31	0.83
Naphthalene, 2,7-dimethyl-	15.46	-	0.88	0.68
Naphthalene, 2-ethenyl-	15.69	-	0.42	-
Naphthalene, 1,4-dimethyl-	15.82	-	2.20	1.70
2-Propyn-1-ol, 3-(4-methylphenyl)-	15.89	-	0.47	-
Biphenylene	15.90	0.46	-	-
1,4-Benzenediol, 2,6-dimethyl-	16.00	-	0.38	-
Phenol, 4-ethyl-2-methoxy-	16.06	0.97	6.70	7.31
1,1'-Biphenyl, 4-methyl-	16.23	0.91	-	-
Acenaphthene	16.44	-	0.37	0.38
1,3-Benzenediol, 4-propyl-	16.50	-	0.42	0.34
Dibenzofuran	16.68	2.44	-	-
1-Naphthalenol	16.88	0.69	1.79	1.44
2-Naphthalenol	17.01	-	0.42	0.38
1,1'-Biphenyl, 3-methyl-	17.23	0.83	2.11	1.28
Naphthalene, 2-(1-methylethenyl)-	17.39	-	0.33	0.82
1H-Phenalene	17.48	-	-	0.65
Fluorene-9-methanol	17.50	-	0.65	-
Fluorene	17.68	0.41	3.53	4.24
trans-3-(2-Nitrovinyl)pyridine	17.80	0.73	-	-
2-Naphthalenol, acetate	17.83	-	0.53	-
1-Naphthalenol, 2-methyl-	18.26	1.62	-	-

1-Naphthalenol, 4-methyl-	18.38	0.52	-	-
Dibenzofuran, 4-methyl-	18.12	-	0.72	0.61
Dibenzofuran, 4-methyl-	18.31	-	0.47	0.49
9H-Fluoren-9-one	19.03	-	0.74	1.01
9H-Fluorene, 1-methyl-	19.09	-	0.38	0.33
3H-Benz[e]indene, 2-methyl-	19.19	-	-	0.45
(E)-Stilbene	19.21	-	0.53	-
Benzene, 2,6-dimethyl-1-(phenylmethyl)-	19.33	-	-	0.24
Benzo[b]benzofuran-2-carboxaldehyde	19.56	-	-	0.27
4-[2-(4-Methylphenyl)ethenyl]pyridin	19.58	-	0.36	-
Phenanthrene	19.93	0.88	5.91	7.11
Benzenamine, 4,4'-methylenebis-	20.80	-	0.29	-
Anthracene	20.12	-	-	1.66
2-Dibenzofuranol	21.03	-	0.33	-
Phenanthrene, 1-methyl-	21.17	-	1.14	1.48
Anthracene, 1-methyl-	21.28	-	0.71	-
Anthracene, 9-methyl-	21.29	-	-	0.43
Benzaldehyde, 3,5-dichloro-2-hydroxy-	21.37	-	1.09	1.59
2,6-Diisopropyl-naphthalene	21.89	0.34	-	-
2-Propenoic acid, 3-(2-naphthalenyl)-	22.16	-	-	0.31
9,10-Bis(bromomethyl)anthracene	22.55	-	-	0.37
Fluoranthene	22.78	-	0.54	1.56
10,18-Bisnorabieta-5,7,9(10),11,13-pentaene	22.83	0.44	-	-
Pyrene	23.30	-	0.65	1.33
2(1H)-Quinolinone, 4-phenyl-	23.44	0.35	-	-
Pyrene, 1-methyl-	23.83	-	-	0.67
Retene	23.96	0.55	-	-
11H-Benzo[a]fluorene	24.25	-	-	0.34
Triphenylene	26.08	-	-	0.26
Sum		100.00	99.63	99.45

4.5.1.4 Permanent gases composition and properties

The influence of reforming temperature on the composition of the TCR-2 gases can be seen in Table 4.14 and Figure 4.14. With increase in reforming temperature, there is a significant increase in the hydrogen from 9 vol % (500 °C) to 15 vol % (700 °C).

However, the composition of methane, carbon monoxide and carbon dioxide decrease with the increase in the reforming temperature. This is due to the fact that methane, carbon monoxide and carbon dioxide reacts to form more hydrogen according to Table 4.8 (Reactions 1, 2, 4 & 5) indicating forward water gas shift reaction and methane reforming reaction. Small amounts of C2, C3 and C3+ were detected at all three reforming temperatures and there was no significant effect of reforming temperature observed on its composition.

Table 4.14 Composition of the TCR-2 gases produced from softwood pellets at different reforming temperatures at a fixed pyrolysis temperature of 450 °C

Reformer Temperature	500 °C	600 °C	700 °C
Gas Composition (Vol %)			
Hydrogen	9.16	13.39	15.09
Methane	32.41	28.46	28.28
Carbon monoxide	25.20	24.73	24.81
Carbon dioxide	32.18	31.58	30.60
C2	0.61	0.73	0.45
C3	0.45	0.68	0.39
C3+	0.00	0.44	0.37

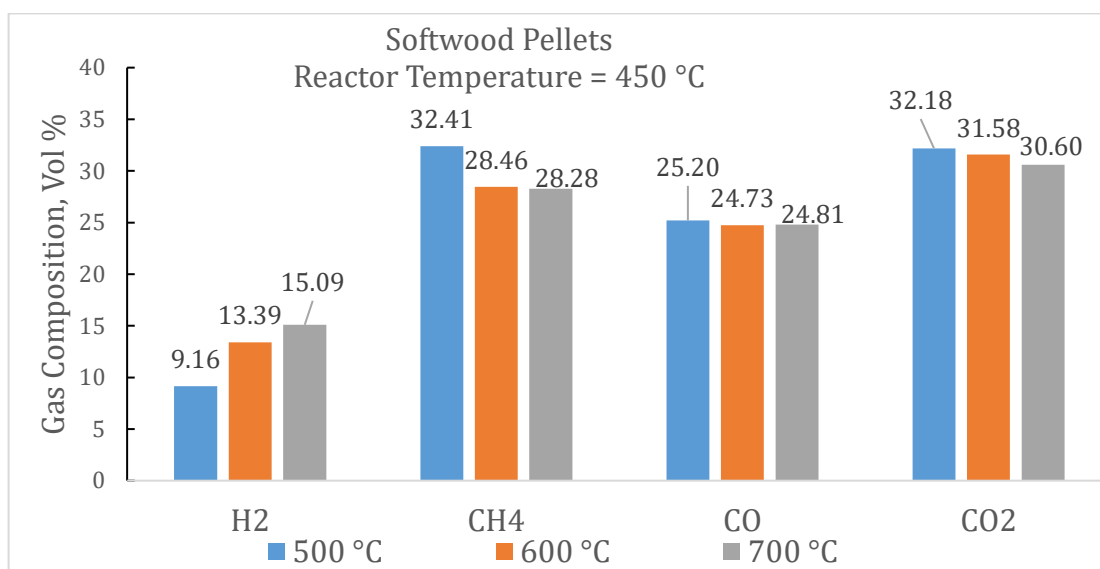


Figure 4.14 Graphical representation of effect of reforming temperature on the TCR-2 gases produced from softwood pellets at a fixed pyrolysis temperature of 450 °C

Thus, higher reforming temperature of 700 °C produces a TCR-2 gas with higher hydrogen content, and lower methane, carbon monoxide and carbon dioxide content.

4.5.2 Effect of Reactor Temperature

The reformer temperature was fixed at 600 °C and the reactor temperature was varied from 400 – 550 °C to observe its effect on the product yield and distribution, and also to establish the optimum conditions for maximum bio-oil yield. The effect of reactor temperature on the product yield and distribution can be seen in Figure 4.15. It can be clearly said that the bio-oil yield increases from 3.8 wt % to 5.86 %, with the increase in reactor temperature from 400 °C to 500 °C. But increasing the reactor temperature further to 550 °C decreases the bio-oil yield. Thus, the bio-oil yield only increases till a certain reactor temperature and decreases on further

increasing the reactor temperature. There is no definite trend in the distribution of biochar, aqueous phase and gas yield on increasing the reactor temperature. Although, it is interesting to note that increasing the reactor temperature from 500 °C to 550 shows a dramatic increase of 47 % in the aqueous phase along with reduction of gases and bio-oil by 10 % and 23 % respectively. There is negligible effect on the bio-char yield with increase in the reactor temperature. This suggests that with increase in the reactor temperature beyond 500 °C, there is a possibility that the bio-oil undergoes secondary cracking that results in the production of product water and permanent gases, thus explaining the increase in aqueous phase and gases at 550 °C.

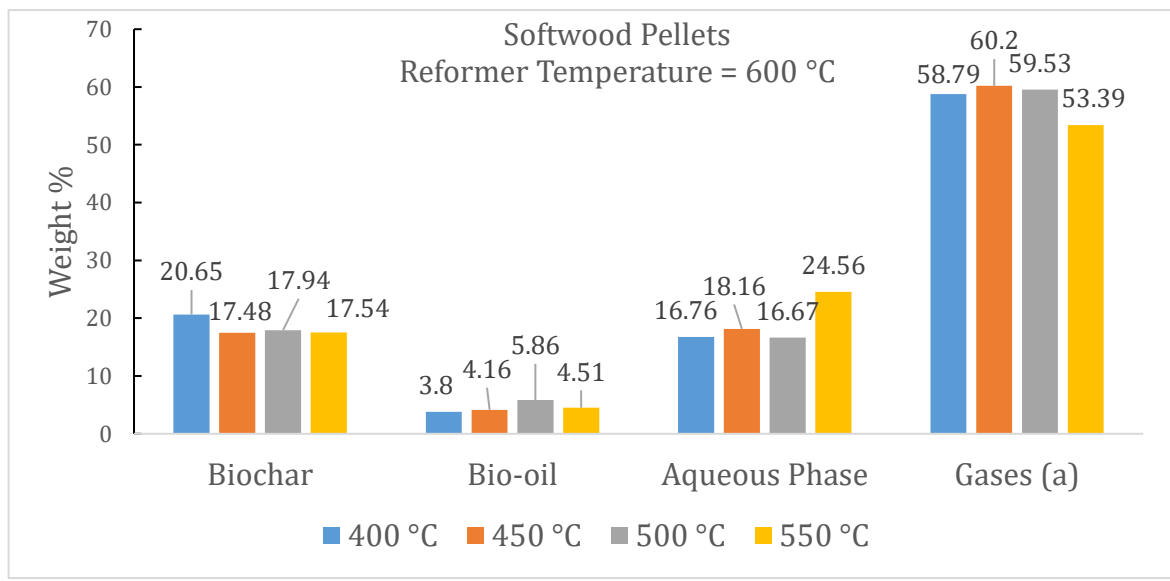


Figure 4.15 Influence of reactor temperature on the product yield and distribution at a fixed reforming temperature of 600 °C

The CHNS analysis results of the biochar and bio-oil produced at different reactor temperatures can be seen in Table 4.15 and Table 4.16 respectively. It can be noted

that there is negligible effect on the composition of the biochar with increase in the reactor temperature. On the contrary, increasing the reactor temperature till 500 °C results in increase of the carbon content and decrease in the oxygen content. But increasing the reactor temperature further to 550 °C decreases the carbon content and increases the oxygen content. The production of bio-oil with higher carbon content and lower oxygen content is favorable.

The bio-oils produced were also analyzed in GC-MS to identify the chemical composition and its variation with the reactor temperature. As can be seen in Figure 4.16, the number of PAHs and MAHs increases quite significantly till a reactor temperature of 500 °C, and then decreases sharply on further increasing the temperature to 550 °C. On the other hand, the number of phenolic compounds and derivatives decreases till a reactor temperature of 500 °C and increases sharply on further increasing the reactor temperature to 550 °C. The number of oxygen-containing compounds such as furans was observed to be lowest at 500 °C (2.80 area %) and increased dramatically at 550 °C (10.67 area %). One of the possible reasons for this trend in the bio-oil composition could be due to presence of excess aqueous phase (24.56 wt % at 550 °C), which results in the formation of more oxygen-containing compounds and phenolic derivatives. Thus, the optimal reactor temperature for bio-oil production from softwood pellets is 500 °C in terms of quality and quantity both.

Table 4.15 Characterization of TCR biochar at different reactor temperatures and a fixed reforming temperature of 600 °C

Reactor Temperature	400 °C	450 °C	500 °C	550 °C
Ultimate analysis (dry basis) (wt %)				
Carbon	93.27	93.26	92.23	93.59
Hydrogen	1.58	1.47	1.45	1.56
Nitrogen	0.11	0.13	0.13	0.11
Sulfur	0.00	0.00	0.00	0.00
Oxygen	5.04	5.14	6.20	4.73
O/C	0.05	0.06	0.07	0.05
H/C	0.02	0.01	0.02	0.02
HHV (MJ/kg)	33.90	32.57	32.04	34.03

Table 4.16 Characterization of TCR bio-oil at different reactor temperatures and a fixed reforming temperature of 600 °C

Reactor Temperature	400 °C	450 °C	500 °C	550 °C
Ultimate Analysis (dry basis) (wt %)				
Carbon	74.91	78.04	78.44	75.94
Hydrogen	6.74	6.71	6.90	6.69
Nitrogen	0.36	0.42	0.47	0.37
Sulfur	0.00	0.00	0.00	0.00
Oxygen	18.00	14.09	14.19	17.01
H ₂ O (wt %)	4.46	5.25	-	3.89
TAN (mg KOH/g)	-	17.14 ± 3.45	-	-
Viscosity (mPas)	-	32.86	-	-
HHV (MJ/kg)	32.23	32.60	33.08	32.63

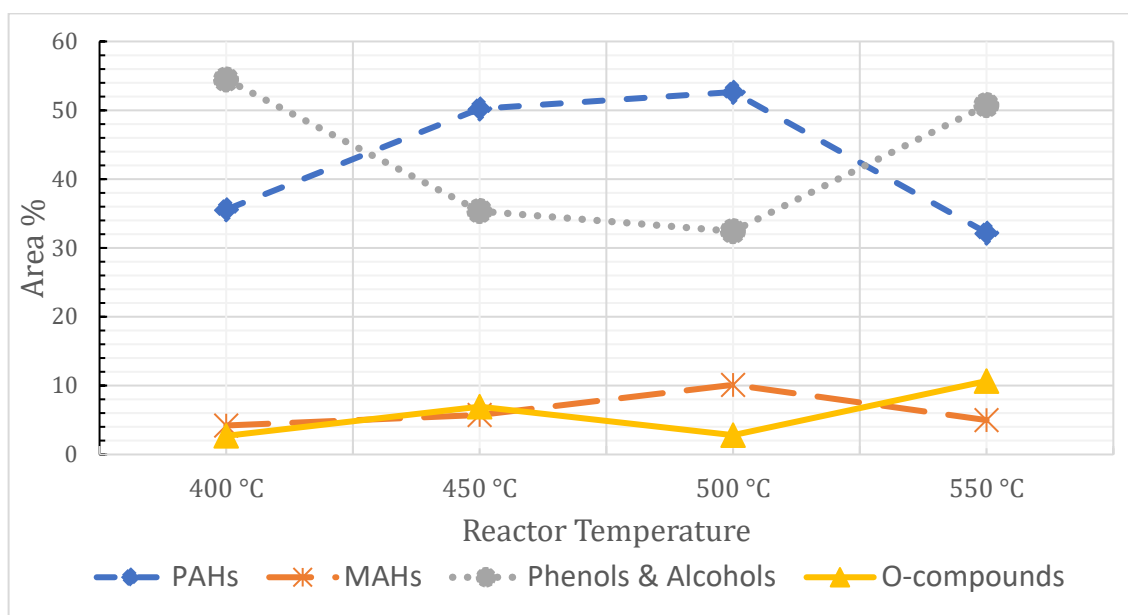


Figure 4.16 Influence of reactor temperature on the composition of the TCR bio-oil at a fixed reformer temperature of 600 °C

The composition of the TCR gases produced at different reactor temperatures are displayed in Figure 4.17. The effect of reactor temperature on the TCR gases can be mainly seen through the hydrogen and carbon monoxide content. The hydrogen content decreases with increase in reactor temperature till 500 °C and increases on further increase in reactor temperature to 550 °C. The opposite trend is observed for carbon monoxide, which increases till 500 °C and decreases on further increasing the reactor temperature to 550 °C. It is interesting to note that the sum of hydrogen and carbon monoxide remains the same. Also, the effect on the methane and carbon dioxide content is almost negligible. This trend in the composition of gases can be explained by the reactions listed in Table 4.8.

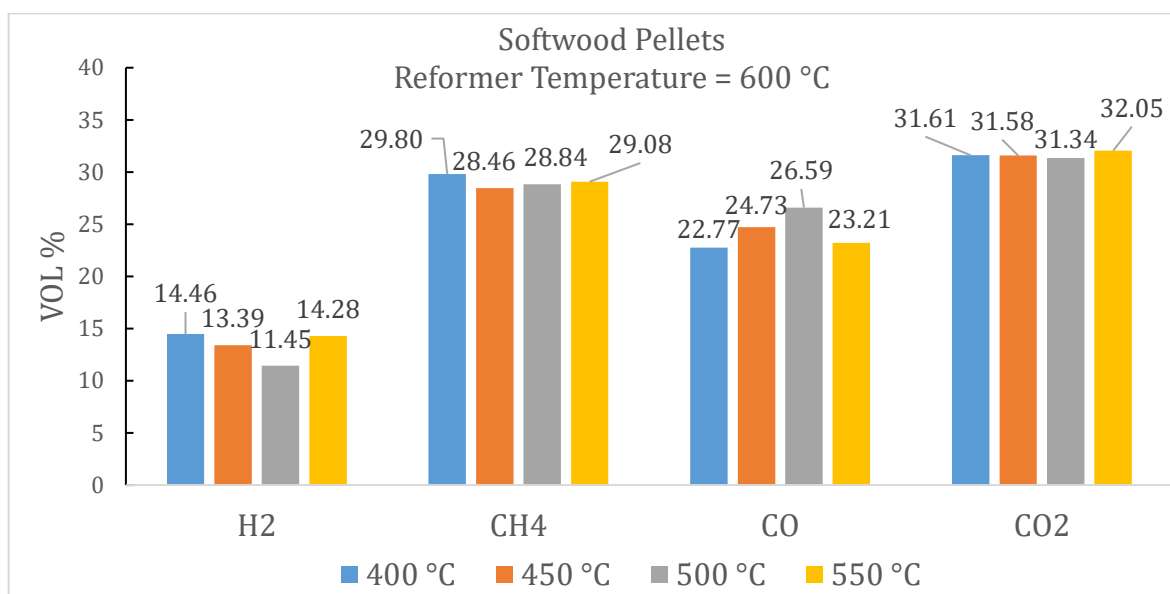


Figure 4.17 Influence of reactor temperature on the TCR gas composition at a fixed reforming temperature of 600 °C

4.5.3 Effect of Biochar Pre-filling

Approximately 500 g of biochar produced from previous experiments is added to the reformer to create a pre-existing biochar bed for catalytic action from the beginning of the experiment. The effect of biochar pre-filling on the product yield and distribution can be seen in Figure 4.18 and Figure 4.19. The presence of pre-existing biochar bed increases the bio-oil, aqueous phase, and the gas yield by decreasing the biochar yield for a reformer temperature of 500 °C. But at a reformer temperature of 600 °C there is minimal to negligible effect on the product yields. The increase in bio-oil, aqueous phase and gas yield is due to the reforming of the pyrolysis products at the beginning of the experiment rather than waiting for the formation of biochar bed. At higher reforming temperatures, the effect of the

biochar pre-filling on the product yield and distribution is almost minimal to negligible.

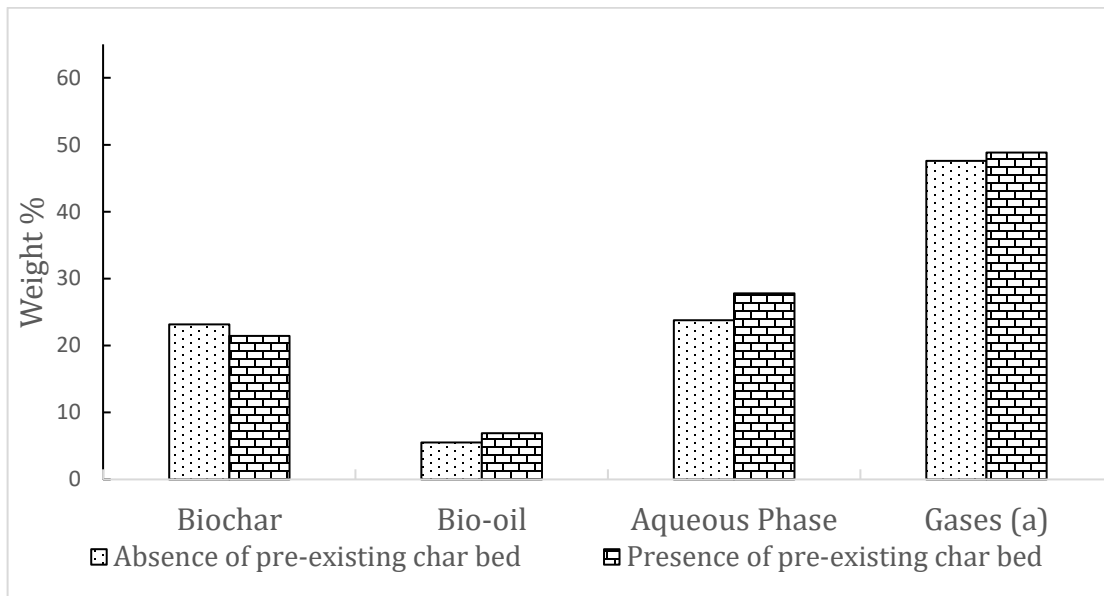


Figure 4.18 Influence of biochar pre-filling on the product yield at a reactor temperature of 450 °C and a reformer temperature of 500 °C

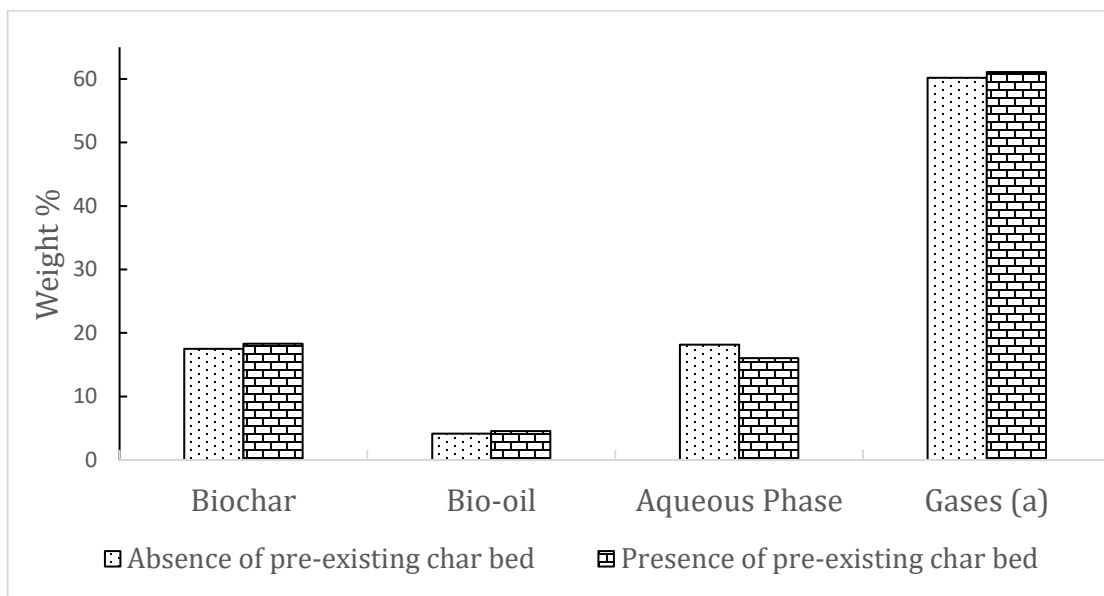


Figure 4.19 Influence of biochar pre-filling on the product yield at a reactor temperature of 450 °C and a reformer temperature of 600 °C

There is no significant effect of biochar pre-filling on the biochar and bio-oil properties. The only significant effect can be seen on the gas composition with increase in hydrogen content and decrease in methane and carbon monoxide content in the presence of biochar pre-filling (Figure 4.20 & Figure 4.21). Presence of biochar pre-filling results in the reforming of pyrolysis products from the beginning, thus increase in hydrogen and reduction of methane and carbon monoxide. This can also be seen in Figure 4.22, where the composition of the TCR gases in the presence of biochar pre-filling remains almost constant throughout the experiment. On the contrary in the absence of biochar pre-filling the hydrogen content increases gradually until a significant amount of biochar bed is formed.

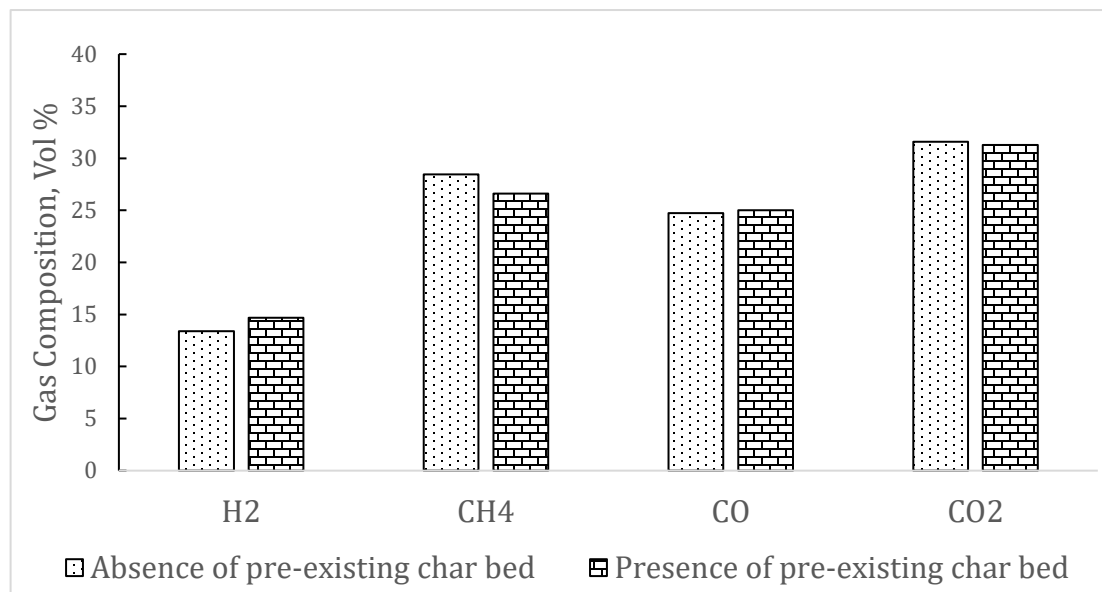


Figure 4.20 Influence of biochar pre-filling on the gas composition at a reactor temperature of 450 °C and a reformer temperature of 500 °C

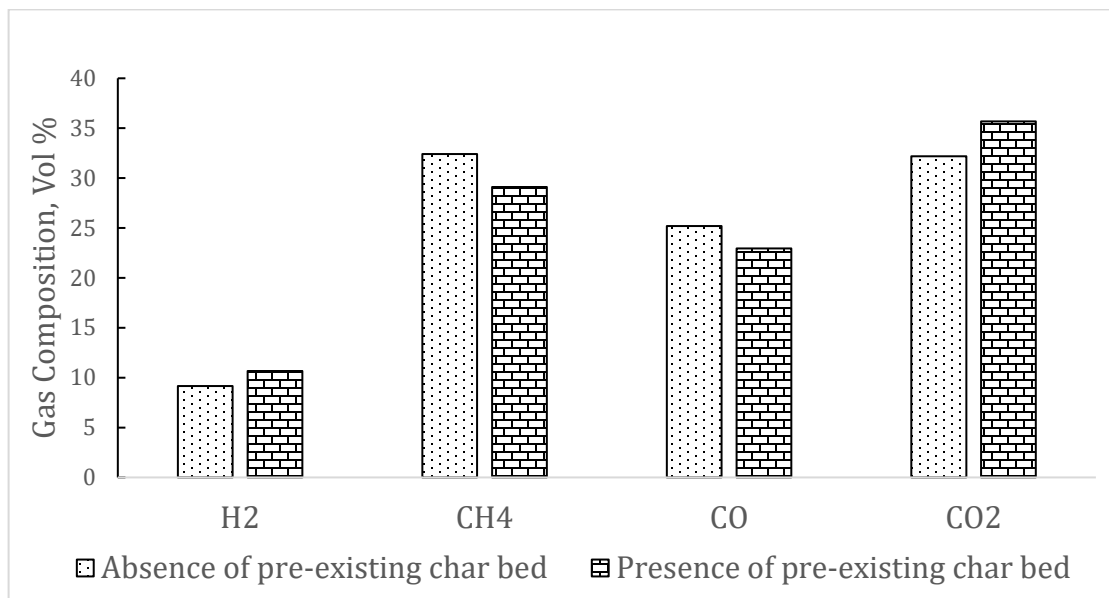


Figure 4.21 Influence of biochar pre-filling on the gas composition at a reactor temperature of 450 °C and a reformer temperature of 600 °C

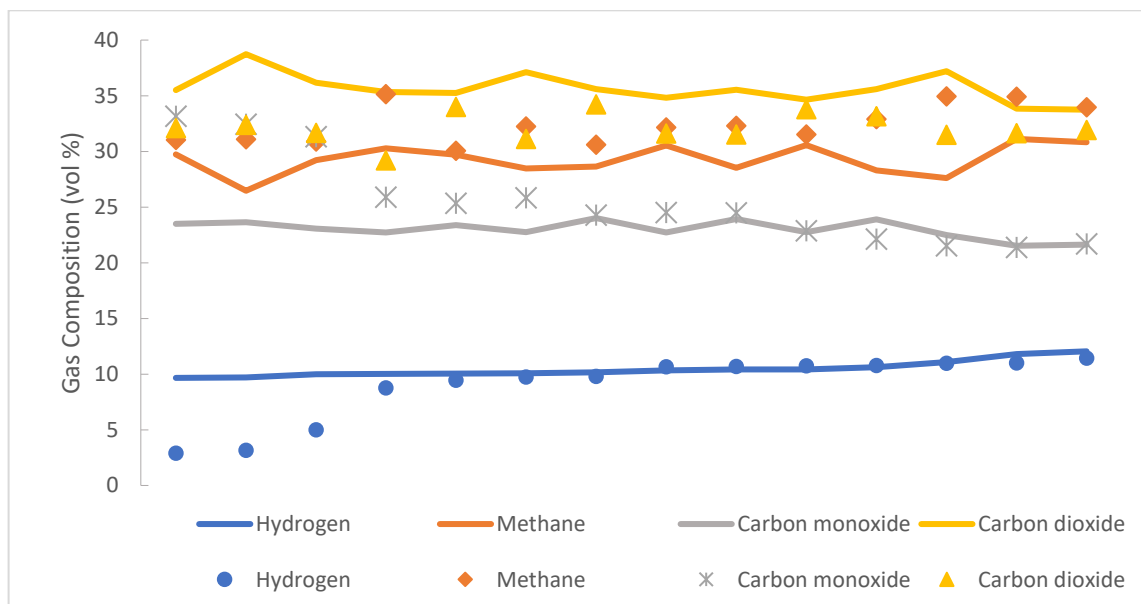


Figure 4.22 Composition of the TCR gases as a function of time throughout the experiment in the presence and absence of pre-existing biochar bed (solid line: presence of biochar pre-filling, dotted line: absence of biochar pre-filling)

Chapter 5

Conclusion and Future Work

5.1 Conclusion

The thermo-catalytic reforming of woody biomass produces combustible gases, fuel grade bio-oil and biochar with enhanced structural properties. It was observed that the composition of woody biomass feedstock had negligible to minor effect on the product distribution and characterization. The gases produced from all three woody feedstocks had similar compositions in terms of hydrogen (13 – 15 vol %), methane (27 – 29 vol %), carbon monoxide (~24 vol %), and carbon dioxide (30 – 31 vol %). The HHV of the gases produced from different woody feedstocks varied between 12.5 – 12.8 MJ/kg. The TCR bio-oil produced from all three woody feedstocks had a low water content and a heating value. The superior quality of the TCR bio-oil is reflected in the O/C ratio of 0.15 and its low TAN number, which is significantly lower than bio-oils from fast pyrolysis [62, 64]. The TCR biochar from all three woody feedstocks had a high heating value and high carbon content, low O/C and H/C ratio.

Increasing the reformer temperature to 700 °C increases the TCR gases yield at the expense of reduction in bio-oil and biochar yields. The produced TCR gases at 700 °C have higher hydrogen content and lower methane, carbon monoxide and carbon

dioxide content. At higher reforming temperatures, the produced bio-oils have lower TAN (6.53 mg KOH/g), viscosity (13.77 mPas), water content (3.41 %) and oxygen content (11.78 %), thus making it on a level that other pyrolysis bio-oils can only reach after HDO treatment. Moreover, the produced biochar had excellent structural and morphological properties ($295.74 \pm 30 \text{ m}^2/\text{g}$ BET surface area) suitable for applications in adsorption, catalysis and soil enrichment.

Increasing the reactor/pyrolysis temperature increase the bio-oil yield till a certain temperature (500 °C) only. Increasing the temperature further results in the decrease of the bio-oil yield. The quality of the bio-oils produced at different pyrolysis temperatures in terms of oxygenated compounds is found to be superior at a reactor temperature of 500 °C. The influence of presence of biochar pre-filling on product yields is almost negligible at higher reforming temperatures. The only major effect can be observed in terms of gas composition over time. Higher contents of hydrogen are observed from the start of the experiment rather than increasing gradually, which was observed in the absence of biochar pre-filling.

Thus, it can be concluded that the thermo-catalytic reforming of woody biomass produces much more superior quality of products at all conditions compared to conventional pyrolysis.

5.2 Future Work

Among all the Canadian biomass feedstocks available, only woody biomass feedstock has been investigated in TCR-2 so far. The next step would be to:

- Experiment with different feedstock such as, agricultural residues (corn stover and wheat straw), organic fraction of municipal solid waste and establish the optimal operating conditions in terms of bio-oil yield and quality.
- Upscale the experiments to a TCR-30 plant and establish the optimal operating conditions in terms of desired product yield and quality.

References

1. Natural Resources Canada. *Electricity facts*. 2019 [cited 2019 August 9]; Available from: <https://www.nrcan.gc.ca/electricity-facts/20068>.
2. Government of Canada. *Greenhouse gas emissions*. 2019 [cited 2019 August 12]; Available from: <https://www.canada.ca/en/environment-climate-change/services/environmental-indicators/greenhouse-gas-emissions.html>.
3. Natural Resources Canada. *How much forest does Canada have?* [cited 2019 August 9]; Available from: <https://www.nrcan.gc.ca/our-natural-resources/forests-and-forestry/state-canadas-forests-report/how-much-forest-does-canada-have/17601>.
4. The Canadian Encyclopedia. *Biomass Energy*. [cited 2019 August 9]; Available from: <https://www.thecanadianencyclopedia.ca/en/article/biomass-energy>.
5. Bridgwater, A., 7 - *Fast pyrolysis of biomass for the production of liquids A2 - Rosendahl, Lasse*, in *Biomass Combustion Science, Technology and Engineering*. 2013, Woodhead Publishing. p. 130-171.
6. Bridgwater, A.V., *Review of fast pyrolysis of biomass and product upgrading*. *Biomass and Bioenergy*, 2012. **38**: p. 68-94.
7. Onay, O. and O.M. Kockar, *Slow, fast and flash pyrolysis of rapeseed*. *Renewable Energy*, 2003. **28**(15): p. 2417-2433.
8. Sadegh-Vaziri, R. and M.U. Babler, *Modeling of slow pyrolysis of various biomass feedstock in a rotary drum using TGA data*. *Chemical Engineering and Processing - Process Intensification*, 2018. **129**: p. 95-102.
9. Yu, S., et al., *Characterization of biochar and byproducts from slow pyrolysis of hinoki cypress*. *Bioresource Technology Reports*, 2019. **6**: p. 217-222.
10. Hornung, A., 8 - *Intermediate pyrolysis of biomass A2 - Rosendahl, Lasse*, in *Biomass Combustion Science, Technology and Engineering*. 2013, Woodhead Publishing. p. 172-186.
11. Kebelmann, K., et al., *Thermo-chemical behaviour and chemical product formation from Polar seaweeds during intermediate pyrolysis*. *Journal of Analytical and Applied Pyrolysis*, 2013. **104**: p. 131-138.
12. Nils Jager, J.N., Andreas Apfelbacher, Robert Daschner, Andreas Hornung, *Two decades of intermediate pyrolysis: A major step towards CHP applicable bio-oils*, F. UMSICHT, Editor.
13. Ouadi, M., et al., *The intermediate pyrolysis of de-inking sludge to produce a sustainable liquid fuel*. *Journal of Analytical and Applied Pyrolysis*, 2013. **102**: p. 24-32.
14. Yang, Y., et al., *Intermediate pyrolysis of biomass energy pellets for producing sustainable liquid, gaseous and solid fuels*. *Bioresource Technology*, 2014. **169**: p. 794-799.

15. Sharifzadeh, M., et al., *The multi-scale challenges of biomass fast pyrolysis and bio-oil upgrading: Review of the state of art and future research directions*. Progress in Energy and Combustion Science, 2019. **71**: p. 1-80.
16. Binder, S., et al., *SYSTEM AND METHOD FOR THERMOCATALYTIC TREATMENT OF MATERIAL AND PYROLYSIS OIL PRODUCED THEREWITH*, F.U. Sulzbach-Rosenberg, Editor. 2014: Germany.
17. Goyal, H.B., D. Seal, and R.C. Saxena, *Bio-fuels from thermochemical conversion of renewable resources: A review*. Renewable and Sustainable Energy Reviews, 2008. **12**(2): p. 504-517.
18. Panwar, N.L., R. Kothari, and V.V. Tyagi, *Thermo chemical conversion of biomass – Eco friendly energy routes*. Renewable and Sustainable Energy Reviews, 2012. **16**(4): p. 1801-1816.
19. Yang, H., et al., *In-Depth Investigation of Biomass Pyrolysis Based on Three Major Components: Hemicellulose, Cellulose and Lignin*. Energy & Fuels, 2006. **20**(1): p. 388-393.
20. Ben, H., *Thermal conversion of biomass and biomass components to biofuels and bio-chemicals*, in *School of Chemistry and Biochemistry*. 2013, Georgia Institute of Technology.
21. Greenhalf, C., *Thermochemical characterisation of various biomass feedstock and bio-oil generated by fast pyrolysis*. 2014, Ashton University.
22. Zanzi, R., *Pyrolysis of biomass. Rapid pyrolysis at high temperature. Slow pyrolysis for active carbon preparation*, in *Trita-KET*. 2001, Kemiteknik: Stockholm. p. 52.
23. Holtzapple, M.T., *HEMICELLULOSES A2 - Caballero, Benjamin*, in *Encyclopedia of Food Sciences and Nutrition (Second Edition)*. 2003, Academic Press: Oxford. p. 3060-3071.
24. Dhyani, V. and T. Bhaskar, *A comprehensive review on the pyrolysis of lignocellulosic biomass*. Renewable Energy, 2017.
25. Patil, N.D., N.R. Tanguy, and N. Yan, *3 - Lignin Interunit Linkages and Model Compounds*, in *Lignin in Polymer Composites*. 2016, William Andrew Publishing. p. 27-47.
26. Collard, F.-X. and J. Blin, *A review on pyrolysis of biomass constituents: Mechanisms and composition of the products obtained from the conversion of cellulose, hemicelluloses and lignin*. Renewable and Sustainable Energy Reviews, 2014. **38**(Supplement C): p. 594-608.
27. Basu, P., *Chapter 3 - Pyrolysis and Torrefaction*, in *Biomass Gasification and Pyrolysis*. 2010, Academic Press: Boston. p. 65-96.
28. Onay, Ö., S.H. Beis, and Ö.M. Koçkar, *Fast pyrolysis of rape seed in a well-swept fixed-bed reactor*. Journal of Analytical and Applied Pyrolysis, 2001. **58-59**: p. 995-1007.
29. Wagenaar, B.M., W. Prins, and W.P.M. van Swaaij, *Pyrolysis of biomass in the rotating cone reactor: modelling and experimental justification*. Chemical Engineering Science, 1994. **49**(24, Part 2): p. 5109-5126.

30. Conti, R., et al., *Thermocatalytic Reforming of Biomass Waste Streams*. Energy Technology, 2017. **5**(1): p. 104-110.
31. TOSYNFUEL. *Technology and Innovation*. [cited 2019 January 14]; Available from: http://www.tosynfuel.eu/?page_id=1937.
32. Ahmad, E., et al., *Integrated thermo-catalytic reforming of residual sugarcane bagasse in a laboratory scale reactor*. Fuel Processing Technology, 2018. **171**: p. 277-286.
33. Jäger, N., et al., *Thermo-Catalytic Reforming of Woody Biomass*. Energy & Fuels, 2016. **30**(10): p. 7923-7929.
34. Kirby, M.E., et al., *The role of thermo-catalytic reforming for energy recovery from food and drink supply chain wastes*. Energy Procedia, 2017. **123**: p. 15-21.
35. Neumann, J., et al., *Production and characterization of a new quality pyrolysis oil, char and syngas from digestate – Introducing the thermo-catalytic reforming process*. Journal of Analytical and Applied Pyrolysis, 2015. **113**: p. 137-142.
36. Neumann, J., et al., *Upgraded biofuel from residue biomass by Thermo-Catalytic Reforming and hydrodeoxygenation*. Biomass and Bioenergy, 2016. **89**(Supplement C): p. 91-97.
37. Neumann, J., et al., *The conversion of anaerobic digestion waste into biofuels via a novel Thermo-Catalytic Reforming process*. Waste Management, 2016. **47**(Part A): p. 141-148.
38. Ouadi, M., et al., *Thermo-catalytic reforming of co-form® rejects (waste cleansing wipes)*. Journal of Analytical and Applied Pyrolysis, 2018. **132**: p. 33-39.
39. Ouadi, M., et al., *Thermo-catalytic reforming of pulper rejects from a secondary fibre mill*. Renewable Energy Focus, 2018. **26**: p. 39-45.
40. Ouadi, M., et al., *Thermo-Catalytic Reforming of municipal solid waste*. Waste Management, 2017. **68**(Supplement C): p. 198-206.
41. Santos, J., et al., *Integrated Intermediate Catalytic Pyrolysis of Wheat Husk*. Food and Bioproducts Processing, 2018.
42. Santos, J., et al., *Integrated intermediate catalytic pyrolysis of wheat husk*. Food and Bioproducts Processing, 2019. **114**: p. 23-30.
43. Mahmood, A.S.N., et al., *The intermediate pyrolysis and catalytic steam reforming of Brewers spent grain*. Journal of Analytical and Applied Pyrolysis, 2013. **103**: p. 328-342.
44. Neumann, J., et al. *Experimental investigation of combustion, performance and emission characteristics of digestate pyrolysis oil in a compression ignition combined heat and power engine*. in *22nd European Biomass Conference and Exhibition*. 2014. Hamburg, Germany.
45. UMSICHT, F. *TCR Fuel*. [cited 2019 January 15]; Available from: https://www.umsicht-suro.fraunhofer.de/en/Our_Solution/BiobasedFuel.html.

46. UMSICHT, F. *TChar for water purification*. [cited 2019 January 15]; Available from: https://www.umsicht-suro.fraunhofer.de/en/Our_Solution/biochar.html.
47. *Standard Test Method for Determination of Total Solids in Biomass*. 2015.
48. Channiwala, S.A. and P.P. Parikh, *A unified correlation for estimating HHV of solid, liquid and gaseous fuels*. *Fuel*, 2002. **81**(8): p. 1051-1063.
49. BSI-British Standards Institution, *Solid biofuels. Determination of calorific value*. 2017: London.
50. Kissinger, H.E., *Reaction Kinetics in Differential Thermal Analysis*. *Analytical Chemistry*, 1957. **29**(11): p. 1702-1706.
51. Kissinger, H.E., *Variation of Peak Temperature With Heating Rate in Differential Thermal Analysis*. *Journal of Research of the National Bureau of Standards*, 1956. **57**.
52. Akahira, T. and T. Sunose, *Method of determining activation deterioration constant of electrical insulating materials*. *Res. Rep. Chiba Inst. Technol. (Sci. Technol.)*, 1971. **16**: p. 22-31.
53. Collazzo, G.C., et al., *A detailed non-isothermal kinetic study of elephant grass pyrolysis from different models*. *Applied Thermal Engineering*, 2017. **110**: p. 1200-1211.
54. Jiang, H., et al., *Pyrolysis kinetics of phenol-formaldehyde resin by non-isothermal thermogravimetry*. *Carbon*, 2010. **48**(2): p. 352-358.
55. Ahmad, M.S., et al., *Kinetic analyses and pyrolytic behavior of Para grass (Urochloa mutica) for its bioenergy potential*. *Bioresource Technology*, 2017. **224**: p. 708-713.
56. Serio, M.A., et al., *Kinetics of volatile product evolution in coal pyrolysis: experiment and theory*. *Energy & Fuels*, 1987. **1**(2): p. 138-152.
57. Scott, S.A., et al., *An algorithm for determining the kinetics of devolatilisation of complex solid fuels from thermogravimetric experiments*. *Chemical Engineering Science*, 2006. **61**: p. 2339.
58. Gašparovič, L., et al., *Calculation of Kinetic Parameters of the Thermal Decomposition of Wood by Distributed Activation Energy Model (DAEM)*. 2012.
59. Ding, Y., et al., *Comparative pyrolysis behaviors and reaction mechanisms of hardwood and softwood*. *Energy Conversion and Management*, 2017. **132**: p. 102-109.
60. BSI - British Standards Institution, *Gas Meters - Diaphragm gas meters*. 2017, BSI - British Standards Institution.
61. Regmi, B.P. and M. Agah, *Micro Gas Chromatography: An Overview of Critical Components and Their Integration*. *Analytical Chemistry*, 2018. **90**(22): p. 13133-13150.
62. Haarlemmer, G., et al., *Analysis and comparison of bio-oils obtained by hydrothermal liquefaction and fast pyrolysis of beech wood*. *Fuel*, 2016. **174**: p. 180-188.
63. Brewer, C.E., et al., *New approaches to measuring biochar density and porosity*. *Biomass and Bioenergy*, 2014. **66**: p. 176-185.

64. Elliott, D.C., et al., *Catalytic hydroprocessing of biomass fast pyrolysis bio-oil to produce hydrocarbon products*. Environmental Progress & Sustainable Energy, 2009. **28**(3): p. 441-449.

Appendix A

The experimental and calculated TGA curves by modified DAEM for wheat straw and corn stover are displayed in Figure 1 & 2.

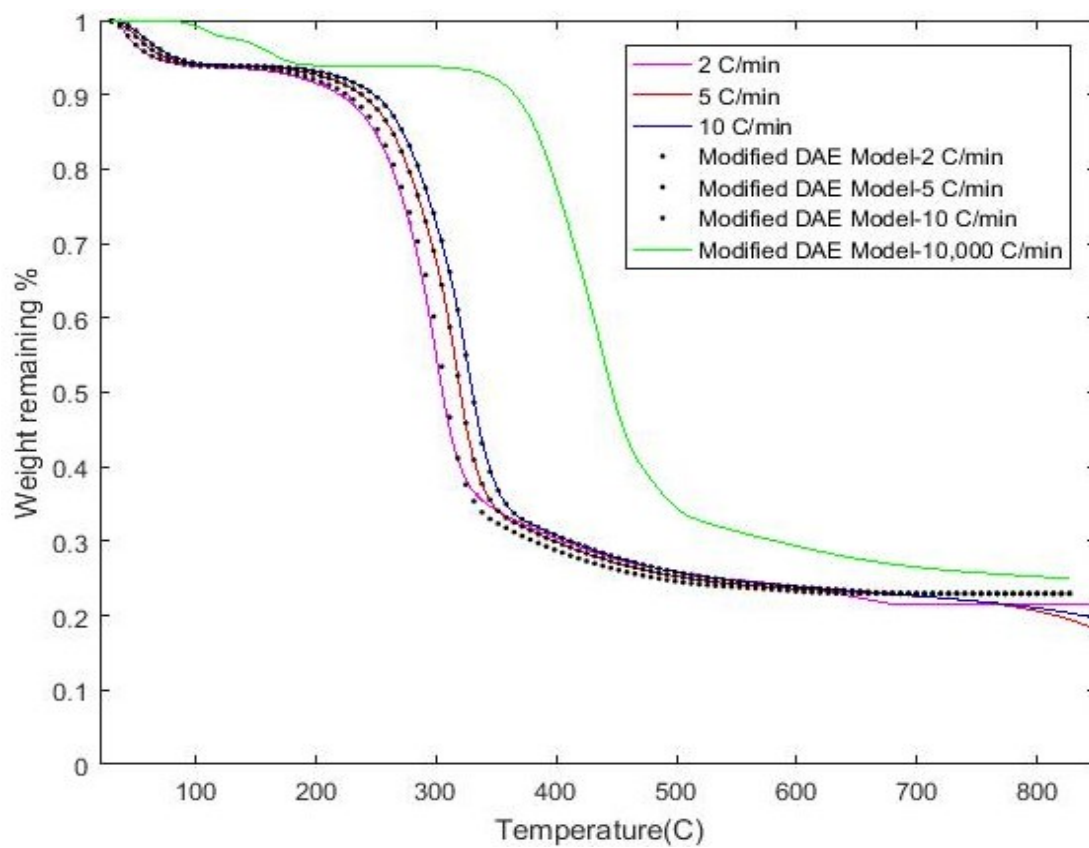


Figure 1 Experimental and modified DAEM curves for pyrolysis decomposition of wheat straw at 2, 5 and 10 °C/min

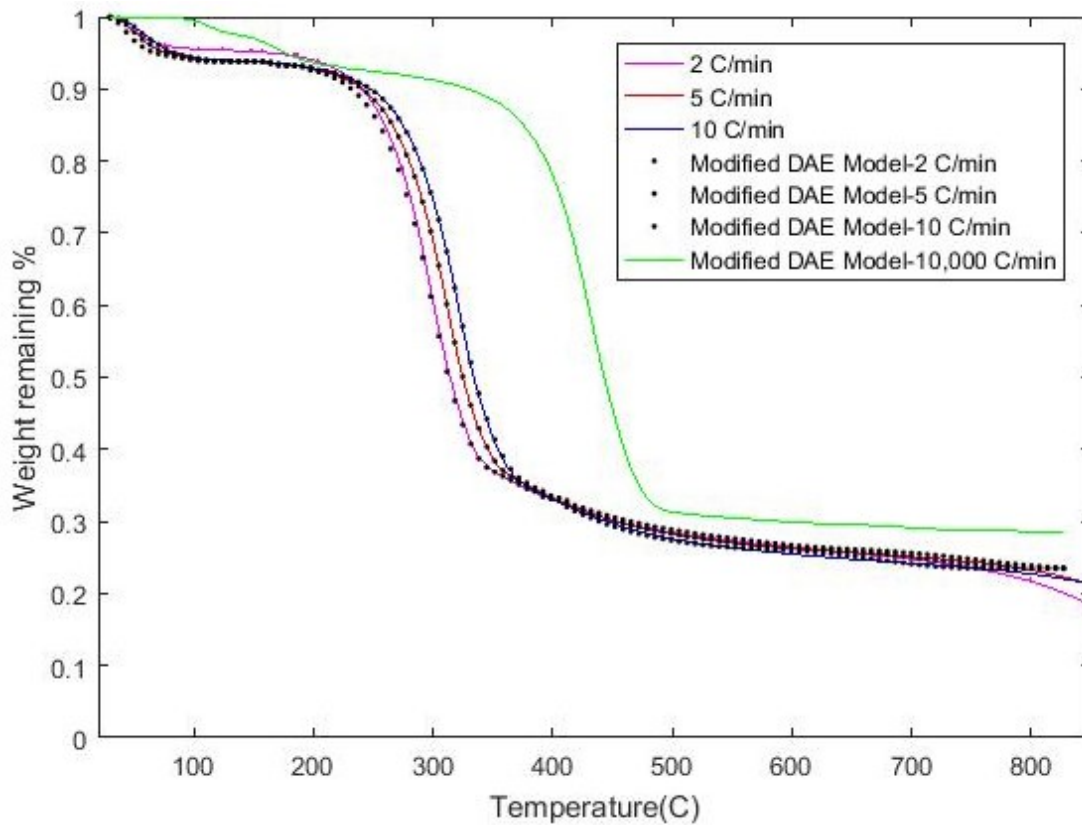


Figure 2 Experimental and modified DAEM curves for pyrolysis decomposition of corn stover at 2, 5 and 10 °C/min

A sample of experimental data taken during and after the completion of experiment is displayed in Figure 3.

The SEM images of biochar produced from hardwood pellets and softwood chips are displayed in Figure 4 & 5.

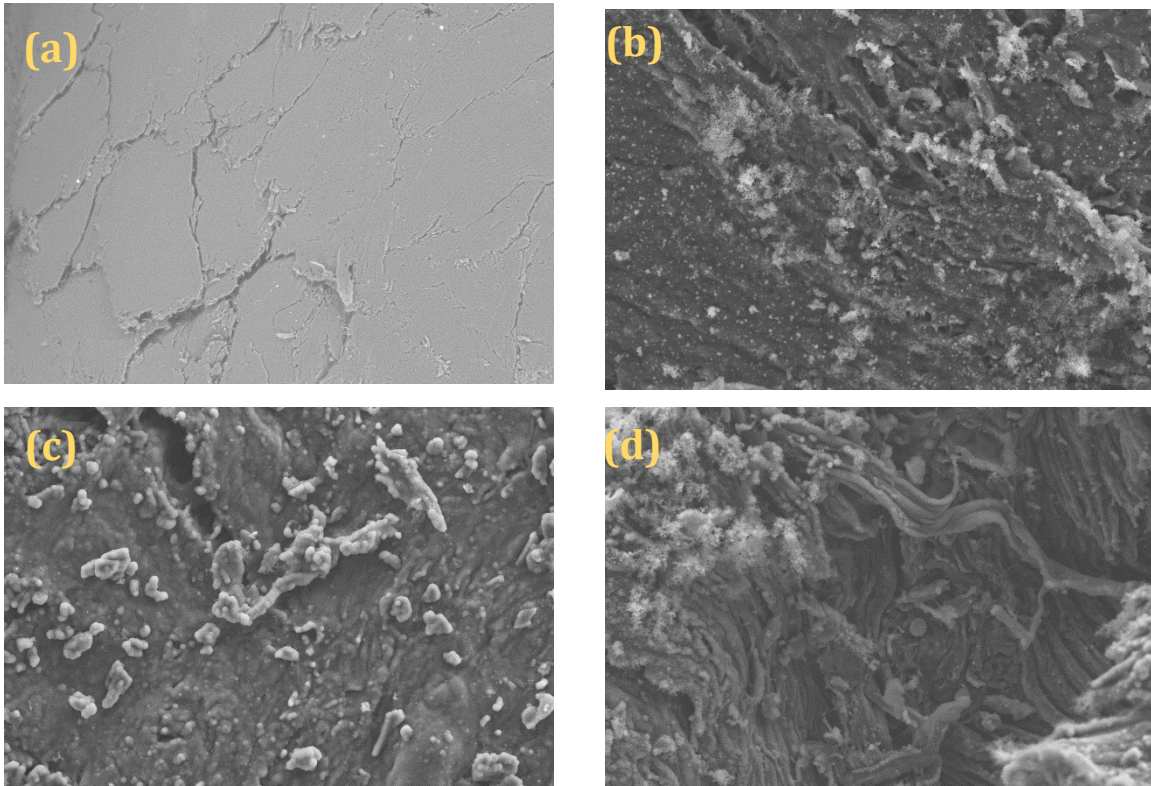


Figure 4 SEM Images of (a) Hardwood pellets (b) Biochar (450, 550) (c) Biochar (450, 600) (d) Biochar (450, 650)

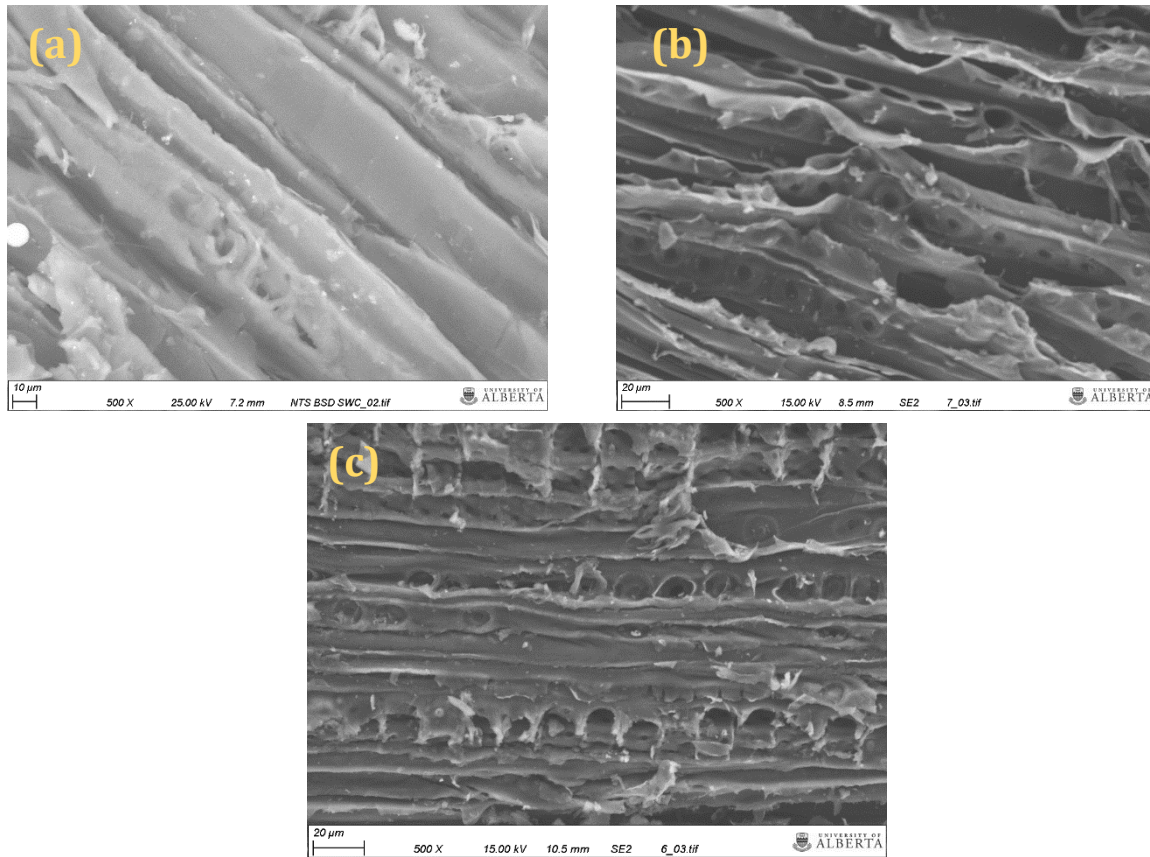


Figure 5 SEM images of the (a) softwood chips (b) Biochar (450, 600) (c) Biochar (450, 650)